The effect of turbulence and shear on the flow around three dimensional square cylinders

Adatia, Aminmohamed

THE EFFECT OF TURBULENCE AND SHEAR ON THE FLOW AROUND THREE DIMENSIONAL SQUARE CYLINDERS

Ph D Thesis

Aminmohamed ADATIA

Aeronautical Engineering Department
QUEEN MARY COLLEGE
University of London

1980

THESIS SUBMITTED TO THE UNIVERSITY OF LONDON
IN PARTIAL FULFILMENT FOR THE DEGREE OF
DOCTOR OF PHILOSOPHY EXAMINATION REQUIREMENTS

ABSTRACT

The effect of turbulence and shear on the flow around square cylinders has been investigated (i) for models without a free end at incidence α in the range $0^{\circ} < \alpha < 45^{\circ}$ for models with and without end plates and, (ii) for models with a free end at $\alpha = 0^{\circ}$ and $\alpha = 45^{\circ}$ for model height ,H, to width ,D, ratio H/D in the range $2 \leq H/D \leq 11$. The Reynolds number, based on the model width was 4.8×10^{4}.

It has been found that end plates are necessary to simulate a two dimensional flow condition in uniform smooth flow provided the wall boundary layer is greater than about 10% of the model span. In other uniform flow conditions, away from the wall boundary layer affected region, which is about the physical thickness of the boundary layer, two dimensionality could be assumed. In linear shear flow, end plates reduced the base pressure in the low velocity region. Two dimensional model results agree well with the published results.

Finite square cross-section cylinders exhibit a free end region of length ℓ_F and a root region. Three regimes, Low H/D, Middle H/D and High H/D are found in all flow conditions. The drag on the finite cylinder in smooth flow is lower than that in turbulent flows. Provided the flow is turbulent, increasing turbulence decreases the drag. For a particular flow condition, increasing H/D ratio increases the drag.

It appears that in the high H/D regime there is a shedding of the free end eddy. The shedding frequency is lower than the shedding frequency in the root region of the cylinder.

The effect of shear can be ascertained by correcting the flow results for the local velocity and thus shear need not be considered a critical flow simulation parameter.

CONTENTS

CONTENTS

ACKNOWLEDGEMENTS

I am very grateful to and would like to thank the following for their help and encouragement.

Roger Montague who did all the modelling

Don Husband who did the photography

The staff and research students (1973-76) in the Aeronautical Engineering Department

Betty Sharples and Cathy Chaffey for typing the thesis

Dr. D.G. Petty my supervisor

NOTATION

A	Constant
A_f	frontal aspect ratio - front width/model height
A_s	side aspect ratio - side face width/model height
a	Longitudinal vortex spacing
B	Constant
b	Lateral vortex spacing; model breadth; grid bar width
C_D	Coefficient of drag
C_{D_c}	Coefficient of drag corrected for blockage
C_{D_s}	Coefficient of vortex street drag
C_P	Coefficient of pressure
C_{P_b}	Coefficient of base/rear/leeward face pressure
C_{P_f}	Coefficient of front/windward face pressure
$C_{P_{b\ell}}$	Coefficient of base pressure based on local velocity
D	Model width; drag
D_s	Vortex street drag
E	Hot wire output voltage
$\overline{E}$	Mean component of E
e	rms value of fluctuating component of E

F(t)	Forcing function
G	Total momentum wake thickness
H	Model height; model span
h	Distance between shear layers emanating from bluff body
K_s	Vortex shedding factor
K_T	Turbulence factor
K_{ts}	Turbulence and shear factor
K_F	Free end factor
k	Stiffness factor
L(x,u)	Turbulence longitudinal length scale
L(z,u)	Turbulence lateral length scale
ℓ	characteristic length
ℓ_F	length of free end region
M	grid mesh length
n	vortex shedding frequency; constant
P	pressure
p'	fluctuating component of P
p	static pressure

P_{ref} pressure at reference point

P_i pressure at position i

P_s vortex shedding component of pressure

P_T turbulence component of pressure

P_F free end component of pressure

$R_{\mathbb{C}}$ Reynolds number based on tunnel centre-line velocity ($R_{\mathbb{C}} = U_{\mathbb{C}}D/\nu$)

R Reynolds number ($R=UD/\nu$); correlation coefficient

R_F free end component of correlation coefficient

R_G Reynolds number based on total momentum wake thickness ($R = UG/\nu$)

R_s vortex shedding component of correlation coefficient

R_T Turbulence component of correlation coefficient

R_{ts} turbulence and shear component of correlation coefficient

S Strouhal number ($S = nD/U$); reduced frequency parameter

S_1 reduced frequency in the model base/root region

S_2 reduced frequency in the model free end region

S_B Bearman universal Strouhal number ($S_B = nb/U_b$)

$S_{\mathbb{C}}$ Strouhal number based on tunnel centre-line velocity ($S_{\mathbb{C}} = nD/U_{\mathbb{C}}$)

S_G Strouhal number based on total momentum wake thickness ($S_G = nG/U$)

S_R Roshko universal Strouhal number ($S_R = nh/U_b$)

t time

U	velocity in x direction
$\overline{U}$	mean velocity component of U
U_o	free stream velocity in x direction
U_b	velocity at edge of boundary layer at separation
$U_{\mathbb{Q}}$	tunnel centre-line velocity in x direction
U_{ref}	refrence point velocity in x direction
U_s	velocity of vortices relative to free stream
u'	fluctuating component of U
u	rms value of fluctuating component of U
x,y,z	cartesian coordinates - x in direction of flow
Y	tunnel dimension in y direction
Z	tunnel dimension in z direction

α	flow incidence
β	damping coefficient
Γ	circulation in one fully formed vortex
Γ_o	total circulation shed from one side duriing one cycle of vortex formation
δ	boundary layer height
ν	kinematic viscosity (= 1.45×10^{-5} m^2/s)
ρ	density of air (= 1.23 kg/m^3); correlation coefficient
ρ_F	free end correlation coefficient component
ρ_s	vortex shedding correlation coefficient component
ρ_T	turbulence component of correlation coefficient
ρ_{ts}	turbulence and shear correlation coefficient component
$\rho(\tau)$	normalized auto-correlation coefficient
ρ_{AB}	spatial correlation coefficient
τ	time constant
θ	velocity fluctuation
ΔS	difference between the reduced frequency in the root region and that in the free end region

CHAPTER 1

INTRODUCTION

Every year considerable damage is caused to buildings and structures by the wind, which also often produces unpleasantly high velocities around tall buildings. With the trend towards tall buildings in cities using modern building techniques with lightweight materials producing lightly damped structures, Building Aerodynamics, and in general Wind Engineering, has become an important discipline.

Since the first Tacoma Narrows Suspension Bridge in the United States oscillated to destruction in 1940 it has become obvious that the wind besides producing a steady load also induces an oscillatory force on the structure and the dramatic collapse of the cooling towers at Ferrybridge in the United Kingdom in 1965 further emphasised the need to understand the nature of wind induced forces on buildings and structures.

Wind loading data on full scale buildings is being obtained in the United Kingdom by the Building Research Station and though this is both time-consuming and expensive it is necessary to provide data to compare with model results in order to validate the wind tunnel techniques.

Early work on building models was done in smooth flow but it soon became apparent that atmospheric flow parameters must be simulated

in the wind tunnel to obtain data representative of full scale buildings. Most wind tunnels, however, have short working sections and artificial methods have had to be used to simulate the atmospheric boundary layer. COUNIHAN (1969), using a combination of elliptic wedge vortex generators, castellated barrier and roughness elements, achieved a good simulation of a natural atomospheric bounday layer. A few wind tunnels with long working sections are in operation notably at the University of Western Ontario, Canada, and at the Colorado State University, U.S.A. The long working section allows for the natural growth of the boundary layer and the neutral atmospheric boundary layer has been reasonably successfully simulated. The boundary layer wind tunnels provide the most reliable source of data for wind engineering in general but the short working section wind tunnels are not a serious limitation, at least for studies of wind effects on buildings. CERMAK (1975) has surveyed the various aspects of wind engineering and cites 222 references.

Considerable work has been done on nominally two dimensional bluff body models, circular cylinders and to some extent flat plates provided the models for determining the basic flow parameters for the flow around two dimensional bluff bodies. The early work naturally extended to bluff bodies resembling buildings and other structures for which a need to understand the effect of the wind, with regards to the flow around and the forces on these structures and the neighbouring environment, became apparent. Models having sharp edges were more

representative of building structures although the emphasis was still on simulating two dimensional flow conditions. The work of BEARMAN (65-72) established the basic parameters that are affected by changing the model-flow configuration. MULHEARN (1973), LEE (1975) did work on two dimensional square cylinder models in flows with varying degrees of turbulence and further established the flow pattern around two dimensional square cylinder models. It is now known that turbulence, oncoming shear and the flow incidence are important factors in determining the flow around two dimensional sharp edged bluff bodies. Further, it now seems also probable that the effect of shear is secondary compared to turbulence (SHARAN, 1977). The relative effect of the turbulence length scale on the various flow parameters is shrouded in controversy with no immediate answer being apparent as to whether turbulence length scale variation has an effect on the flow around the bluff body.

As the two dimensional model results provided the model of the flow around sharp edged bluff bodies, experimental work moved to three dimensional sharp edged bluff bodies which are truly representative of buildings and like structures of importance to Building Aerodynamicists and Wind Engineers. There have developed two methods of obtaining model results for possible full scale comparison. One method is to perform all testing in a wind tunnel that simulates the natural boundary layer as in boundary layer wind tunnels. This method assumes no flow parameters as being of a higher priority, the emphasis being on

simulating the flow at the full scale site. The second methods is to use wind tunnels with short working section, by far the majority of wind tunnels available, and simulate mainly the turbulence characteristics of the flow. This allows for substantially larger models to be used for testing. While the boundary layer wind tunnels provide the better test facility for almost all wind engineering model tests, the short working section wind tunnels can be used to obtain valuable data in at least Building Aerodynamics, provided care is taken to simulate the correct turbulence characteristics (COUNIHAN, 1969). The work of SHARAN (1977) moreover shows, as Sharan says, that the boundary layer portion that needs to be simulated for model testing need only be up to about 3 times the model height. Thus it seems that the short working section wind tunnel need not become obsolete as far as Building Aerodynamics is concerned.

To a large extent, Building Aerodynamics depend on the two dimensional model results to obtain insights into wind related design problems - three dimensional model results being limited to cases related to a full scale building under investigation or to cases covering a small range of model height to width ratio.

Joubert et al (1962) did some work to determine the effect of changing the frontal and side aspect ratios on the flow around models having a height, H, to width, D, ratio in the range $1 < H/D < 4$ and found that the drag coefficient, C_D, was sensitive to changes in the frontal aspect ratio. BRAY (1962)

considered a model of an approximately square cross-section with H/D = 4.5 in a shear flow with a 1/5th power law exponent and found C_D at the ground higher than that at the top. COOK (1971) found a dependence on turbulence length scale for high rise building models having H/D = 3 for longitudinal length scale $L(x,u)$ in the range $0.5 \leq L(x,u)/D \leq 2$. Engineering Sciences Data Unit has produced a Data Item ESDU 71016 (1973) which contains data from various sources. The bulk of the data consists of smooth flow results for two dimensional model configuration. Three dimensional model configuration results are also for smooth flow conditions and the results are extrapolated to two dimensional model values. The data item provides correction methods (graphical) for application to turbulence flows. The surface mounted cube, probably the basic three dimensional sharp edged bluff body, has been investigated for by CASTRO & ROBINS (1977) to determine the flow around the cube in uniform and turbulent streams.

The programme for the present study, therefore, was planned to investigate the effect of turbulence and shear on the flow around a three dimensional square cylinder considered to be representative of a building. Measurements were taken of the surface mean pressures, pressure power spectral density and pressure correlations for the square cylinder model in uniform smooth, uniform turbulent and low turbulence shear flows for models with and without a free end and the data has been compared where possible with the published results.

In Chapter 2, bluff body flow is briefly reviewed; the aspects considered being the vortex street parameters, the flow around circular and sharp-edged cylinders in uniform flows and the flow around a bluff body in non-uniform flow. Chapter 3 describes the experimental procedure, the data reduction methods and the data acquisition equipment used for the study while in Chapter 4 the characteristics of the incident flows are presented and discussed.

For uniform smooth, 0.4% turbulence intensity, and uniform turbulent flows, the results presented and discussed in Chapter 5 are for the model without a free end and incidence in the range $0^{\circ} \leq \alpha \leq 45^{\circ}$ while in Chapter 6 results for the three-dimensional model at $\alpha = 0^{\circ}$ and $\alpha = 45^{\circ}$ for model height to width ratio H/D 2 $\leq$ H/D $\leq$ 11 are presented and discussed. The results for the model without a free end at $\alpha = 0^{\circ}$ and $\alpha = 45^{\circ}$ in approximately linear and 1/6th power law shear flows are presented and discussed in Chapter 7.1 while those for finite cylinders, $2 \leq$ H/D $\leq$ 11 at $\alpha = 0^{\circ}$ and $\alpha = 45^{\circ}$ in an approximately linear shear flow in Chapter 7.2.

In Chapter 8 are presented the conclusions that have been drawn from the present study into the effect of turbulence and shear on the flow around square cylinders with and without a free end.

CHAPTER 2

REVIEW OF BLUFF BODY FLOW

2.1 Introduction

Shear layers, which can be regarded as thin layers of vorticity, develop in flows having a velocity gradient, such as in a boundary layer. If no separation occurs in the flow over a surface, the vorticity is confined to the boundary layer. The viscosity effect is present only in the boundary layer and thus the pressure distribution can be found, at least approximately by inviscid flow theory. However, if separation takes place, vorticity is present elsewhere in the fluid and in general, the pressure distribution can be found only by experiment.

For bluff bodies, except at very low Reynolds numbers, separation always takes place. (The Reynolds number, $R = U \ell/\nu$ where U is a representative velocity, ℓ is a characteristic length which for a bluff body is typically the body width and ν is the kinematic viscosity.) TANEDA 1968) investigated the flow around a circular cylinder and a flat plate normal to the flow at very low R, and found that the circular cylinder first shows signs of separation at $R \simeq 6$ while separation at the edges of the normal flat plate first occurs at the very low R about 0.4. Once the flow has separated, the shear layers, which are unstable, roll up into vortices and for symmetrical

bluff bodies an attached vortex pair is formed behind the body. Taneda found that this vortex pair, called the standing 'vortex', elongates in the streamwise direction with increasing R and the length of the 'vortex' increases linearly with R. The standing 'vortex' eventually becomes unstable and finally breaks down as R is further increased and Taneda found a value R ≃ 30 for a circular cylinder and R ≃ 25 for a normal flat plate for this critical R. For a circular cylinder this critical R is now regarded to be about 40. The breakdown of the standing 'vortex' leads to a different arrangement of vortices in the wake, a double row of asymmetrically arranged vortices with the vortices shed alternately from either side of the body - the Karman vortex street.

ROSHKO (1954) investigated the relationship between the frequency of vortex shedding from circular cylinders and Reynolds number and found that the Reynolds number range of periodic vortex shedding is divided into two distinct subranges; a stable vortex street range, $40 \lesssim R \lesssim 150$, where regular streets are formed with no turbulent motion developing within the street and an irregular range, $R \gtrsim 300$, where the vortex street is composed of turbulent fluid. The Strouhal number $S = nD/U$, where n is the vortex shedding frequency, D the cylinder width and U is the free stream velocity, was found in the stable range to be proportional to R while in the irregular range S was essentially constant. In the intermediate range,

$150 \lesssim R \lesssim 300$, which Roshko called the transition range, no regular periodicity could be found in the wake. Considerably more research has been done on circular cylinders than on any other bluff body and the circular cylinder work has been instrumental in forming a basis for the understanding of the separated flow behind bluff bodies.

In the present review emphasis has been placed on the vortex shedding Reynolds number range and the review mainly considers the vortex street parameters and the flow around circular cylinders and bluff bodies with fixed separation points.

2.2 Vortex Street Parameters

Von Karman (see Lamb) investigated the stability of an idealized potential flow model of the vortex street wake which forms behind a bluff body. He showed that only the asymmetrical double row of vortices, FIGURE 1a, is stable to first order disturbances and only if the ratio of distance, b, between the rows to distance, a, between two consecutive vortices called the spacing ratio , b/a, is equal to 0.281. In a vortex street stability review paper, WILLE (1960) points out that theory seems to indicate that vortex streets can not exist since they are unstable to second order disturbances but, vortex streets can be produced. Wille suggests the possibility that the theory considers a completely different situation from the real vortex street wake flow since all vortex street stability theories assume an established vortex arrangement whereas in a real street stability may be affected by viscosity, the vortex age, etc; the vortex street wake that is observed is still developing. Moreover, experimental results do not support the Karman spacing ratio. There is a considerable discrepancy in the experimental results for the spacing ratio, values ranging from 0.20 to 0.40 and even higher. The difficulty is in defining the centres of the voritices. HOOKER (1936) considered a real vortex which has a core of finite radius whose centre is the point of zero velocity and maximum vorticity.

In a vortex street the points of zero velocity and maximum vorticity do not coincide. Whereas the point of maximum vorticity is unchanged, the point of zero velocity moves further out, its distance from the centre of the street increasing almost linearly with time. Thus a spacing ratio based on vorticity centres remains constant while the spacing ratio based on velocity centres increases linearly. TIMME (1959), reported by WILLE (1966), showed the validity of the Hooker vortex model and FIGURE 1b shows the result of the application of the Hooker model; the results also show that the spacing ratio increases with distance downstream from the cylinder. It is now known that both the lateral and longitudinal spacing grow with distance downstream but the latter slower than the former (Wille).

Another difficulty in experimental investigation of the vortex street is the location of the centre of rotation. BERGER (1964) found a signal having a minimum amplitude at double frequency, indicative of the middle of the street, and two symmetrically positioned outer signals of maximum amplitude but no characteristic hot wire probe signal for the centre of rotation of a vortex. BEARMAN (1965) measured velocity fluctuation $\theta = u'/U_o$, where u' is the rms value of the velocity fluctuations and U_o is the free stream velocity, across the wake of a two dimensional model with a blunt trailing edge and found that θ had a

peak and that maximum occurred at a distance equal to one base height from the model rear face. Downstream of the body the θ peaks converge up to a position of maximum θ and then diverge. Bearman proposed that the position of maximum θ is the start of the fully formed vortex; the region between the body producing the vortices and the fully formed vortex being the formation region. The lateral spacing of the vortices, Bearman suggests, could be obtained, at least to a first approximation, from the peaks in θ taken from traverses across the wake.

KRONAUER (1964) showed that, if the vortex street drag is taken to be that given by the von Karman vortex street model where the drag is given by:

$$C_{D_s} = \frac{4}{\pi} \left(\frac{U_s}{U_o} \right)^2 \left\{ \coth^2 \pi \frac{b}{a} + \left(\frac{U_o}{U_s} - 2 \right) \pi \frac{b}{a} \coth \pi \frac{b}{a} \right\}$$

$$\text{where } C_{D_s} = D/\tfrac{1}{2}\rho a U_o^2 \qquad \ldots\ldots (1)$$

D_s is the vortex street drag, U_o the free stream velocity, U_s is the velocity of the vortices relative to the free stream, a the longitudinal spacing , b the lateral spacing and ρ density of the fluid, C_{D_s} is very insensitive to the spacing ratio b/a; C_{D_s} passing through a broad minimum. He then proposed a new stability criterion that for a given vortex velocity, U_s, the vortex street adjusts itself into a configuration giving a minimum C_{D_s}. The

criteria can be expressed as:

$$\left\{ \frac{\partial C_{D_s}}{\partial (b/a)} \right\} \frac{U_s}{U_o} = \text{const} = 0 \qquad ..(2)$$

The validity of the Kronauer criterion has been shown, although indirectly, by BEARMAN (1967) through the formulation of a universal Strouhal number. This is discussed in more detail later.

ROSHKO (1954a) had proposed a universal Strouhal number, S_R, based on distance h between the two shear layers, which spring from the body, as the length scale and the velocity, U_b, at the edge of the boundary layer at the separation point such that

$$S_R = nh/U_b$$

where n is the shedding frequency. Applying Bernoulli Equation upstream and in the wake.

$$U_b = U_o \ (1 - C_{P_b})^{1}/2 \qquad ..(3)$$

or

$$U_b = kU_o \text{ where } k = (1 - C_{P_b})^{1}/2 \qquad ..(4)$$

where C_{Pb} is the base pressure coefficient. Thus

$$S_R = \frac{S}{k} \frac{h}{D} \qquad ..(5)$$

where S is the Strouhal number (S = nD/U), D is the body width. The value h can be obtained by the notched hodograph method developed by ROSHKO (1954b).

GERRARD (1966) found that there was a considerable discrepancy when circular cylinder results were compared with Roshko's on the universal Strouhal number plot and attributed this to the level of free stream turbulence in the two experiments. Gerrard also compared the results on the basis of a plot of S_G (=nG/U) as a function of R_G (=UG/ν) where G, the total wake momentum thickness, is the length scale, and found that at high R, S_R and S_G are equivalent but at R_G = O[10^3] there was again a considerable spread. This discrepancy, according to Gerrard, is due to the state of the shear layers, emanating from the body, which later roll up into vortices. When the flow is laminar, it seems that the Strouhal number itself is the universal non-dimensional frequency parameter while at high R when the flow is turbulent S_R and S_G are equally good. In the range when the position of transition in the shear layers is moving towards the body (§ 2.1), laminar and turbulent layers are present in the formation region and neither S_R nor S_G represent the wake. From further considerations of the wake and the vortex shedding frequency for a circular cylinder, Gerrard concluded that there are two simultaneous characteristic scales, the length of the formation region and the width to which the free shear layers diffuse. A formulation of a universal Strouhal number applicable to various bluff bodies both

with and without wake interference was proposed by BEARMAN (1967). The length scale used was the lateral spacing distance, b, and U_b the velocity giving the Bearman universal Strouhal number, S_B, so that:

$$S_B = nb/U_b \qquad ..(6)$$

which can be shown to be

$$S_B = \frac{S}{k}\,\frac{b}{D} \qquad ..(7)$$

S and k are both measured quantities while b/D could be found using either the Karman or the Kronauer stability criterion. Bearman evaluated S_B and k for bluff bodies with wake interference, splitter plates and base bleed, and found that over most of the range of k, S_B based on the Kronauer criterion, was a constant at 0.181 whereas the Karman criterion gave S_B which decreased monotonically with k. On comparing the wakes of various bluff bodies based on the Kronauer criterion, it was found that at low values of k, $k \to 1$, S_B decreases. Bearman suggests that at these low values of k some other length scale becomes important and the wake similarity model based on the lateral spacing, b, breaks down. The constancy of S_B, based on the Kronauer criterion, over a wide range of k for a variety of bluff bodies with and without wake interference, as Bearman says lends much support to the Kronauer vortex street stability criterion.

Experimental investigations have shown that the total amount of circulation Γ_σ shed from one side of a bluff body during one cycle of vortex formation is more than the circulation, Γ, found in one fully formed vortex; the ratio Γ / Γ_o has been found to be about 0.6. Wood, cited by MAIR & MAULL (1971), in an experimental study reported a value 0.66. ABERNATHY & KRONAUER (1962) proposed a theoretical model and their predicted ratio Γ/Γ_o was 0.61. A model for the vortex formation region due to GERRARD (1966) explains this loss of circulation. A part of the circulation in one shear layer is transferred across to the other shear layer and some circulation is transferred into the recirculation region immediately behind the base; the vortex being shed when its supply is cut off by the transferred shear layer from the opposite side. Gerrard also showed that the diffusion length-the thickness of the shear layer at the end of the formation region where the layer is drawn across the wake, is of fundamental importance to the determination of the vortex shedding frequency.

BEARMAN (1972) showed that the base pressure value depends upon the distance from the body at which the vortices are formed; the further downstream that the vortices form the higher the base pressure. Wake interference, with splitter

plates (and base bleed) , caused the base pressure to rise and increased the size of the separated region behind the body; the vortices not being able to form until after the splitter plate. Bearman suggests that it is the entrainment process during vortex formation that sustains the low base pressure; the removal of entrained fluid balanced by an induced reversed flow into the formation region (Gerrard's formation model) with the vortex formation region adjusting to an equilibrium position determined by the base cavity volume, the shed vorticity and the base pressure.

2.3 Sharp-edged Bluff Bodies in Uniform Flows

In experiments with a two dimensional flat plate normal to the flow, TANEDA (1968) observed that the Reynolds number at which standing vortices first appear was as low as $R \simeq 0.4$ and that the breakdown of the vortex pair occured at $R \simeq 25$ leading to the establishment of the Karman vortex street. The emanating shear layer from the fixed separation points undergo transition; the distance to transition from separation being x_t. GARTSHORE (1973) found that for rectangular two dimensional prisms x_t is given by

$$x_t/h = kR^{-1/2} \qquad ..(8)$$

where h is the frontal dimension of the two dimensional prism with $k \simeq 5$.

Hence for $R > 3\ 10^4$ $\quad x_t < .05h$

Gartshore however, comments that equation (8) may underestimate x_t because of the difficulty in exactly defining transition and the inability to accurately account for the interaction between the shear layers and the body.

GARTSHORE (1973) cites LANEVILLE (1973), who found that for short rectangular prisms, the drag coefficient increased with increasing R becoming essentially constant for $R \gtrsim 3\ 10^4$. These two results thus suggest, as Gartshore says, that the addition of free stream turbulence, if it simply promotes early transition in the shear layers, is unlikely to alter the flow pattern significantly if $R > 3\ 10^4$.

The pressures and forces on sharp edged bluff bodies have been found to be sensitive to the type of incident flow, be it smooth, turbulent, uniform or sheared, and the incidence of the flow relative to the body. The sharp edged body most frequently considered has been square section cylinder in a nominally two dimensional configuration.

For a cylinder with a face normal to the flow, VICKERY (1966) found that the base pressure coefficient, C_{P_b}, increased with an increase in the level of turbulence. BEARMAN (1972) collected results from various workers and FIGURE 2 shows the variation of C_{P_b} with turbulence intensity. Detailed measurements of the mean and fluctuating pressures around the cylinder in flows with varying degrees of turbulence intensity have been made by LEE (1975a). The work showed that an increase in the level of turbulence intensity led to a more complete pressure recovery towards the rear of the side faces of the square prism. Both Vickery and Lee found that the axial correlation length decreased with turbulence. Vickery had measured the length in smooth flow to be 5.6D; D is body width, which had decreased to about 3.6D at 10% turbulence intensity. Lee found the correlation length to have decreased from about 4.1D in smooth flow to about 0.96D in 12½% turbulence intensity. When the turbulence intensity increased from 0.5% to 12.5% Lee found that

the vortex shedding strength was reduced by a factor of 5. From his measurements, Lee built the following picture of the flow around a square prism at zero incidence (FIGURE 3). In the absence of turbulence in the incident flow, the shear layers originating at the front corners of the prism curve outward and form the Karman vortex street in the wake close behind the body. The proximity of this vortex formation region gives rise to a large fluctuating pressure C_p', on the rear face in addition to the low base pressure coefficient C_{P_b}, and a high coefficient of drag, C_d. With the introduction of turbulence in the flow shear layers undergo transition, from their initial laminar state to turbulent behaviour, nearer the front corners resulting in an increased entrainment and thickening of the shear layers. The mean centre line of the shear layers may also curve inwards towards the sides of the body. The result of either or both of these processes is that there will be an intermittent reattachment of the mean shear layer to the side faces. This in turn will inhibit vortex formation immediately behind the body as occurs in smooth flow, and the vortices will be formed further downstream of the body reducing C_p', increasing C_{P_b} and decreasing C_D.

Flow visualization of the flow around a square cylinder in smooth and turbulent flow, having an intensity about 8% showed that the incidence α_R at which separated layers from the 'leading' corner reattached on to the side face decreased

with turbulence (MULHEARN, 1973). Mulhearn suggested that even when reattachement does not occur, as at $\alpha < \alpha_R$, the shear layers are closer to the body. When reattachment has taken place the flow separates at the leading corner and reattaches on the side face. There is now a back flow towards the leading corner, the secondary flow separating at a point before the corner, setting up a separation bubble. The flow patterns for the prism at incidence are shown in FIGURE 4.

McLaren et al (1969a, 1969b) in experiments with square cylinders at incidence found that at $\alpha = 0^\circ$, C_D decreased and C_{P_b} increased with increasing turbulence intensity. As α was increased to 15°, the difference in C_D for various turbulence levels became small but as α was further increased the difference in C_D for various turbulence levels again become large. Between $\alpha = 10^\circ$ and $\alpha = 20^\circ$ the effect of turbulence on C_D was found to be negligible; the greatest difference in C_{P_b} (and thus C_D) were found to occur in the symmetrical flow cases $\alpha = 0^\circ$ and $\alpha = 45^\circ$. LEE (1975a) found that as α is increased, C_D has a minimum and then increased for increasing α. The incidence for minimum C_D decreased with increasing turbulence intensity, minimum C_D occurring in smooth flow at $\alpha = 12\frac{1}{2}^\circ$, in flow having turbulence intensity 6.5% at $\alpha = 10^\circ$, in 8% intensity at $\alpha = 9\frac{1}{2}^\circ$ and in 12½% intensity at $\alpha = 8^\circ$.

Before reattachment of the flow on the side face, the proximity of the body and the shear layers causes the vortices to form further from the body raising C_{P_b} and decreasing C_D. Once reattachment has taken place the rear of the side face becomes the new separation point and the flow pattern does not alter with increasing α. Increasing α now widens the wake and the drag increases.

Assymmetry in the flow is introduced as α is increased giving rise to a side force. This reaches a maximum at the reattachment angle α_R and then decreases with increasing α becoming zero when the flow is again symmetrical at $\alpha = 45^{\circ}$ (LEE, 1975a).

Measurement of the Strouhal number, S, showed that S increases with α reaching a maximum at the reattachment angle α_R. Lee associated this variation in S with the variation in C_D with α. To quote "The minimum in the mean drag is thought to be associated with a minimum wake width, and hence a minimum longitudinal vortex spacing, if a constant ratio of vortex spacing to wake width is presumed. This would lead to an increase in the frequency of vortex shedding, and thus to an increase in the Strouhal number". BEARMAN (1967) had found that when the product $C_D.S$ was plotted against $k = (1 - C_{P_b})^{\frac{1}{2}}$ a good correlation was obtained. Lee obtained good agreement with Bearman's results which further supports the formulation of the Bearman universal Strouhal number, S_B, and in turn

the Kronauer stability criterion (§ 2.1).

The work of McLaren et al had shown that besides the turbulence intensity, the turbulence scale relative to the size of the cylinder also had an effect on C_D. At $\alpha = 0^o$, C_D was found to have a distinct maximum for longitudinal length scale L(x, u), to cylinder width D, ratio L(x,u)/D in the range 1.2 to 1.6. For larger L(x,u)/D, C_D tended to a constant value as L(x,u) was increased. At $\alpha = 45^o$ all C_D results for all turbulence intensities collapsed on to one curve with a maximum C_D at L(x,u)/D 1.4; again as L(x,u)/D became large C_D tended to a constant value. COOK (1971), working in the range $0.5 \leq L(x,U)/D \leq 2$ on high rise building models with a height to width ratic of 3, also found that the fluctuating flow and surface pressure characteristics are strongly dependent on the turbulence scale. BEARMAN (1972) however, could find no base pressure, C_{P_b}, variation with length scale, L(x,u)/D, although the later was varied through an order of magnitude range. FIGURE 2 taken from Bearman (1972) however, shows the variation of C_{P_b} with turbulence intensity for a square section cylinder at $\alpha = 0^o$ for a range of L(x,u)/D values. Plotted against turbulence intensity, C_{P_b} values fall within a band with about 12% scatter.

Although over most of the turbulence intensity range covered, 0% to 12%, there is not a significant variation in C_{P_b} with length scale, at turbulence intensity about 5%, C_{P_b} for L(x,u)/D = 1 is about 10% higher than C_{P_b} for L(x,u)/D = 3 and the same sort of variation is found at turbuelence intensity about 8%.

LEE (1976) did a series of tests to determine the effect of length scale, L(x,u)/D, on C_D by varying the length scale for a given turbulenece intensity and found that length scale does have an effect upon C_D. Lee found, FIGURE 5, that C_D has a maximum at $L(x,u)/D \simeq 1$ followed by a minimum in the range $1.5 < L(x,u)/D < 2$. At high values of L(x,u)/D, C_D tended to a constant value which was greater than that at low values of L(x,u)/D; PETTY (1972) having shown that high turbulence scales cause an attenuation of the turbulence intensity while at low lenth scales the intensity is amplified and as already seen, the effect of decreased turbulence intensity is to increase C_D.
Measurements of the base pressure, C_{P_b}, and drag coefficient C_D, on rectangular section cylinders have been made by BEARMAN & TRUEMAN (1972) who found that for a range of depth, d, to breadth b, ratios at $\alpha = 0^{\circ}$ C_D reaches a maximum (=2.94) when d/b = 0.62 and that the maximum is associated with regular vortex shedding. Further increase in depth decreases C_D.

It is argued that until the critical d/b ratio, as the depth increases the size of the separated cavity decreases while the vortices form at the same distance downstream of the separation point. With increasing d the body is closer to the vortex formation region which leads to a reduction in C_{P_b} and thus an increase in C_D. At d/b = 0.62 the separating shear layers just clear the rear corner and the vortices form closest to the body giving a maximum C_D. It would appear that in turbulent flows since the vortex formation region is increased the critical d/b ratio would be higher. However, the maximum C_D value would be lower than 2.94 for smooth flow because in turbulent flows the base pressure at $\alpha = 0^o$ is lower than that in smooth flow.

The rectangular section model results extend the range of the correlation product C_DS versus k but also show a weak dependence on a second parameter which Bearman & Trueman suggest to be the diffusion length scale proposed by GERRARD (1966) (§2.1). Once again, the results were found to be incomaptible with the Karman stability criterion.

2.4 Bluff Bodies in Non-Uniform Flows

Investigations into the effect of a non-uniform free stream velocity profile on the base pressure and the vortex shedding of blunt based body have been made by MAULL & YOUNG (1972) and MAIR & STANSBY (1975). Maull & Young used a model spanning the tunnel but did not use any end plates while Mair & Stansby also used end plates.

Mair and Stansby found that for circular cylinders the base pressures (180^{o} from the front stagnation line) were influenced by end boundaries for cylinder height, H, to width, D, ratio $H/D < 20$, and that for $H/D > 20$ a tendency towards constant $C_{Pb\ell}$ - the base pressure coefficient based on centre-line velocity.

Vortex shedding from the bluff body in a shear flow was found by Maull & Young, to occur in distinct cells with almost discontinuous jumps, in the reduced frequency, from one cell to the next. Mair & Stansby also found that if end plates extended a short distance downstream (4D) the cell boundaries moved with time but when longer end plates were used well defined cells were formed. The boundaries between the vortex shedding cells coincided with the points of inflexion, found on the curve giving spanwise distribution of C_{P_b}, in both the experiments. Mair and Stansby argue that a uniform shedding frequency over the whole span is

not to be expected since this would require a variation of the local Strouhal number across the span in inverse proportion to the stream velocity. Thus vortex shedding in cells of limited spanwise extent is to be expected with a constant frequency within each cell.

Maull and Young did some further work to try and determine the formation of the cell boundaries and concluded that development of longitudinal vortices in the flow direction leads to the cell pattern of vortex shedding.

Mair and Stansby suggest that the action of the cylinder on the shear flow leads to a concentration of streamwise vorticity which interacts with the shed vortex so that the strengths of the shed vortices vary along the span and this causes the cell pattern to develop.

Mair and Stansby by using different lengths of end plates found that the streamwise vortices generated in the boundary layer on the wall of the tunnel can in some cases, disturb the wake and cause fluctuations of the cell boundaries. At the end of each of the cylinders, the wall boundary layer leads to the formation of a horseshoe vortex, which effects the flow field. It is argued that if the effects of viscosity on the development of the secondary flow are neglected, the strength of each horseshoe vortex should be

independent of boundary layer thickness. However, the velocities induced by the horseshoe vortices are substantially reduced by a reduction of boundary layer thickness. Mair and Stansby explain this by considering that the solid boundary represents an image horseshoe vortex of opposite sign on the other side of the boundary. With the thinner boundary layer the real vortex and its image are closer together so that their effects cancel each other more effectively.

On a model with a free end, model height H to model width D ratio H/D = 15, MAULL & YOUNG (1972) found that the pressure distribution could be split into three regions; a root region extending at least 6D from the floor, a central region of approximately constant base pressure and a tip region which has lower base pressures.

It was found that in the central region the base pressure coefficient based on local velocity was the same as in uniform flow, but that the boundary layer affected the base pressure in the root region where the actual pressure distribution rather than the local coefficient was very similar to that on the root of the model in uniform flow.

The spectra of velocity fluctuations due to the vortex shedding at various spanwise positions in uniform flow showed that the main shedding occurred at almost constant frequency over the entire span with a slight frequency shift at some spanwise stations. In shear flow, however, the root region exhibits only one shedding frequency but at spanwise distances within the central region a new peak was observed, the size of which increases, relative to the root frequency, with distance away from the root. In the lower tip region another peak appears and again its size relative to the central region frequency peak increases as the free end is approached Maull & Young suggest that the frequency shift in the root central region area is again caused by the presence of a longitudinal vortex. The flow over the free end is complicated by the presence of very powerful trailing vortices together with some sort of bubble caused by the flow down the back of the body. Maull and Young could give no explanation for the two frequencies in the tip region spectra.

2.5 Three Dimensional Models

The effect of varying the frontal and side aspect ratios, for a model with a face normal to the flow, on the C_D of a building model in smooth flow was investigated by JOUBERT, STEVENS & PERRY (1962). The models considered gave a range of frontal aspect ratio, AF, of $0.255 \leq AF \leq 1.042$ and the side aspect ratio, As, range of $0.0317 \leq As \leq 0.26$, with the model height to width ratio H/D range of $1 \leq H/D \leq 4$. Joubert et al found that C_D was sensitive to AF but quite insensitive to changes in As. The results of Joubert et al also show that as H/D is increased the drag coefficient C_D increased.

BRAY (1962) considered a model of a building of approximately a square cross-section with a height to width ration H/D = 4.5 in a shear flow with a 1/5th power law exponent. Bray obtained C_D based on the local velocity at various heights and on the width of one face, and found that the local C_D was higher at the ground than at the top. Bray found this to be due to relatively larger suctions, at the ground, in the wake compared the local dynamic head.

Engineering Sciences Data Unit (ESDU) issued a Data Item 71016 (1973) for fluid forces, pressures and moments on rectangular blocks where surface mounted blocks in smooth flow have been also considered. The ESDU 'data' showed that the force coefficient, Cx, in the wind direction for

the model at $\alpha = 0^{o}$ has a maximum at breadth to width ration b/d 0.66 for model height to width ratio in the range 20 $\leq$ H/D $\leq$ 5. As H/D becomes smaller than 5 the maximum in C_x occurs at b/D towards 1. The magnitude of C_x also decreases with decreasing H/D. The variation of C_x with b/D is similar to the variation of C_D with a/b found by BEARMAN & TRUEMEN (1972) for two dimensional rectangular models (§ 2.3). For three dimensional models it would appear that the flow over the top surface introduces a kind of base bleed into the wake resulting in an increase in base pressure and hence a reduction in the force coefficient C_x. The flow around the model however, remains essentially the same as the two dimensional model- increasing b/D has the effect of bringing the rear of the model closer to the vortex formation region and hence reducing the base pressure. For H/D < 5 the top surface flow also affects the flow reattachment at the rear corner of the side face so that the separating shear layers are pushed wider and thus a larger b/D change can be accommodated.

SHARAN (1977) investigated the effect of turbulence and shear on the pressure distribution around building models of square cross-section and having height to width ratio of 2 and 3 and found that turbulence characteristics of the flow exercised primary influence on the flow around the models while shear had a secondary influence. The models were considered in flows having turbulence intensity in

the range 9 - 16% and the shear flow had a power law exponent between 0.2 and 0.4. Using models to give a range of simulated boundary layer height, δ , to model height, H, ratios δ/H, Sharan found that for $\delta/H \geq 3$, the pressure coefficients on the windward and leeward sides did not show any significant variation, suggesting that for wind tunnel work the boundary layer height of at least 3 times the building height should be simulated. The experiments also showed that the suction on the roof continues to decrease with increasing δ/H.

A method of changing the shear flow profile while leaving the turbulence characteristics practically unchanged would, as suggested by Sharan, be to reduce the flow velocity by a non-insignificant factor which would cause a significant change in the shear flow profile in terms of absolute velocity. This method is applicable since the flow around buildings reacts to actual shear flow profile and not to the non-dimensional shear flow.

CHAPTER 3

EXPERIMENTAL PROGRAMME

Introduction

This chapter describes the various equipment that was built for the programme, the standard commercial apparatus that was used, the data reduction methods used with the corresponding data acquisition equipment and the experimental procedures adopted.

3.1 Wind tunnels

Two wind tunnels in the Aeronautical Engineering Department were used for these tests. These were (i) The Blowdown Tunnel and (ii) The No. 4 Closed Return Tunnel.

3.1.1 The Blowdown Tunnel

This wind tunnel is an open return type with a closed rectangular working section, 1.016m wide x 0.77m high x 2.12m long, having a contraction ratio 5.6:1. A second section, 2.12m long, was added so that it could house a traversing mechanism. Planar grids could be introduced at the beginning of the working section; the maximum velocity that can be attained, without the presence of any grid, is about $30ms^{-1}$.

3.1.2 No. 4 Closed Return Tunnel

This is a closed return tunnel with a closed rectangular working section 528mm wide x 381mm high x 1.3m long and

has a contraction ratio of 9.3:1 with the working section vented to atmosphere at the downstream end. Again planar grids could be introduced at the beginning of the working section and the maximum wind velocity obtainable without any grid being present is about 30ms^{-1}.

3.2 Experimental Models

Three model cylinders with a square cross-section were made, two of which, 48mm x 48mm and 114mm x 114mm, were used in the Blowdown tunnel and the third, 24mm x 24mm, was used in the No. 4 Closed Return Tunnel, and these are described in the following sections, together with the end plates made to be used with the 48mm model.

3.2.1 48mm model

This model was made from a duraluminum channel section, side thickness 2mm, with the fourth side being a removable (sliding) TUFNEL panel. One end of the cylinder was closed, the other being left open to allow for the passage of tubes to pressure taps on the model. A part circumferential pressure tap distribution, having eleven taps, was provided and was positioned to be at mid-span when the model spanned the height of the Blowdown tunnel. FIGURE 5a shows the tap positions on the model and also the face identification sequence adopted. At flow incidence $\alpha = 0^{o}$, Face A is normal to the flow and then in anticlockwise direction Face B, Face C and Face D;

faces B and D being the side faces. At $\alpha = 45^{\circ}$ the corner between Faces A and B is pointing into the flow; Faces A and B being windward faces and C and D the leeward faces.

At the centre of faces A, B and C, a single spanwise row of pressure taps was provided for each face. FIGURE 6 shows the distribution for Face A and also indicates the tap positions for faces B and D.

On the 48 mm model each pressure tap had a diameter 0.762 mm and could be connected to the required data acquisition equipment through flexible tubes.

3.2.2 114mm model

This model was made of three Tufnel panels, thickness 4mm, joined together with the fourth side being a removalbe sliding panel. One end was closed whilst the other was open to allow for the passage of tubes. Fifteen pressure taps were provided in one quadrant on the closed end, the distribution shown in FIGURE 5b. Each pressure tap had a diameter of 1.524mm and could be connected by a legth of tubing to a recording instrument.

3.2.3 24mm model

This model was made of a duraluminum tube of side thickness 1mm. Four pressure taps were provided one at the centre of each face and all at the same spanwise position. The

model was long enough so that the pressure taps could be positioned at any station along the width of the No. 4 Closed Return Tunnel by traversing the model. Each tap diameter was 0.381mm and could be connected to a measuring instrument through a flexible tube.

3.2.4 End plates

Two similar end plates were made for use with the 48mm model in the Blowdown Tunnel. Each end plate was a rectangular 530mm x 635mm, 2mm thick duraluminum plate with rounded corners and edges. A turntable was inserted flush into the plate to allow rotation of the model. The end plate was supported on circular rods, diameter 5mm, and with the model in position and with a face parallel to a plate edge, the plate edge extended 2D in front of the model, 5D to each side of the model, and 12D to the rear of the model, D being the width of the model. The end plates were 104mm below the roof and 106mm above the floor of the tunnel giving an effective span of 560mm.

3.2.5 Model mounting and axes system

The 48mm and 114mm models both used in the Blowdown Tunnel had similar mountings. Each model was mounted on a turntable through the roof of the working section along the tunnel centre line at a distance 2.55m downstream from the beginning of the working section. The model end could slide in through the turntable and could

be positioned anywhere between the roof and the floor of the tunnel. When the model spanned the tunnel, the end of the model rested on the floor. For the 48mm model when end plates were present at the roof and the floor, the very small gaps between the cylinder and the end plate hole were sealed with 'Sellotape'. However, for finite cylinder configuration when only the roof end plate was present, these gaps were not sealed since it was necessary to change the model height while keeping the tunnel flow on.

FIGURE 7a shows the axes system adopted for the blowdown tunnel; x-axis is along the flow direction and z-axis along the model span. Z represents the tunnel dimension in the z direction, the height, and Y the dimension in the y-direction, the width.

The 24mm model, used in the No. 4 Closed Return Tunnel, was mounted at a distance 0.88m from the grid position through two circular plates which were set into portholes at the sides of the working section so that the model spanned the width of the tunnel. The cylinder could slide through the plates and thus the single set of pressure taps on the model could be positioned at any station along the width of the tunnel. The inevitable gaps between the cylinder sides and the support plate hole were not sealed.

The axes system adopted for the No. 4 Closed Return Tunnel is shown in FIGURE 7b; x-axis is along the flow direction and z-axis is along the cylinder span. Again Z represents the tunnel dimension along the z-axis (the width) and Y represents the dimension along the y axis (the height).

The axes system adopted for the model, shown in FIGURE 7c, was such that the z-axis was along the model span.

3.3 Grids

Two types of grids were used in the study and these were (i) turbulence producing grids and (ii) grids to produce a shear flow.

3.3.1 Turbulence Grids

Three grids were made and each was of the square mesh flat bar type and made from 8mm thick wooden sheets by cutting out the square mesh sections. Two grids, GR1 and GR2 had the same mesh arrangement while the third, GR3, had a different arrangement; in GR3 the gap between the first horizontal bar, i.e. the bar along the width of the tunnel, and the section roof/floor was about a mesh length whereas in GR1 and GR2 this gap was about half a mesh length. TABLE 1 gives the geometrical characteristics of the turbulence grids GR1, GR2 and GR3. GRO is the case with no grid.

3.3.2 Shear Flow Grids

Grids for producing a shear flow were made by arranging circular bars on a frame to give a varying blockage across the tunnel. Three grids were made; SH1 for use in the Blowdown Tunnel with SH2 and SH3 for use in the No. 4 Closed Return Tunnel. TABLE 1 gives the geometry of the grids. Grid SH1 was built using the design method of OWEN & ZIENKIEWICZ (1957) while grids SH2 and SH3 were constructed using the method of COWDREY (1967).

3.4 Data acquisition equipment for grid calibrations

3.4.1 Hot wire anemometer

A Thermo Systems Incorporated (T.S.I.) constant temperature anemometer model 1054A was used with the DISA type P01 single sensor hot wires. The anemometer could be operated in either the non-linear or linearized output modes, the linearizer used being the T.S.I. model 1117 Linearizer.

3.4.2 Correlator

Correlation measurements were made using a DISA type 55D70 Correlator which has an optimum frequence range of 2Hz-200kHz. For autocorrelation measurements, the correlator was used in conjunction with a DISA type 55D75 Time Delay Unit and a DISA type 52B01 Sweep Motor Drive Unit. The frequency response in this mode of operation

operation was 2Hz-10kHz. The autocorrelation equipment gave a trace output of the autocorrelation function with time delay, and the output was recorded on a graph using a Bryans XY Recorder type 29000 A4.

3.5 Data reduction methods for grid calibrations

3.5.1 Hot wire calibration procedure

The hot wire to be used was calibrated in smooth flow against a Pitot-static tube positioned so that the static holes were in the same downstream plane as the hot wire; the wire calibrated for a velocity range from about 1 ms^{-1} to about 25ms^{-1}. Once the first calibration was completed, the hot wire orientation was not altered during any investigative procedure for which the hot wire was being used. At the end of the experimental run the hot wire was recalibrated in smooth flow and if the two calibrations were significantly different the results for the particular experimental run were discarded. If the two calibrations showed a slight difference only in the high velocity region this was not considered to be significantly different since the tests were done at velocities much lower. For these cases, however, the results obtained from the two calibrations were averaged.

3.5.2 Calculation of velocity and turbulence intensity

BRUUN (1976) has compared non-linear calibration procedures for the evaluation of hot wire data and from the evaluations

of the hot wire data obtained from four linearization methods it was shown that the actual method of linearization is of no importance provided the linearization procedure is carried out accurately.

In the present study the linearization method used to evaluate the hot wire data for the mean velocity and turbulence intensity was the power law relationship.

$$E^2 = A+BU^n \qquad \ldots (9)$$

where E is the measured output voltage, U the flow velocity with A,B, and n constants to be determined. The exponent n is assumed to be a constant in the velocity range considered.

The mean velocity, $\bar{U}$, is obtained once the hot wire has been calibrated by using equation

$$\bar{U} = \{(\bar{E}^2-A)/B\}^{1/n} \qquad \ldots (10)$$

where $\bar{E}$ is the measured mean output voltage.

By measuring the fluctuating component of the output voltage E, the turbulence intensity of the flow can be calculated. Consider that the measured voltage E is the sum of a mean voltage $\bar{E}$ and a fluctuating component whose rms value is e, and this corresponds to the flow velocity U which is also a sum of the mean $\bar{U}$ and a fluctuating quantity with rms value u. Thus

$$E = \bar{E}+e$$

$$\text{and } U = \bar{U}+u \qquad \ldots (11)$$

From equation (11) and assuming $(e/\bar{E})^2 << 1$ and $(u/\bar{U}) << 1$ it can be shown that the turbulence intensity u/U is given by

$$\frac{u}{\bar{U}} = \frac{2\bar{E}e}{n(\bar{E}^2-A)} \qquad \ldots (12)$$

3.5.3 Longitudinal correlation length

The longitudinal correlation length, L(x,u), was estimated from the normalized autocorrelation function measurements. The autocorrelation function, $R(\tau)$ for a time dependent function X(t) for which the fluctuation component X'(t) is such that $\overline{X'(t)} = 0$ is given by

$$R(\tau) = \frac{\overline{X'(t).X'(t+\tau)}}{\overline{X'(t)^2}} \qquad \ldots (13)$$

where τ is the time dealy from time t and the overbar represents the mean value. The normalized autocorrelation function, $\rho(\tau)$, is defined

$$\rho(\tau) = R(\tau)/R(0) \qquad \ldots (14)$$

The length scale in the streamwise direction, the longitudinal length scale, L(x,u) can then be estimated using the Taylor hypothesis of 'frozen' turbulence by the relationship

$$L(x,u) = \bar{U} \int_0^\infty \rho(\tau)d \qquad \ldots (15)$$

where $\bar{U}$ is the mean velocity in the x direction.

3.5.4 Lateral correlation length

The turbulence lateral length scale L(z,u), for the lateral displacement in the z direction and the velocity component U in the x direction was estimated from the relationship

$$L(z,u) = \int_0^\infty \rho_{AB} dz \qquad \ldots (16)$$

where ρ_{AB} is the correlation coefficient between the fluctuating velocity component at station A and station B a distance z apart; ρ_{AB} is defined as

$$\rho_{AB} = \frac{\overline{U'_A . U'_B}}{\sqrt{\overline{U'^2_A}}\ \sqrt{\overline{U'^2_B}}} \qquad \ldots (17)$$

with U' the fluctuating velocity component.

3.6 Grid flow calibration procedure

The properties measured in the flow behind the various grids were the following.

(i) Mean velocity profiles

(ii) Local turbulence intensity profiles

(iii) Longitudinal length scales L(x,u)

(iv) Lateral length scales L(z,u).

Except for the mean velocity profiles for the shear grids where a Pitot-static tube was used, all measurements were made using a hot wire. Mean velocity profile for shear grid SH1 was, however, also measured using a hot wire.

In the Blowdown tunnel at a distance 2.55m downstream of the grids and at about the model plane, velocity and turbulence intensity profiles were measured in the z direction for all flow conditions while in the y direction at about the tunnel centre line, velocity profiles were obtained for flow conditions GRO, GR1 and GR2.

Shear grid flows SH2 and SH3 were calibrated for velocity profiles in the z-direction, using a Pitot-static tube, at tunnel centre line and about 20mm ahead of the model position; the distance downstream of the grids being 860mm. All calibrations were done at tunnel centre line velocities in the range 12-15 ms^{-1}.

Autocorrelation measurements were made for grids GR1, GR2 and SH1 with the hot wire probe at tunnel centre and 2.55m downstream of the grids. The mean flow velocity was obtained with a Pitot-static tube positioned near the hot wire with the static holes in line with the hot wire. For grids GR1 and GR2 the time delay, τ, range was 0-30 msecs while for grid SH1, τ was in the range 0-10 msecs. The mean velocities at which the autocorrelations were obtained were (i) GR1 at 12.3 ms^{-1}, (ii) GR at 12.8 ms^{-1} and (iii) SH1 at 13.1 ms^{-1}.

No measurements were made for grids SH2 and SH3 in the No. 4 Closed Return Tunnel.

Spatial correlation measurements for spatial distance in z direction were made in the Blowdown tunnel for grids GR1, GR2 and SH1, using hot wires aligned to the y-axis at a distance 2.5m downstream of the grids and about 50mm to one side of the tunnel centre, $y/Y = 0.5$. The stationary reference wire was at position $z/Z = 0.5$. The flow velocities, measured using a Pitot-static tube, were (i) for GR1 $12ms^{-1}$, (ii) for GR2 $10ms^{-1}$ and (iii) for SH1 $14ms^{-1}$.

Again, no measurements were made for grids SH2 and SH3 in the No. 4 Closed Return Tunnel.

The results of the flow properties measured for the various grids are presented and discussed in Chapter 4.

3.7 Experimental procedure for surface mean pressure measurements

3.7.1 Manometers

Two manometers were used for mean pressure measurements and these were:

(i) A standard multitube manometer with alcohol as the working fluid and having graduation marks in steps of 0.2 inch which allowed readings to be made to within $\pm$ 0.05 inch.

(ii) A Furness micromanometer having a range $\pm$ 25mm of water with the output recorded using a digital voltmeter, a Schulumberger Time Domain Analyser JM 1860. Pressure

taps on the model were connected through a switch which enabled a sampling of one tap at a time.

The pressure taps from the 48mm and 114mm models were connected to the manometer using flexible tubes about 4.5m long while the reference Pitot-static tube had connecting tube lengths about 2.5m long. The 24mm model pressure taps had tubes about 2m long.

3.7.2 Circumferential and top surface pressures

Due to the physical size of the models, a compelte circumferential or top surface pressure tap distribution could not be provided and the following method was adopted for obtaining the complete pressure distributions. For a flow incidence α, the pressures at the available taps were recorded, the model then rotated through a right-angle and the pressures at the new tap positions measured. The model could be positioned to within $1/8^{th}{}^{o}$ of the required incidence. The sequence was repeated until the complete pressure distribution for the incidence had been obtained.

Circumferential mean surface pressures were measured on the 48mm model in a two-dimensional and three-dimensional configuration at various flow incidences. The model configurations and flow conditions for which the circumferential pressures were measured are given in TABLE 2.

The reference Pitot-static tube was at tunnel centre line z/Z = 0.5 about 4D from the model and about 6D from the tunnel wall and in the model plane.

Pressures on top surface of a three-dimensional model were taken on the 114 mm model in the Blowdown tunnel for model height, H, to width, D ratio of 3.3 and at flow incidence $\alpha = 0^{\circ}$ and 45° for flows GR0, GR1 and GR2. The reference Pitot-static tube was in the model plane and at the model top which was at the tunnel centre, about 3D from the model and about 5D from the tunnel wall.

3.7.3 Spanwise mean surface pressures

These pressures were measured on the 48mm model for the model spanning the tunnel and for the model height, H, to width D ratio in the range $2 \leq H/D \leq 11$ $\alpha = 0^{\circ}$ and 45° for flow conditions GR0, GR1, GR2 and SH1. For the model spanning the tunnel measurements were made both for the cases with and without end plates being present while for the finite cylinders the end plate at the roof, from where the model was suspended, was present. The reference Pitot-static tube was in the model plane at centre line z/Z = 0.5 and about 4D from the model and 6D from the tunnel wall.

Spanwise pressure distribution was also obtained for the 24mm model for flows SH2 and SH3 at $\alpha = 0^{\circ}$ by traversing the single set of pressure taps across the tunnel. The

Pitot-static tube was at tunnel centre-line $y/Y = 0.5$ about 2D ahead of the model and about 3D away from the model.

In TABLE 3 are given the model configurations and the flow conditions for which spanwise pressure distributions were measured.

3.7.4 Data reduction procedure for surface mean pressures

The measured surface mean pressure, P, was converted to coefficient of pressure, C_p, using the logitudinal (x direction) free stream velocity measured by a Pitot-static tube as the reference; C_p given by the relationship

$$C_p = \frac{P - P_{ref}}{\frac{1}{2}\rho U_{ref}^2} \qquad \ldots (18)$$

where P is the measured surface mean pressure

P_{ref} the reference static pressure

U_{ref} the reference velocity

ρ the density of air (= 1.23 kg/m^3).

3.8 Pressure transducer system

Two pressure transducers, DISA type 51f32 Low Pressure Transducer, were used for obtaining a measure of the fluctuating pressure. The transducer system comprised of the transducer connected through a DISA type 51E32 Oscillator to a DISA type 51E01 Reactance Converter, with the surface pressure tap connected to the transducer through a flexible tube of internal diameter 1.5 mm and length 0.5 m. The system was calibrated for frequency response in the following way. The transducer system was

connected to a pressure source so that a sudden pressure drop could be induced and the response of the system to the step input was recorded on a transient recorder. Assuming that during the transient the flow in the connecting tube is laminar and that the fluid and transducer behave in an elastic manner, the system can be shown to behave as an elastic system with single degree of freedom with the response given by equation

$$\frac{d^2P}{dt^2} + \beta \frac{dP}{dt} + kP = F(t) \qquad \ldots \quad (19)$$

where P is the pressure detected by the transducer, β is the damping coefficient, k is the stiffness factor, and F(t) is the forcing function.

FIGURE 8 shows the response of the transducer system to a step input and the corresponding frequency response calculated using equation 19.

3.9 Power spectral density analysis

3.9.1 Spectrum analyser

A Hewlett Packard model 3580A spectrum analyser was used for the pressure PSD analysis. The analyser model is a low frequency instrument optimized for use in the 5Hz to 50kHz range. The spectral analyser was operated to give 1Hz bandwidth resolution for a 50Hz frequency scan. During

operation it was found that the analyser had a frequency shift of about 1 Hz over a period of operation of about half hour. The analyser gives a trace output for the PSD sweep.

3.9.2 Experiemental procedure for PSD measurements

PSD measurements were made, along the span of the model, of the pressure fluctuations on the side face of the 48mm and 24mm models at $\alpha = 0^{o}$ for model flow configurations given in Table 4. As only two transducers were available, for each flow condition it was necessary to remove the 48mm model from the tunnel, position the transducers at new spanwise stations and reintroduce the model into the flow for further PSD measurements. For the 24mm model the PSD measurement technique was similar to that used for the spanwise pressure distribution (§3.7.3). The reference velocity was measured at the same position as for pressure measurements.

3.10 Spanwise pressure correlations

At $\alpha = 0^{o}$ on the 48mm model, pressure P_B on the side face B and pressure P_D on the side face D both at the same spanwise position were obtained using the transducer system (§3.9.1) and correlated using the DISA correlator (§3.4.2). The correlation coefficient R is defined

$$R = \frac{\overline{P'_B P'_D}}{\sqrt{(\overline{P'^2_B}\ \overline{P'^2_D})}} \qquad \ldots (20)$$

where P' is the fluctuating component (such that $P = \bar{P} + P'$) and the suffixes indicate the model face. R was measured in the flow conditions GR0, GR1, GR2, and SH1 for

(i) Model spanning the tunnel and with both end plates present for pressures at mid-span poisition.

(ii) Three-dimensional cylinders for H/D ratios 2,4,6-11 at various spanwise positions. Again the end plate at the base of the cylinder was present.

3.11 Flow visualization procedure

A mixture of Saturn Yellow powder paint and paraffin was spread as a thin layer on model surface where flow pattern was to be visualized. The flow in the tunnel was then started from rest and set to a constant velocity. After about 10 minutes when the paint particles had established the surface flow the tunnel flow was stopped and any excess paraffin allowed to evaporate. When the flow pattern had dried the model was removed from the tunnel and the pattern illuminated by an ultraviolet source was photographed.

Flow patterns were obtained for the top surface of 114mm model at H/D = 3.3 and at $\alpha = 0^{\circ}$ and 45° in smooth flow and a highly turbulent flow. Turbulence was introduced using grid GR2 and because of model mounting position for flow visualization in the Blowdown tunnel, the model was only about 5 grid mesh lengths downstream of the grid. No

measurements were made of the turbulence level in the flow.

3.12 Blockage corrections

MASKELL (1963) proposed that the blockage correction for bluff bodies may be looked at as a velocity increment. However, RANGA RAJU & SINGH (1975) have shown that blockage corrections cannot be looked at as a velocity increment. Ranga & Singh found that for flat plates of different blockage although the base pressure changes considerably with blockage ratio the pressure distribution on the upstream face of the plate is practically independent of blockage; if blockage corrections could be looked at as a velocity increment the pressure distribution on both faces ought to be affected by blockage. RANGA RAJU & GARDE (1970) suggested an equation for blockage correction of the form

$$C_{D_c} = C_D(1-H/D)^n \qquad \ldots \quad (21)$$

where C_{D_c} is the corrected drag coefficient

C_D the measured drag coefficient

H/D is the blockage ratio

and n a constant determined by experiment.

For square cylinders the value of n was found to be 1.18. Ranga & Singh suggest that equation (21) can be adapted for three-dimensional objects by replacing the ratio H/D by the ratio of the projected area of the body to the tunnel cross-section.

For the present study the blockage correction factors, calculated using the Ranga & Singh method, were 0.95 for the 48mm model spanning the blowdown tunnel and 0.93 for the 24mm model spanning the No. 4 Closed Return Tunnel. Consequently no blockage correction has been applied to the results of the present study.

CHAPTER 4

FLOW CHARACTERISTICS

Introduction

The longitudinal velocity and turbulence intensity profiles, the autocorrelation functions and the lateral spatial correlation measured in the two wind tunnels for the various flow conditions are presented and discussed in this chapter.

4.1 Velocity and Turbulence Intensity Profiles

Velocity profiles are presented with the local velocity, U, non-dimensionalized with the centre-line velocity , U_{ℓ} , and the distance from the wall normalized with the appropriate tunnel span length.

In FIGURE 9 the velocity profiles in the z and y direction for the turbulence grids and the no grid case are shown. For the z-direction velocity profile, the substantially non-uniform flow for grid GR3 is probably due to the different mesh distribution used. The mesh length, M, spacing between the first bar and tunnel wall would give, after reflection at the wall, an effective gap 2M thus producing an uneven blockage across the span. The first bar spacing for GR1 was 0.63M and for GR2, 0.5M; the slight increase in velocity at the wall for GR1 would then be due to the larger gap at the wall after 'reflection'. In the y direction, the gap between the first bar and tunnel wall

for GR1 and GR2 was 0.25M and 0.44M respectively. There was no velocity increment region for either of these grids; the velocity defect produced by the greater blockage was probably compensated for by the tunnel wall boundary layer. It would appear that to obtain a uniform velocity profile in the region away from the wall boundary layers, the square mesh type grid should have a half mesh length gap between the first bar and the tunnel wall.

By positioning end plates at appropriate distances from the tunnel wall a region of uniform flow could be obtained where the boudnary layer with its significant vorticity has been removed and, in this region, tests for uniform flow conditions could be carried out. End plates were placed 104mm from the roof (z/Z = .135) and 106mm from the floor (z/Z = .86) which gave uniform flow for GR0 and GR2 while eliminated most of the velocity increment region of GR1.

In FIGURE 10 the z direction velocity profiles for the three shear flow grids SH1, SH2 and SH3 are shown. For SH1 both the hot wire and Pitot-static tube measurements are presented. Away from the wall boundary layer region, SH1 had a profile which was mde up of two linear portions, the intersection region being at about the centre line. The gradients of the two portions is not too different and to an approximation the flow SH1 could be considered to be a linear shear flow. Grid SH2 had a linear profile away

from the wall boundary layer regions, $0.1 < z/Z < 0.8$; beyond $z/Z \simeq 0.8$ the velocity was almost uniform. Flow SH3 had a simple power law profile, at least square curve fit giving the relationship

$$\frac{U}{U_{\mathfrak{E}}} \simeq 1.1 \left(\frac{z}{Z}\right)^{1/6} \qquad \ldots \quad (22)$$

where U is the velocity at z,

$U_{\mathfrak{E}}$ is the centre line velocity

and Z is the tunnel width

This power law profile, with the exponent $\simeq 0.17$, corresponds to that found in the open country; urban areas having the exponent in the range 0.28 to 0.35. Isolated tall structures like cooling towers are perhaps the types of structures which would be in open country.

Turbulence intensity profiles for all grids in the Z direction are presented in FIGURE 11. The turbulence intensity is given as a percentage of the local velocity. Away from the boundary layer regions, the local turbulence intensity distributions are uniform for all grids; the approximate values in this region being 0.4% for grid GR0, 5.7% for grid GR1, 9.1% for grid GR2, 1.7% for grid SH1, 2% for grid SH2 and 1.7% for grid SH3. Turbulence intensity distributions for SH2 and SH3 have been obtained from STRADLING (1975). These values of turbulence intensities

are too low compared to the atmospheric turbulence intensity in urban areas where turbulence intensities are typically in the 10% - 30% range. To have tried to obtain high turbulence intensity in the tunnel would have resulted in non-uniform flow and it was important to consider the turbulence and flow non-uniformity in isolation.

It was felt that the 0.4% to 9.1% turbulence intensity range available would be sufficient to indicate the possible effects of turbulence on the behaviour of the flow around the cylinders.

The turbulence properties of the flows measured in the two tunnels are summarized in TABLE 5.

4.2 Correlation Measurements

The auto correlation and the spatial correlation distributions for three grids, GR1, GR2 and SH1 are presented in FIGURE 12. The normalized auto correlation coefficient is plotted against a non-dimensionalized time delay parameter, $U\tau/L(x,u)$, where U is the mean velocity, τ the time delay and L(x,u) the estimated longitudinal length scale. The spatial correlation coefficient is plotted against spatial distance z normalized with the lateral length scale L(z,u).

The collapse of the data onto a single curve for all the grids for both correlation functions suggests that the turbulent eddy characteristics are similar for all flow cases and that at distances sufficiently downstream of the grids the particular grid type, square mesh-flat bar type or circular rod type, is not significant in determining the turbulence characteristics. The ratio L(z,u)/L(x,u) for the grids was found to be 0.44 for grid GR1, 0.51 for grid GR2 and 0.53 for grid SH1.

In TABLE 5 are given the various turbulence length scales estimated from the correlation measurements for flows GR1, GR2 and SH1.

4.3 Summary

The flow properties measured in the two wind tunnels are summarized in TABLE 5.

CHAPTER 5

TWO DIMENSIONAL MODEL IN UNIFORM FLOWS

Introduction

Mean pressure distributions, Strouhal numbers and correlation coefficients of the pressure fluctuations on the model were obtained for the 48mm model, to investigate the effect of flow incidence and turbulence. The results are compared with those published and where possible the results are presented in the same form as the published results.

5.1 Spanwise Surface Mean Pressures

STANSBY (1974) has reported that when a circular cylinder spans a wind tunnel, the tunnel wall boundary layers have a significant effect on the pressure in the base region. From experiements to investigate the effect of removing the wall boundary layers by using end plates, Stansby found that the addition of end plates caused a substantial reduction of base pressure and hence an increase in drag which suggests, as Stansby says, that the results for drag and pressure distributions on circular cylinders obtained without end plates are not representative of two-dimensional flow.

The effects of flow non-uniformities on the mean forces on a two-dimensional square cylinder have been studied by

LEE (1975b) and the results showed that for a model with a face normal to the flow, axial flow non-uniformtiy is responsible for an axial variation of the mean drag coefficient, whether based on local axial dynamic head or any constant dynamic head value, the reason being that the pressures on the front face respond directly to the incident dynamic head profile whilst the base pressures have a constant axial value. Lee also found that end plates had no effect on either limiting the region of end effects on the body or in preventing the axial variation of mean drag on the body for non-uniform flow. The region of end effects was found to be confined to an axial length corresponding approximately to the physical thickness of the upstream wall boundary layer.

Lee argued that the wall boundary layer effect observed by Stansby was because of the late flow separation on the circular cylinder in the boundary layer regions where the turbulence is higher. The later flow separation in the boundary layer would cause a variation in the spanwise base pressure and this is shown when end plates are not present on a circular cylinder. For the square cylinder however, the separation points are fixed and there is found no spanwise effect of the boundary layer, the rise in base pressure would then solely be due to the higher turbulence intensity in the wall boundary layer.

For the present study, the effect of end plates on the spanwise base pressures on the 48 mm model at $\alpha = 0^{o}$ for flows with turbulence intensities 0.4%, 5.7% and 9.1% is shown in FIGURE 13. The end plates only remove the boundary layer affected regions except in smooth flow , 0.4% turbulence intensity, where end plates reduce the base pressure. This could be because of the rather large wall boundary layer ($\simeq$ 100 mm) present in the tunnel giving rise to thick horseshoe vortices, at the ends of the cylinder, which would affect the base region flow. The horseshoe vortices induce a flow into the base region, introducing a kind of base bleed which would lead to an increase in the base pressure (MAULL & YOUNG, 1972).

It would appear that the effect of end plates on square cylinders is to only remove the wall boundary layer affected regions. For smooth flow however, wall boundary layers 10% of the model span and larger, seem to have the effect of increasing the base pressure and end plates should be present for these flow conditions. Thus provided the wall boundary layer is less than 10% of the model span, a square cylinder spanning a wind tunnel could be considered to be two dimensional in the region away from the wall boundary layer region.

In FIGURE 14 are presented the spanwise mean C_p on the 48 mm model at $\alpha = 0^{o}$ and 45^{o} for the model with end plates and in uniform flows. Suffix f refers to the front and windward faces while suffix b refers to the rear

and leeward faces. Positive C_{p_f} at $\alpha = 45^{\circ}$ indicates that the flow is attached over the windward face while at $\alpha = 0^{\circ}$ C_{p_f} follows the dynamic head. At $\alpha = 0^{\circ}$ C_{p_b} increases with increasing turbulence intensity. C_{p_b} being - 1.33 in smooth flow , 0.4% intensity, - 1.16 in 5.7% turbulence intensity flow, and -0.99 in 9.1% turbulence intensity flow. At $\alpha = 45^{\circ}$, however, C_{p_b} does not show much variation with turbulence, C_{p_b} being about - 1.2. The increase in C_{p_b} with turbulence at $\alpha = 0^{\circ}$ indicates that with increasing turbulence the vortices are formed further away from the rear of the model (BEARMAN, 1972), while at $\alpha = 45^{\circ}$ it would seem that the vortices form at about the same distance downstream of the model irrespective of the flow turbulence intensity. It may

5.2 Circumferential surface mean pressures

The mean C_p around the 48 mm model spanning the tunnel without end plates for flow incidence α, range $0^{\circ} \leq \alpha \leq 45^{\circ}$ for smooth flow GR0, and flows GR1 and GR2 with turbulence intensities 5.7% and 9 1% respectively are presented in FIGURES 15 - 23 inclusive. FIGURES 24 and 25 show the distribution at $\alpha = 0^{\circ}$ and 45° respectively for the model with end plates in the three uniform flow conditions and shear flow SH1. In smooth flow GR0 , the slight decrease in

C_P at the centre of Face C is more pronounced for the model with end plates. The large wall boundary layer (§4.1) causes some inflow into the base region resulting from the horseshoe vortices - the inflow increasing the pressure (§2.2). Shear flow SH1 results are reduced to C_P using the local velocity and the distribution is very similar to the smooth flow case. Increasing turbulence shows an increased base pressure (Face C) where the distribution has become uniform; on the side faces there is an increased pressure recovery region towards the rear of the side faces.

By integrating the mean C_P distributions mean drag coefficient, C_D, and mean lift coefficient C_L, were obtained at the various flow incidences; the results are presented in FIGURE 26, with the forces reduced to coefficient form using the cylinder width, D, as the reference length.

As α is increased C_D falls to a minimum at α_R and then increases with α. C_L decreases with α to a minimum at α_R and then increases with increasing α. At large values of α, $\alpha > 20^\circ$, C_L is small, of the order 0.1 and changes sign, once for smooth flow and twice for turbulent flows. The value of α_R decreases with increasing turbulence intensity; the α_R values being $12\frac{1}{2}^\circ$ for smooth flow, 11° for 5.7% turbulence intensity and 9° for 9.1% turbulence intensity. At $\alpha > \alpha_R$ the reverse is the case.

Following the results on the scale length effect on the mean forces on square cylinder published by LEE (1976) (§2.3) the results for the present study were plotted on to Lee's and FIGURE 27 shows the variation of C_{P_b} at $\alpha = 0^{\circ}$ with turbulence length scale parameter L(x,u)/D where D is the model width. C_{P_b} has been corrected using Maskell's blockage correction which is a velocity increment method and similar to that used by Lee. The values of L(x,u) have been obtained by using the results of BAINES (1949) for grid flows since Lee's values have also been obtained from the same source. The relationship used by Lee to convert the lateral length scale L(z, u), measured by Baines, to L(x, u) was

$$L(x, u) = 2.5L\ (z, u) \qquad \ldots \quad (23)$$

The results are in good agreement with Lee but since sufficient fresh data points are not available it is difficult to give any conclusive evidence on the scale length effect on the mean forces on square cylinders.

5.3 Strouhal Number and Correlation Coefficient

Pressure PSD measurements on the side face of the 48mm model at $\alpha = 0^{\circ}$, with end plates present, in uniform flows showed that there was a definite peak for all span-wise positions with the Strouhal Number S (= nD/U) constant along the span but S decreased with increasing turbulence.

Correlation coefficient, ρ , at mid-span position between pressures on opposite side faces for 48mm model at $\alpha = 0^{o}$ and with end plates present was found to be large and negative suggesting a definite periodicity. The table below gives the values of S and ρ in uniform flows.

Flow	L(x,u)/D	L(x,u)/D	TURB %	Strouhal Number S	Correlation Coefficient ρ
GR0	SMOOTH	FLOW	0.4	0.126	-0.86
GR1	1.31	0.58	5.7	0.123	-0.82
GR2	1.75	0.88	9.1	0.119	-0.64

The decrease in the correlation coefficient with increasing turbulence may be explained as follows. The correlation coefficient, ρ , between pressures P_1 and P_2, say, is given by:

$$\rho = \frac{\overline{P_1' P_2'}}{\sqrt{(\overline{P_1'^2}\ \overline{P_2'^2})}} \qquad \ldots \quad (24)$$

where P_i' is the fluctuating component of P_i.

If P_i' is now considered to be a sum of a vortex shedding component P_{si}' say, and a component due to turbulence P_{Ti}' so that

$$P_i' = P_{si}' + P_{Ti}' \qquad \ldots \quad (25)$$

then

$$\rho = \frac{(P'_{S1} + P'_{T1})\ (P'_{S2} + P'_{T2})}{\sqrt{(P'_{S1} + P'_{T1})^2}\ \sqrt{(P'_{S2} + P'_{T2})^2}} \qquad \ldots (26)$$

Assuming that the RMS fluctuating components at the two side faces are equal for the model at $= 0^{o}$ so that:

$$\overline{(P'^{2}_{S1})} = \overline{(P'^{2}_{S2})} = \overline{(P'^{2}_{S})} ;$$

$$\overline{(P'^{2}_{T1})} = \overline{(P'^{2}_{T2})} = \overline{(P'^{2}_{T})} ;$$

$$\overline{(P'^{2}_{1})} = \overline{(P'^{2}_{2})} = \overline{(P'^{2})} \qquad \ldots (27)$$

and that the cross product terms are zero

$$\overline{(P'_{si}\ P'_{T1})} = 0 \qquad \ldots (28)$$

the correlation coefficient, ρ , can then be expressed as

$$\rho = K_s \rho_s + K_T \rho_T \qquad \ldots (29)$$

a sum of the vortex shedding component and a turbulence component where:

$$\rho_s = \frac{\overline{P'_{s1}\ P'_{s2}}}{\overline{P'^2_s}} \quad ,$$

$$K_s = \left\{ 1 + \frac{\overline{P'^2_T}}{\overline{P'^2_s}} \right\}^{-1} \quad ,$$

$$\rho_T = \frac{\overline{P'_{T1}\ P'_{T2}}}{\overline{P'^2_T}} \quad ,$$

$$K_T = \left\{ 1 + \frac{P'^2_s}{\overline{P'^2_T}} \right\}^{-1} \qquad \ldots (30)$$

For purely periodic shedding and with no turbulence being present $\rho = -1$.

Thus the realtive negativeity of ρ would indicate the vortex shedding strength and the vortex shedding dominance of the flow around the cylinder. Since the effect of turbulence is to mix the flow, increased turbulence would disrupt the vortex shedding and make ρ more positive.

The product $C_D.S$ was plotted against base pressure function $k = (1-C_{p_b})^{\frac{1}{2}}$ for the 48mm model at $\alpha = 0^\circ$ and is shown in FIGURE 28. As found by BEARMAN (1967) and LEE (1976a)

there is a good correlation suggesting that the Bearman bluff body wake model (§ 2.1) is a good representation of the wake flow for two dimensional bluff bodies.

5.4 Summary

As found by other workers, the flow around a two dimensional square cylinder is affected by (i) the flow incidence and (ii) the level of turbulence intensity. The reulsts in the present study support the flow patterns that have been suggested by MULHEARN (1973) and LEE (1975) (§ 2.3). It has not been possible to conclude on the effect of length scale observed by McLAREN et al (1969) and by LEE (1976).

The effect of end plates is to remove the wall boundary layer affected regions. In smooth flow it seems that provided the boundary layer region is less than 10% of the model span, the results obtained away from the wall boundary layer affected regions can be considered to be representative of two dimenstional flows. However, for wall boundary layers greater than 10% of the model span, end plates should be present to give a representation of two dimensional flow conditions. For turbulent flows it appears that two dimensional flow conditions are simulated away from the wall boundary layer affected regions.

The universal Strouhal Number suggested by BEARMAN (1967) and the corresponding wake model is a good representation of two dimensional bluff body flow.

CHAPTER 6

THREE DIMENSIONAL SQUARE CYLINDERS IN UNIFORM SMOOTH AND TURBULENT FLOWS

Introduction

Surface mean pressures, pressure power spectral density, pressure correlations and flow visualization results for three dimensional square cylinders in uniform flows, with various turbulence levels, are presented and discussed in this chapter. The cylinder aspect ratio, taken to be the cylinder height, H, to width, D, ratio, H/D, varied in the range $2 \leq H/D \leq 11$.

Only two incidences have been considered, namely, $\alpha = 0^{o}$ and $\alpha = 45^{o}$. Initially it was hoped to also consider an intermediate angle, but as the experimental programme proceeded, it became apparent that if intermediate angles were to be tested for, a range of values, $0 < \alpha < 16$, would have to be considered in order to develop a picture of the flow around the model at intermediate angles. This however, would have made the experiemental programme much too long and consequently it was decided against testing for intermediate angles.

6.1 Top Surface Mean Pressures and Flow Visualizations

Top surface mean pressures were taken on the 114mm model for a height to width ration H/D = 3.3 and for $\alpha = 0^{o}$ and $\alpha = 45^{o}$ in uniform smooth flow (GR0) and uniform turbulent flows with turbulence intensities 5.7% and 9.1%. Flow visualization patterns were obtained on the top

surface and on the 'ground plate' leeward of the model, for the model in a smooth flow and a highly turbulent flow, with H/D = 3.3 and at $\alpha = 0^{o}$ and $\alpha = 45^{o}$. The results are presented and discussed in this section.

FIGURE 29 shows the mean C_p distribution on the top surface of the 114mm model at $\alpha = 0^{o}$ for the three flow conditions. In smooth flow (GR0) C_p is uniform over the surface while a pressure recovery occurs towards the rear of the top surface in turbulent flows in a manner similar to that on the side face of a two-dimensional model at $\alpha = 0^{o}$(§ 5.2). It would appear that turbulence entrains more fluid into the separating shear layers which thicken more rapidly and appraoch the body towards the rear, leading to a pressure recovery. As turbulence increases there is an increased suction at the side edges.

For the model at $\alpha = 0^{o}$ in smooth flow, PLATE 1 shows the top surface flow and FIGURE 30 the streamline pattern over the free end. As expected from the pressure distribution (Figure 29), the flow separates from the leading edge and does not reattach on the surface; a reverse flow being present in the separated flow region.

The top surface flow and the streamline pattern over the free end for the model at $\alpha = 0^{o}$ in a highly turbulent flow are shown in PLATE 2 and FIGURE 31 respectively. In this case the flow separates from the leading edge and reattaches

near the trailing edge setting up a separation bubble. A recirculating flow is set up in the bubble giving a secondary separation towards the font edge. The fluid between the leading edge and the secondary separation line is drawn out towards the sides probably due to the suction at the side edges and this would also account for the outward flow at the sides.

FIGURE 32 shows the mean C_p distributions on the top surface of the model at $\alpha = 45^{\circ}$ for flows with turbulence intensities 0.4% (smooth flow), 5.7% and 9.1%. It is found that increased turbulence increases the suction over the surface and produces a larger region of fairly uniform pressure over the trailing edge triangle. The flow visualization pattern obtained in smooth flow is shown in PLATE 3 and that in a highly turbulent flow in PLATE 4. FIGURE 33 shows the top surface flow pattern for the model at $\alpha = 45^{\circ}$. The top surface flow at $\alpha = 45^{\circ}$ is similar to that over a delta wing with the vortices forming at the leading corner and lifting off the surface. The conical vortex forms a secondary separation line near the windward edge and it is probably the high suction below the vortex that draws the fluid from the windward edge towards the secondary separation line.

Standing vortices at the 'ground' are closer to each other in smooth flow and the vortices are further from the model in turbulent flow unlike the $\alpha = 0^{\circ}$ case. At $\alpha = 45^{\circ}$ the base bleed depends on the strength of the conical vortices

and since these are stronger in turbulent flow the 'ground' vortices would move further away from the model.

6.2 Spanwise Surface Mean Pressure Distributions

FIGURE 34 shows the spanwise mean C_p distribution of the 48mm model at $\alpha = 0^o$ for the front and rear faces for the cylinder range $2 \leq H/D \leq 11$ in smooth flow GR0, 5.7% turbulence intensity flow GR1 and 9.1% turbulence intensity flow GR2. The spanwise distance, z ,is non-dimensionalized with the model height H. The rear face C_p was also plotted against z non-dimensionalized with model width, D, for the three flows and FIGURE 35 shows the distribution for H/D = 2 - 6 and FIGURE 36 for $7 \leq H/D \leq 11$.

The centre of the front face is at stagnation pressure except near the free end where the flow accelerates over the surface towards the free end. Higher suction on the top surface caused by the separating flow, would also tend to accelerate the flow towards the free end.

Pressures on the rear face are more indicative of the flow around the cylinder and of the variations introduced by changing H/D. The spanwise pressure distribution shows that there are two regions (i) a free end region where C_p decreases towards the free end and (ii) a root region, from the root of the cylinder to the beginning of the free end region, where C_p is more or less uniform. Over the range

of H/D considered, there appear to be three regimes depending on the cylinder H/D for each flow condition. At low H/D ratios say, H/D $<(H/D)_L$, C_p decreases from the root to the tip in a manner similar to that in the free end region for high H/D ratio cylinders, H/D $>(H/D)_L$, and no separate root region is apparent. The magnitude of the pressures are however, not as low as those found for the free end region for H/D $>(H/D)_L$. In fact for this regime C_p valves are the highest.

For cylinders with H/D $>(H/D)_L$ a definite root region and a free end region can be observed and two H/D regimes can be identified. For both the regimes the root region C_p is constant with z/D . For the range $(H/D)_L < H/D < (H/D)^*$ say, the middle H/D regime, the magnitude of the root region C_p is about the same for all cylinders in this regime while for H/D $>(H/D)^*$, the high H/D regime, C_p in the root region decreased with increasing H/D. Towards the end of the root region there is a slight increase in C_p before C_p again starts decreasing in the free end region. This type of C_p distribution could be taken as typical of high H/D regime. FIGURE 37 shows a schematic represenatation of the variation of the spanwise rear face C_p with H/D - the three regimes being (i) Low H/D regime where H/D $< (H/D)_L$, (ii) middle H/D regime with $(H/D)_L < H/D < (H/D)^*$ and (iii) high H/D regime where H/D $> (H/D)^*$.

In the high H/D regime, as H/D increases from (H/D)*, the root region C_p becomes more negative and tends towards C_{pb} value for two dimensional models. It could be that in the high H/D regime, the top surface flow into the leeward area can extend downwards to only a certain degree before turning again towards the free end. This low point would form a boundary beyond which the free end region flow would have diminishing effect as H/D increases. As H/D increased, the root region length increases and C_p approaches two-dimensional value. In smooth flow however, for H/D = 11 the root region C_p(= -0.9) is significantly higher than C_{pb}(= -1.33). This may be because in smooth flow there is no top surface reattachment and a large 'base bleed' is introduced. H/D greater than 11 may possibly give root region C_p approaching smooth flow C_{pb}.

The rear face C_p distribution in all uniform flow conditions shows that C_p decreases with increasing H/D. Since the front face C_p is constant over most of the span the drag on the cylinders would also increase as H/D increases. Results of Joubert et al (1962) (§2.5) show a similar tendancy of the drag force for the cylinders in the range $1 < H/D < 4$.

SHARAN (1977) had found that increasing turbulence intensity caused the rear face C_p to increase. Present results show that in turbulent flows increasing turbulence increases the base region C_p for the high H/D regime while for other cylinders it is difficult to determine the effect of turbulence

on the base region C_p. In smooth flow, root region C_p values for all cylinders are higher than those found for turbulent flows. Again this could be due to the increased inflow into the leeward region in smooth flow as there is no flow reattachment on the top surface.

For the free end region in the high H/D regime, C_p increases with increasing turbulence but for other regimes, C_p increases with turbulence only in turbulent flow cases; C_p in smooth flow being higher than that in turbulent flows.

SHARAN only considered non-smooth flows and his conclusion that increasing turbulence intensity caused the rear face C_p to increase appears to be true only for non-smooth flow conditions.

In smooth flow the lower C_p in the free end region, for the high H/D regime, may be because there is no flow reattachment on the top surface and the flow comes down the leeward face nearer the rear surface whereas in turbulent flow the reattachment on the top surface (or the shear layer deflection by the top surface) would cause the flow to come down a distance away from the rear surface giving a higher C_p than that in smooth flow. The slight increase in C_p towards the free end in the high H/D regime (FIGURE 37) may be an indication of the downward flow from the top surface turning towards the rear face and returning upward to the free end with a kind of circulation bubble set up in the

free end region. FIGURE 38 shows the flow pattern over finite cylinders in smooth and turbulent flows.

FIGURE 39 shows the C_p distribution on the windward and leeward faces for cylinder range $2 \leq H/D \leq 11$ at $\alpha = 45^{\circ}$ for smooth flow (GR0), 5.7% turbulence intensity flow (GR1) and 9.1% turbulence intensity flow (GR2).

On the windward face, C_p distribution is similar to that for $\alpha = 0^{\circ}$; the strong tip vortex (§ 6.1) drawing the fluid towards the free end. Positive C_p indicates that the flow is attached over the face at least up to the mid face position.

On the leeward face C_p decreases towards the free end until there is a slight pressure recovery near the free end; the recovery becoming more pronounced as H/D increases. This pressure recovery may be due to a reversed flow induced onto the leeward face by the trailing top surface 'delta wing' vortex. As H/D increases there is a greater suction in the free end region indicating that the strength of the top surface vortex also increases with these changes.

The general flow characteristics at $\alpha = 45^{\circ}$ do not show any significant difference from the $\alpha = 0^{\circ}$ case.

$(H/D)_L$ tends to decrease from a value between 5 and 6 in

smooth flow (GR0) to a value between 4 and 5 in turbulent flow GR1, 5.7% turbulence intensity to around 4 in 9.1% turbulence intensity flow GR2. Likewise (H/D)* also decreases with increasing turbulence. (H/D)* in smooth flow is found to be between 9 and 10 while in 5.7% turbulence intensity flow GR1 (H/D)* is between 6 and 7. As turbulence in the flow increases, the boundaries between the various H/D regimes become difficult to define and it is difficult to determine the (H/D)* value for flow GR2, 9.1% turbulence intensity.

The decrease in $(H/D)_L$ with turbulence may be realted to the reattachment or deflection of the top surface flow. The extent the top surface flow travels down the leeward side decreases as the top surface flow is deflected by or reattaches on the top surface. It may be possible that once a turbulence condition is reached when the top surface flow reattaches on the surface, further increase in turbulence would not alter $(H/D)_L$. It would be interesting to find the response in flow with turbulence intensity higher than 9.1%.

The decrease in (H/D)* with turbulence is probably related to the $(H/D)_L$ value. If a critical length of base region must exist for the cylinder to be in the high H/D regime then this condition would be satisfied at a lower cylinder H/D for the condition where $(H/D)_L$ is smaller, hence the decrease in (H/D)* with decreasing $(H/D)_L$.

6.3 Spanwise Pressure Power Spectral Density

Results presented and discussed in this section are the spanwise pressure Power Spectral Density (P S D) measurements on the 48mm model at $\alpha = 0^{o}$ for pressures on a side face for smooth flow (GR0) and flow with turbulence intensities 5.7% (GR1) and 9.1% (GR2). PSD is plotted on an arbitrary scale against a reduced frequency parameter nD/U, where n is the frequency, D (=48mm) is the model width and U is the reference free stream velocity.

FIGURE 44 shows the PSD distributions for H/D = 11 and 10 and FIGURE 45 for H/D = 9 and 8 for the model in smooth flow GR0.

For H/D = 11, 10 and 9 two peaks are found at reduced frequency S_1 in the base region and S_2 in the free end region with S_1 being greater than S_2. At certain spanwise positions two peaks appear, their relative size depending upon the spanwise position. The spectral peak is narrow in the lower root region becoming broader towards the free end. The size of the peak also decreases towards the free end. At H/D = 8 a broad band spectral peak is found in the base region with no peak being detected towards the free end. It was also found that for $H/D \leq 7$ no spectral peak could be detected at any spanwise position.

In turbulent flows GR1, 5.7% turbulence intensity and GR2 9.1% turbulence intensity, PSD distributions were obtained

for H/D = 2,4,6,7,8,9,10 and 11. The results are present in FIGURES 46 - 49 for flow GR1 and in FIGURES 50 - 53 for flow GR2.

In flow GR1, 5.7% turbulence intensity, S_1 and S_2 are found for H/D = 11 - 6 and as in smooth flow S decreases with decreasing H/D with S_1 tending towards S_2. Twin peaks for certain spanwise positions are found for 9 H/D 11. The spectral peaks become broad and decrease in size towards the free end and with decreasing H/D. At H/D = 11, however, the peak at z/H = 0.08 is smaller than at z/H = 0.18 which could be due to the interference from the floor. Unlike smooth flow, all cylinders show a spectral peak for the spanwise positions tested.

PSD distributions obtained in flow GR2, 9.1% turbulence intensity (FIGURES 50 - 53) show a pattern similar to that found in flow GR1 and GR0. The spectral peaks are not as large as found in flow GR1 and GR0 and the peaks are also braoader. ΔS does not decrease as rapidly as in the other flows. At no spanwise station however, were twin peaks observed for any cylinder.

It would seem that for the H/D range where a free end peak occurs the flow from over the top surface does not quite reach the 'ground' but turns towards the rear face before reaching the 'ground' and is then drawn upwards towards the low pressure region of the free end. The eddy

thus formed would subsequentlv be 'shed' downstream at the free end region frequency S_2. The base region frequency S_1 probably corresponds to eddies shed in this region from the sides of the cylinder.

In the H/D range where both S_1 and S_2 are observed, the difference ΔS between S_1 and S_2 becomes smaller, with S_1 tending towards S_2 as H/D decreases. It could be that the free end eddy is much stronger than the base region eddy and where H/D is not large the free end eddy disrupts the base region flow as it now reaches the 'ground' and can not form the free end eddy of the higher H/D cylinders. This could be the reason for not finding s spectral peak in the free end region for H/D = 8 in smooth flow. The top surface flow never now returns up to the free end to form the eddy to be shed.

It seems that the extent of the free end region, length ℓ_F, depends on the degree of turbulence and the cylinder H/D ratio. It appears that in the high H/D regime ℓ_F is constant for atleast turbulent flows. There might be a correspondence between the free end region length ℓ_F and the Low H/D regime limit $(H/D)_L$ - the Low H/D regime really being the free end region with no base region.

In turbulent flows a spectral peak is observed for all cylinders while in smooth flow only for H/D >7 is there a spectral peak found. This again indicates that as with the spanwise mean pressures, (§6.2) smooth flow results do not quite give the flow pattern to be expected in full size conditions.

6.4 Spanwise Pressure Correlations

Correlation coefficients for pressures on opposite side faces on the 48mm model at $\alpha = 0^{\circ}$ were measured at various spanwise positions for smooth flow (GR0), 5.7% turbulence intensity flow (GR1) and flow GR2 having 9.1% turbulence intensity; the results are presented in FIGURE 54 a,b,c respectively. The correlation coefficient, R, is plotted against spanwise distance z, non-dimensionalized with model width D(=48mm) for H/D = 8 - 11 for flow GR0 and H/D = 2,4 and 6 - 11 for flows GR1 and GR2.

In all flow conditions and for all H/D the pressure correlation coefficient, R, becomes more positive with distance towards the free end with a sharp increase in the free end region. As with the mean pressure distribution (§ 6.2) the correlation coefficient distribution can also be divided into a free end region and a base region. In the base region, as H/D increases, R, becomes more negative and in the lower base region, R, tends towards the two dimensional value for the corresponding flow condition (§ 5.3).

The correlation coefficinet, R, on three dimensional cylinders may be considered to be composed of fluctuating components such that the fluctuating pressure, P_i, now has an additional term corresponding to the free end effect so that $P_i = P_{si} + P_{Ti} + P_{Fi}$ ... (30)

where P_{si} is the vortex shedding component

P_{Ti} is the turbulence componts

P_{Fi} is the free end effect component.

The correlation coefficient, R, can then be expressed as the sum of the vortex shedding, turbulence and free end components so then $R = k_s R_s + k_T R_T + k_F R_F$ ... (31)

where k_i is a constant to be determined and

R_i is the correlation component.

Since the effect of the free end is to introduce a tip vortex and hence, intorduce further turbulence, it may be assumed that the free end term $k_F R_F$ varries in the same manner as the turbulence term $k_T R_T$ and be always positive, making R more positive. The vortex shedding term $k_s R_s$, depends on the vortex shedding strength which decreases with distance towards the free end and with decreasing cylinder H/D (§6.3). For three dimensional cylinders then, the correlation coefficient would tend to be more positive than that found for two dimensional model in the same flow conditions.

Considering the power spectral density distributions (§6.3) and the correlation coefficient distributions on the cylinders it appears that where the free end eddy has affected the cylinder flow to a large extent, R, is generally more positive. At H/D = 8 in smooth flow where no base shedding frequency was found, R, over the entire span is positive suggesting that the flow is almost completely dominated by the free end effect. Thus it appears that for three dimensional cylinders the more positive the value of R from the corresponding two dimensional configuration value, the greater is the influence of the presence of the free end.

6.5 Summary

The flow around a three dimensional square cylinder in uniform smooth and turbulent flows exhibits a free end region and a base region for finite cylinders in the range $2 \leq H/D \leq 11$. Three regimes are found to exist, these being

i) Low H/D regime $\quad H/D < (H/D)_L$

ii) Middle H/D regime $\quad (H/D)_L < H/D < (H/D)^*$

iii) High H/D regime $\quad H/D > (H/D)^*$

In turbulent flows it appears that the length, ℓ_F, of the free end region, in the high H/D regime, decreases with increasing turbulence. It was not possible to determine ℓ_F from the limited test data available.

For a cylinder, provided the flow is turbulent, increasing turbulence casuses a decrease in the drag while for a

particular uniform flow condition increasing the cylinder H/D ratio causes the cylinder drag to increase. The effect of decreasing drag on the cylinder with increasing turbulence is only found for turbulent flows - smooth flow drag being lower than that in turbulent flows.

The flow over the free end moves downward into the leeward region introducing a kind of 'base bleed'. If the cylinder is tall enough, high H/D regime, this top surface flow does not reach the ground and moves in towards the cylinder and consequently up to the free end. This sets up an eddy which is 'shed' at a reduced frequency S_2. The base region sheds vortices, formed from the shear layers from the separating flow at the cylinder sides, at a reduced frequency S_1. As H/D gets smaller the free end eddy envelopes a greater portion of the cylinder and eventually reaching up to the ground and completly disrupting the base region vortices. When H/D increases, S_1, tends to the two dimensional vortex sheddding reduced frequency. In all cases S_1 is greater than S_2.

The relative effect of the free end on the flow around the finite cylinder compared to the flow around a two dimensional configuration seems to be indicated by a more positive value of the pressure correlation coefficient for pressures on the side faces.

CHAPTER 7

SQUARE CYLINDER IN SHEAR FLOWS

Introduction

To investigate the effect of shear on the flow around a square cylinder mean pressures, pressure power spectral density and pressure correlation measurements were made on square cylinder models in two configurations, and the results are presented and discussed in two sections. The two configurations considered were as follows:

(i) Model without a free end

(ii) Finite model with a free end.

7.1 Square Cylinder Without a Free End in Shear Flows

In this section, results for spanwise mean C_p, Power Spectral Density and Strouhal number measured on the 48mm and 24mm models are presented and discussed.

To determine the effect of the tunnel boundary layer on the pressure distribution along the span of the model, in a shear flow, spanwise pressures were measured on the 48mm model at $\alpha = 0^{\circ}$ in shear flow SH1 both with and without the end plates and FIGURE 55 shows C_p based on tunnel centre-line velocity, $U_{\mathbb{C}}$, on the front face, C_{p_f}, and rear face, C_{p_b}.

C_{P_f} follows the dynamic head in the tunnel and the end plates remove the tunnel boundary layer region. C_{P_b} shows that the end plate decreases the pressure in the low velocity end. However, in both cases, C_{P_b} decreases away from the low velocity end until there is some recovery at the top end where the effect of the end plate is not very significant.

FIGURE 56 shows spanwise C_P in shear flow SH1 with end plates on the 48mm model at $\alpha = 0^\circ$ and 45° and on 24mm model at $\alpha = 0^\circ$ in shear flows SH2 and SH3. C_{P_f} and C_{P_b} are based on U_t while $C_{P_{b\ell}}$ is C_P on the rear/leeward face based on the local velocity.

C_{P_f}, in all flows, follows the dynamic head in the tunnel. C_{P_f} in flow SH1 for $\alpha = 45^\circ$ being lower than flow $\alpha = 0^\circ$ because at $\alpha = 45^\circ$ the pressure taps are no longer along the stagnation pressure line.

C_{P_b}, at $\alpha = 0^\circ$, decreases along the span, in going from the low velocity end to the high velocity region, until there is some pressure recovery near the top velocity end. C_{P_b} is constant in the lower half of the model and then increases slightly along the span.

In flow SH1 at $\alpha = 0^\circ C_{P_b}$ is constant up to $z/H \simeq .4$ after which it decreases slightly before increasing towards the high velocity end. However, at $\alpha = 45^\circ$ $C_{P_{b\ell}}$ increases from the low velocity end to the high velocity end with

the slope greater for $z/H > .6$. $C_{P_{b\ell}}$ in flow SH2 is almost constant in the range $0.1 < z/H < 0.7$ beyond which it increases. In the lowest region of the cylinder, C_{P_b} although being constant is less than that for the rest of the span. Flow SH3 shows that for $z/H > .2$ there is a very small decrease at $z/H \simeq 0.5$ with $C_{P_{b\ell}}$ increasing at either side. In the region below $z/H \simeq .2$ $C_{P_{b\ell}}$ increases along the span as the velocity increases.

The flow model proposed by MAULL and YOUNG (1972) attempts to explain the pressure distributions obtained on models without a free end and in a shear flow. It is argued that the vorticity in the shear flow and in the tunnel boundary layer induce velocities along the span of the model. This introduces a type of "base bleed" into the model-floor region and this increases the pressure in these areas. Since the boundary layer vorticity aguments the vorticity in the low velocity end of the shear flow, the "base bleed" is higher and consequently C_{P_b} is higher than that found at the high velocity end. Away from the end regions the induced velocity is almost constant with a consequent very little "base bleed" and the base pressure coefficient. $C_{P_{b\ell}}$ based on the local velocity would be constant. The regions where $C_{P_{b\ell}}$ is not constant would thus indicate regions where the induced velocities produce significant "base bleed". In flow SH3 where the shear at the high velocity end is not too large the induced base bleed would be small. This probably accounts for the almost constant

$C_{P_{bl}}$ away from the low velocity region.

The constancy of $C_{P_{bl}}$ in the region not affected by the induced velocities suggests shear flow effects may be taken account of by considering the flow parameters with respect to the local velocity when smooth flow results could be used.

Pressure PSD along the span for model at $\alpha = 0^{o}$ in flow SH1 on the 48mm model and in flow SH2 on the 24mm model is shown in FIGURE 57. The PSD is plotted on an arbitrary scale against a reduced frequency parameter $nD/U_{\mathcal{L}}$ where n is the frequency, D the model width and $U_{\mathcal{L}}$ is the tunnel centre-line velocity.

In both flows, the PSD shows peaks at a reduced frequency that increases along the span and in flow SH2, at certain spanwise stations two peaks are observed, the reduced frequencies of these peaks corresponding to the frequency of the single peaks in the adjacent regions. This suggests (Maull & Young) that shedding occurs in cells at a centre frequency which is distinct for each cell; the two frequencies found in the region where the two adjacent cells overlap.

FIGURE 58 shows the spanwise Strouhal Number, $S_{\mathcal{L}}$, based on the tunnel centre-line velocity U so that $S_{\mathcal{L}} = nD/U_{\mathcal{L}}$, for 48mm model in shear flow SH1 and for 24mm model in shear flows SH 2 and SH3 for the models at $\alpha = 0^{o}$.

As observed by Maull & Young (1972), the Strouhal Number distribution shows the cell pattern across the span with a distinct jump in S from one cell to the next.

Both Maull and Young (1972) and MAIR and STANSBY (1975) suggest that the action of the cylinder on the shear flow leads to a concentration of streamwise vorticity which interacts with the shed vortex so that the strengths of the shed vortices vary along the span which leads to the formation of the cell pattern.

It seems that the streamwise vorticity occurs in "pockets" along the span and each cell corresponds to the position of this streamwise vorticity. It is probable that the number of these streamwise vorticity "pockets" increases with the amount of shear in the flow. Mair and Stansby (1975) argue that vortex shedding in cells of limited spanwise extent is to be expected with a constant frequency within each cell. This would explain the difference in the number of cells found in each of the shear flows. Shear flow SH1 being much weaker than flow SH2 although both are uniform shear flows (§ 4).

The results of the spanwise pressures and Strouhal Number measurements on square cylinders without a free end and in a shear flow are similar to those obtained by Maull and Young (1972) for a bluff body without a free end and in a shear flow. The flow patterns suggested by Maull and

Young for this model-flow configuration seems to represent the experimental condition well.

7.2 Three Dimensional Square Cylinders in a Shear Flow

Mean pressures at $\alpha = 0^{\circ}$ and $\alpha = 45^{\circ}$ and pressure PSD and correlations at $\alpha = 0^{\circ}$ taken on the 48mm model in shear flow SH1 for the model height, H, to width, D, ratio in the range $2 \leq H/D \leq 11$ are presented and discussed in this section.

7.2.1 Spanwise Surface Mean Pressures

Spanwise mean C_P for the 48mm model at $\alpha = 0^{\circ}$ and 45° for the cylinder range $2 \leq H/D \leq 11$ are shown in FIGURE 59; C_{P_f} is C_P on the front and windward faces while C_{P_b} is the C_P on the rear and leeward faces. Both C_{P_f} and C_{P_b} are based on U as the reference velocity and C_P is plotted against spanwise distance, z, non-dimensionalized with cylinder height H. C_{P_b} at $\alpha = 0^{\circ}$ plotted against Z/D for flows SH1 and smooth flow GR0 are shown in FIGURE 60 for H/D = 2-6 inclusive and in FIGURE 61 for H/D = 7-11 inclusive.

The pressure distribution pattern in shear flow is similar to that found in uniform flows (§6.2). As would be expected from the position of the pressure taps along the stragnation line, C_{P_f} at $\alpha = 0^{\circ}$ follows the dynamic head in the tunnel except near the faree end where C_{P_f} decreases; the free end

allowing the air to accelerate over the cylinder top. At $\alpha = 45^{o}$, positive C_{P_f} indicates, as in uniform flows, that the flow is attached over the windward face of the cylinder.

At both 0^{o} and 45^{o}, C_{P_b} shows the presence of the free end and base regions and also the three H/D regimes found in uniform flows (§6.2). Again increasing H/D causes a stronger tip vortex and hence greater suctions in the free end. The slight recovery at the free end at $\alpha = 45^{o}$ would again be due to the induced back flow from the trailing vortex.

As observed in uniform flow conditions (§6.2) at both $\alpha = 0^{o}$ and $\alpha = 45^{o}$, C_{P_b} shows the presence of the three H/D regimes found in uniform flows; (i) the low H/D regime, $H/D < (H/D)_L$ (ii) the middle H/D regime, $(H/D)_L < H/D < (H/D)^{*}$, (iii) the high H/D regime, $H/D > (H/D)^{*}$.

In the shear flow, unlike uniform flows, at $\alpha = 45^{o}$ the three H/D regimes are well defined.

In the high H/D regime, as H/D increase, C_{P_b} decreases and in this case C_{P_b}, in the root region, would tend towards the C_{P_b} value on a cylinder without a free end in a shear flow away from the induced "base bleed" effects (§7.1).

The critical H/D ratio values in shear flow SH1 are: $(H/D)_L$ between 4 and 5 while $(H/D)^*$ is around 6. Smooth flow values were found to be $(H/D)_L$ between 5 and 6 with $(H/D)^*$ between 9 and 10 (§6.2). From FIGURE 60 and 61 it is seen that for $H/D < 5$, C_{P_b} values in shear flow are higher than those obtained in smooth flow while the reverse is the case for $H/D > 5$. The vorticity in the shear flow would be inducing a kind of base bleed behind the cylinder causing the C_P to rise. As H/D increases it is probable that the now much stronger tip vortex would be drawing the fluid from the leeward region causing C_P to fall.

For most of the cylinders there is remarkable similarity in the rear face C_P distribution in the shear flow and in uniform smooth flow.

The mean pressure distribution on finite square cylinders in shear flow SH1 suggests a flow pattern similar to that found in uniform flows (§6.2) and as found with uniform flows, changes in the flow characteristics from the smooth flow conditions alters the $(H/D)_L$ and $(H/D)^*$ values from those observed in smooth flow.

The very much similar C_P distribution on the rear face for the cylinders at $\alpha = 0^o$ for shear flow and smooth flow tends to suggest, as with cylinders without a free end, that the

shear effects may be accommodated by considering the smooth flow results and applying the local velocity as the normalizing factor.

Considering the C_{P_b} distribution in shear flow and in uniform flows, smooth and turbulent, the effect of shear is not as large as that of turbulence. Sharan (1977), working with models having H/D ratio of 2, suggested that the effect of shear on the flow around finite cylinders was secondary compared to the effect of turbulence and the present results also lead to the same conclusion.

The decrease in drag with increasing H/D ratio found in uniform flows (§6.2) is also found in shear flow conditions since C_{P_b} becomes more negative as H/D increases while the front face C_P is essentially constant for all cylinders and over most of the span.

7.2.2 Spanwise Pressure Power Spectral Density

Pressure PSD and correlation coefficient measurements were taken on the 48mm model at $\alpha = 0^\circ$ in shear flow SH1 for cylinder H/D = 2,4,6,7,8,9,10 and 11, and the results are presented and discussed in this section.

FIGURES 62-65 show the PSD plotted on an arbitrary scale against a reduced frequency parameter nD/U_{ℓ} for all the cylinders.

As suggested by the mean pressure results (§7.2.1) the PSD distributions also exhibit a pattern similar to that obtained on three dimensional cylinders in uniform flows (§6.4). It is found that there is a peak in the PSD distribution at reduced frequency S_1 in the base region while the peak in the free end region is at the lower reduced frequency S_2; the difference, ΔS, between S_1 and S_2 becoming smaller as H/D decreases and reducing the zero for H/D in the low H/D regime. Also the size of the peak decreases with distance towards the free end and as H/D decreases. For H/D = 1,10 and 9 definite base and free end regions can be observed with an intermediate region which exhibits two peaks at S_1 and S_2, the size of each peak depending upon the relative spanwise position.

Twin peaks are found near the root of the cylinder for H/D = 8 and at H/D = 7 a slight indication at the lowest root position tested for . For cylinders with H/D $\leq$ 6 the PDS scale is magnified 5 times and H/D = 6 shows a distribution similar to that at H/D = 8, except that the peak at S_1 is much smaller than the peak at S_2, suggesting that twin peaks may be occuring up to H/D $\simeq$ 6. Only single peaks could be observed for H/D = 4 and 2.

The PSD distribution on finite cylinders in shear flow suggests a flow pattern similar to that in uniform flows (§ 6.3) in that for the high H/D regime there is eddy

shedding from the lower part of the cylinder at a reduced frequency S_1 and that the top surface flow curls over into the leeward region and the eddy thus formed is shed at reduced frequency S_2. There appears to be no over-riding effect of shear on the flow pattern except perhaps that the shear would tend to "drag upward" the top surface eddy and thus the returning flow would reach the floor for a H/D smaller than that found in smooth flow. This perhaps explains the small peaks at S_1 found for H/D = 6 in shear flow SH1.

7.2.3 Pressure Correlations

FUGURE 54d shows the pressure correlation coefficient, R, measured at various spanwise positions for cylinder H/D = 2, 4, and 6-11, for the 48mm model at $\alpha = 0^{\circ}$ in shear flow SH1. R is plotted against spanwise distance, z, non-dimensionalized with model width D (= 48mm). Figure 54 also shows R found in uniform flow conditions (§6.4).

In the free end region, as H/D becomes small, R near the free end becomes more positive, while for H/D > 8, R, in the lower base region, decreases with increasing H/D and tends to large negative values as H/D becomes large. The free end distribution is similar to that in uniform smooth flow in that except for H/D = 2 as H/D decreases from H/D = 11, the free end vlaue of R becomes more positive. The trend towards a more negative R in the lower root region as H/D becomes large again is the same as foundin uniform flow conditions.

Using the argument of equation 30, the correlation coefficient R can be expressed as:

$$R = K_s R_s + K_{ts} R_{ts} + K_F R_F \quad \ldots \quad (32)$$

where $K_{ts}R_{ts}$ is the turbulence and shear component.

As with uniform flows, in shear flow also the more positive the value of R, the greater the effect of the free end on the flow around the cylinder.

7.2.4 Summary

In linear shear flow SH1 with turbulence intensity 1.7% the flow pattern over finite square cylinders is not different from the flow pattern discernable in uniform flows from the mean pressure, pressure PSD and pressure correlation measurements made on the cylinders.

The trends found in the low turbulence shear flow are similar to that found in uniform smooth flow and it would seem that the shear flow effect can be accommodated into the smooth flow results by considering the local velocity as the normalizing parameter. However, it does appear that the deviation from smooth flow produces results that can not really be predicted from just considering smooth flow results in isolation. As observed by Sharan (1977) the effect of shear on the flow around finite square cylinders is secondary compared to the effect of turbulence.

CHAPTER 8

CONCLUSIONS

The effect of turbulence and shear on the flow around square cylinders has been investigated for models without a free end at incidence in the range $0^{\circ} \leq \alpha \leq 45^{\circ}$ and for model with a free end at $\alpha = 0^{\circ}$ and $\alpha = 45^{\circ}$ for the model height to width ratio $H/D\ 2 \leq H/D \leq 11$ at Reynolds number, based on model width, of 4.8×10^{4}.

It has been found that for the model having a side normal to the flow and without a free end, in uniform smooth flow, turbulence intensity 0.4%, end plates reduced the base pressure besides removing the wall boundary layer affected regions and it seems that for wall boundary layer greater than 10% of the model span, end plates are necessary to simulate a two dimensional flow configuration. However, in uniform turbulent flows, turbulence intensities 5.7% and 9.1% with turbulence scale to model width ratio L(x,u)/D 1.31 and 1.75 respectively, away from the wall boundary layer affected regions two dimensionality could be assumed. The wall boundary layer affected region was of the order of the physical thickness of the layer. In an approximately linear shear flow, turbulence intensity 1.7% with L(x,u)/D =0.69, end plates reduced the base pressure in the low velocity region but had no effect at the high velocity end.

The results obtained for the surface mean pressure distributions and Strouhal number for two dimensional square cylinder and for model without a free end in shear flows agree with the

published data and support the flow models proposed by MULHEARN (1973) and LEE (1975) for two dimensional models and that proposed by MAULL & YOUNG (1972) for a bluff body without a free end in a shear flow.

Finite square cross-section cylinders having a height, H, to width, D, ratio in the range $2 \leqslant H/D \leqslant 11$ exhibit a free end region and a root region. Three regimes are found to exist in uniform smooth and turbulent flows and also in low turbulence linear shear flow. The regimes are:

(i) Low H/D regime with $H/D < (H/D)_L$

(ii) Middle H/D regime with $(H/D)_L < H/D < (H/D)^*$

(iii) High H/D regime with $H/D > (H/D)^*$

Provided the flow is turbulent, increasing turbulence causes a decrease in the drag on the cylinder. The drag on the cylinder in smooth flow is lower than that found for the cylinder in turbulent flow. For a particular flow condition, increasing the cylinder H/D ratio leads to an increase in the drag on the cylinder.

From the limited data available for the length, ℓ_F, of the free end region, it appears that ℓ_F is a function of turbulence and is probably related to $(H/D)_L$.

The present set of results suggests the following flow pattern around finite square cross-section cylinders.

The flow over the free end moves downward into the leeward region. If the cylinder is tall enough, high H/D regime, this top surface flow does not reach the "ground" but turns back towards the free end forming an eddy, which is shed at a reduced frequency S_2. The root region sheds vortices, formed from the separating flow at the cylinder sides, at a reduced frequency S_1. As H/D decreases the free end eddy envelopes a larger portion of the cylinder, and eventually the eddy reaches the ground and completely disrupting the root region vortices. The free end eddy still comes down near the leeward face but as H/D gets smaller, low H/D regime, the free end flow does not have the curvature to bring it down nearer the leeward face and the leeward face just "sees" a separated flow wake with none of the characteristics found for the high and middle H/D regimes.

It appears that as turbulence increases the increased flow mixing causes the free end flow to reattach on the top surface causing the flow to curve into the leeward region further away from the cylinder. In smooth flow there is no flow reattachment and the free end flow turns into the leeward region close to the cylinder, the increased flow bleed into the leeward region causing an increase in the rear face C_p values.

The flow around finite cylinders in linear shear flow with low turbulence intensity is similar to that in uniform flows. In shear flow there is the effect of the flow vorticity causing an additional flow bleed into the leeward region and for cylinders in the low H/D regime; and perhpas the lower end of

the middle H/D regime, the rear face C_p is higher than that found in smooth flow. As H/D increases the stronger tip vortices counteract the flow bled at the lower end and rear face C_p becomes lower than that in smooth flow.

The trends in low turbulence linear shear flows follow the smooth flow results more closely than the turbulent and it would appar that the effect of shear may be taken into account by applying the local velocity as the normalising factor.

As reported by Sharan (1977), the effect of shear may be considered to be secondary to the effect of turbulence on the flow around finite square cross section cylinders. The present results also seem to indicate that unlike two dimensional model configurations, smooth flow results may not form the lower end of the series of results for the flow around finite square cylinders. The effect of increasing turbulence intensity within turbulent flows is to decrease the drag but the drag in smooth flow is lower than that in turbulent flow.

It would seem that for model tests the simulation of flow turbulence characteristics should be of great importance and the effect of shear can then be accounted for by applying the local velocity as the normalising factor. The experimental parameters to be simulated can be reduced to turbulence parameter matching which may not be too difficult to achieve in short wind tunnels.

REFERENCES

1. ABERNATHY, F.H. & KRONAUER, R.E. (1962); The formation of vortex streets; Journal of Fluid Mechanics 13, part 1, 1-20.

2. BAINES, W.D. & PETERSON, E.G. (1949); An investigation of flow through screens; Iowa Institute of Hydraulics, July, 1949.

3. BAINES, W.D. (1963); Effects of velocity distribution on wind loads and flow patterns on buildings; NPL Symposium No. 16, June 26-28, 1963. HMSO.

4. el BAROUDI, M.Y. (1960); Measurement of two-point correlations of velocity near a circular cylinder shedding a Karman vortex street; University of Toronto Institute of Aerophysics, Tech. Note 31 (January, 1960).

5. BEARMAN, P.W. (1965); An investigation of the flow behind a two-dimensional model with a blunt trailing edge and fitted with splitter plates; Journal of Fluid Mechanics 21, part 2, 241-255.

6. BEARMAN, P.W. (1967); On vortex street wakes; Journal of Fluid Mechanics 28, part 4, 625-641.

7. BEARMAN, P.W. (1969); On vortex shedding from a circular cylinder in the critical Reynolds number regime; Journal of Fluid Mechanics 37, part 3, 577-585.

8. BEARMAN, P.W. (1972); Investigation into the effect of base bleed on the flow behind a two dimensional model with a blunt trailing edge; Aeronautical Quarterly, 485-507.

9. BEARMAN, P.W. (1972); Some recent measurements of the flow around bluff bodies in smooth and turbulent streams; Symposium on External Flows, University of Bristol, 4-6 July, 1972.

10. BEARMAN, P.W. & TRUEMAN, D.M. (1972); An investigation of the flow around rectangular cylinders; Aeronautical Quarterly, August,1972, 229-237.

11. BERGER, E. (1964); Unterdrueckung der laminaren wirbelstroemung und des Turbulenzcinsatzes der Karmanschen wirbelstrasse im Nachlauf eines schwingenden Zylinders bei Kleinen Reynoldzahlen; Jarb WGLR, 164-172.

12. BERGER, E. (1964); Bestimmung der hydrodynamischen Grossen einer Karmanschen Wirbelstrasse aus Hitzdrahtmessungen bei kleinen Reynoldschen Zahlen, Z. Flugwiss. 12, Heft 2, 41-59.

13. BERGER, E. & WILLE, R. (1972); Periodic flow phenomena; Annual review of Fluid Mechanics 4, 313-340.

14. BLOOR, M.S. (1964); The transition to turbulence in the wake of a circular cylinder; Journal of Fluid Mechanics 19, part 2, 290-304.

15. de BRAY, B.G. (1962); Wind pressures on Multi-Storey Buildings; Engineering, July 6, 1962, 10-11.

16. BRUUN, H.H. (1976); A digital comparison of linear and non linear hot wire data evaluation; Journal of Physics E: Scientific Instruments 1976, 9, 53-57.

17. CASTRO, I.P. & ROBBINS, A.G. (1977); The flow around a surface-mounted cube in uniform and turbulent streams. Journal of Fluid Mechanics 79, Part 2, 307-336.

18. CERMAK, J.E. (1975); Applications of fluid mechanics to wind engineering - A Freeman Scholar Lecture; ASME Journal of Fluids Engineering, March, 1975, 9-38.

19. CHEN, C.F. & MANGIONE, B.J. (1969); Vortex shedding from circular cylinders in sheared flow; AIAA Journal 7, 1211-1212.

20. COOK, N.J. (1971); The effect of turbulence scale on the flow around high-rise building models; Ph.D. Thesis, University of Bristol.

21. COUNIHAN, J. (1969); An improved method of simulating an atmospheric boundary layer in a wind tunnel; Atmospheric Environment 3, 197-214.

22. COWDREY, (1967); Simple method for the design of wind tunnel velocity grid; NPL Note 1055, May, 1967.

23. FAGE, A. (1934); Photographs on fluid flow revealed with an ultramicroscope Proc. Roy. Soc. A. vol. 144, 381-385.

24. GARTSHORE, I.S. (1937); Effects of free stream turbulence on the drag of rectangular two dimensional prisms; University of Western Ontario, BLWT 4-73.

25. GASTER, M. (1969); Vortex shedding from slender cones at low Reynolds numbers; Journal of Fluid Mechanics, 38, part 3, 565-576.

26. GASTER, M. (1971); Vortex shedding from circular cylinders at low Reynolds numbers; Journal of Fluid Mechanics 46, part 4, 749-756.

27. GERRARD, J.H. (1961); An experimental investigation of the oscillating lift and drag of a circular cylinder shedding turbulent vortices; Journal of Fluid Mechanics 11, part 2, 244-256.

28. GERRARD, J.H. (1965); A disturbance sensitive Reynolds number range of the flow past a circular cylinder; Journal of Fluid Mechanics 22, part 1, 187-196.

29. GERRARD, J.H. (1966a); Three dimensional structure of the wake of a circular cylinder; Journal of Fluid Mechanics 25, part 1, 143-164.

30. GERRARD, J.H. (1966b); The mechanics of the formation region of vortices behind bluff bodies; Journal of Fluid Mechanics 25, part 2, 401-413.

31. HAMA, F.R. (1957); Three dimensional vortex pattern behind a circular cylinder; Journal of Aerospace Sciences 24, 156-158.

32. HOMANN, F. (1936); Einfluss grosser Zachigkeit bei Stroemung um Zylinder und Kugel; Forch. Ing. Wes. 7, 1-10.

33. HOOKER, S.G. (1936); On the action of viscosity in increasing the spacing ratio of vortex streets; Proc. Roy. Soc. (A), 154.

34. HUMPHREYS, J.S. (1960); On a circular cylinder in a steady wind at transition Reynolds numbers. Journal of Fluid Mechanics 9, 603-

35. JONES, G.W. Jr., CINCOTTA, J.J. & WALKER, R.W. (1969); Aerodynamic forces on a stationary and oscillating circular cylinder at high Reynolds numbers; NASA. Tech. Rep. TR R-300.

36. JOUBERT, P.N., STEVENS, L.K., & PERRY, A.E. (1962): The effect of aspect ratio on wind forces on building models. Civil Engineering Transactions, September, 1962, 75-78.

37. KOVOSZNAY L.S.G. (1949); Hot wire investigation of the wake behind cylinders at low Reynolds numbers; Proc. Roy. Soc. London Series A 198, 174-190.

38. KRONAUER, R.E. (1964); Predicting eddy frequency in separated wakes; Paper presented at the I.U.T.A.M. Symposium on concentrated vortex motions in fluids, University of Michigan, Ann Arbor, Michigan, 6-11 July, 1964.

39. KUCHEMANN, D. (1965); Report on the I.U.T.A.M. symposium on concentrated vortex motions in fluids; Journal of Fluid Mechanics, 21, part 1, 1-20.

40. LEE, B.C. (1974); The surface pressure field experienced by a two-dimensional square prism; Central Electricity Research Laboratories, Laboratory Note No. RD/L/N 17/74.

41. LEE, B.E. (1975a); The effect of turbulence on the surface pressure field of a square prism; Journal of Fluid Mechanics 69, part 2, 263-282.

42. LEE, B.E. (1975b); An investigation of the effects of flow on non-uniformities on the mean forces on a two-dimensional square prism, Report BC23, Dept. of Building Science, University of Sheffield.

43. LEE, B.C. (1976); Some effects of turbulence scale on the mean forces on a bluff body; Journal of Industrial Aerodynamics 1, (1975-1976), 361-370.

44. MAIR, W.A. & MAULL, D.J. (1971); Bluff bodies and vortex shedding - A report on Euromech 17; Journal of Fluid Mechanics 45, part 2, 209-224.

45. MAIR, W.A. & STANSBY, P.K. (1975); Vortex wakes of bluff cylinders in shear flow; SIAM J. APPL. MATH 28, No. 2, 519-540

46. MALTBY, R.L. (1962); Flow visualization in wind tunnels using indicators; AGARDograph 70.

47. MARRIS, A.W. (1964); A review on vortex streets, periodic wakes, and induced vibration phenomena; ASME Journal of Basic Engineering 86, 185-196.

48. MASKELL, E.C. (1963); A theory of the blockage effects of bluff bodies and stalled wings in a closed tunnel; Aeronautical Research Council R & M 3400.

49. MATTINGLEY, G.E. (1962); University of Maryland TN No. BN-295.

50. MAULL, D.J. & YOUNG, R.A. (1972); The wake of a bluff body in a non-uniform flow; Symposium on External Flows, University of Bristol, 4-6 July, 1972.

51. McLAREN, F.G., SHERRATT, A.F.C., & MORTON, A.S. (1969a, 1969b); Effect of free stream turbulence on the drag coefficient of bluff sharp-edged cylinders; Nature 223, 828-829, Nature 224, 908-909.

52. MORKOVIN, M.V. (1964); Flow around circular cylinders; Proceedings of ASME Symposium on Fully Separated Flows, 102-118.

53. MULHEARN, P.J. (1973); Stagnation and reattachment lines on a cylinder of square cross-section in smooth and turbulent flows; Nature Physical Science 241, 165-167.

54. OWEN, P R. & ZIENKIEWICZ, K.H. (1957); The production of uniform shear flow in a wind tunnel; Journal of Fluid Mechanics 2, 521-531.

55. PENDERGAST, V. (1958); Measurements of two-part correlations of the surface pressure on a circular cylinder; University of Toronto, Institute of Aerophysics, Tech. Note 23.

56. PENWARDEN, A D. (1973); Acceptable wind speeds in towns; Building Science 8, No 3, 259-267.

57. PETTY, D.G. (1972); The distortion of turbulence by a circular cylinder; Symposium on External Flows, University of Bristol, 4-6 July 1972.

58. PHILLIPS, O.M. (1956); The intensity of aeolian tones; Journal of Fluid Mechanics 1, 607-624.

59. RANGA RAJU, K.G. & GARDE, R.J. (1970); Resistance of an inclined plate placed on a plane boundary in two dimensional flow; ASME Journal of Basic Engineering 92, 21-31.

60. RANGA RAJU, K.G. & SINGH, V. (1975); Blockage effects on drag of sharp-edged bodies; Journal of Industrial Aerodynamics 1 (1975-1976), 301-309.

61. ROSHKO, A. (1954a); On the drag and shedding frequency of two-dimensional bluff bodies; NACA TN 3169.

62. ROSHKO, A. (1954b); A new hodograph for free streamline theory; NACA TN 3168.

63. ROSHKO, A. (1961); Experiments on the flow past a circular cylinder at very high reynolds numbers; Journal of Fluid Mechanics 10, part 3, 345-356.

64. SALLET, D.W. (1969); On the spacing of Karman vortices; ASME Journal of Applied Mechanics, 370-372.

65. SALLET, D.W. (1973); The lift force due to von Karman's vortex wake; AIAA Journal of Hydronautics 7, No. 4, 161-16

66. SCHAEFER, J.W. & ESKINAZI, S. (1959); An analysis of the vortex street generated in a viscous fluid; Journal of Fluid Mechanics 6, 241-260.

67. SCHMIDT, L.V. (1966); Fluctuating force measurements upon a circular cylinder at Reynolds numbers up to 5×10^6; paper presented at NASA meeting on Ground wind problems in relation to launch vehicles; Langley Research Center, June 7-8 1966.

68. SHARAN, V.K.R. (1977); On the influence of the characteristics of the flow on pressure distribution around building models with a view to simulating the minimum height of atmospheric boundary layer; Int. J. Mech.Sci 19, 387-397.

69. STANSBY, P.R. (1974); The effects of end plates on the base pressure coefficient of a circular cylinder; The Aeronautical Journal, January 1974, 36-37.

70. STRADLING, P. (1975); Vortex shedding in a shear flow; Part III project, Aero. Eng. Dept., Queen Mary College, University of London.

71. TANEDA, S. (1956); Experimental investigation of the wakes behind cylinders and plates of low Reynolds numbers; Journal of Phys. Soc. Japan 11, No. 3, 302-307.

72. TANEDA, S. (1965); Experimental investigation of vortex streets; J.Phys.Soc. Japan 20, No 9, 1714-1721.

73. TANEDA, S. (1968); Standing twin vortices behind a thin flat plate normal to the flow; Reports of Research Institue for Applied Mechanics, 16, No 54, 155-163.

74. TANI, I. (1964); Low-speed flows involving bubble separations; Progress in Aeronautical Sciences 5, 70-103.

75. TIMME, A. (1957); Uber die Geschwindigkeitsverteilung in Wirbeln; Ingenieur-Archiv 25, 205-225.

76. TRITTON, D.J. (1959); Experiments on the flow past a circular cylinder at low Reynolds numbers; Journal of Fluid Mechanics 6, 547-567.

77. TRITTON, D.J. (1971); A note on vortex streets behind circular cylinders at low Reynolds number; Journal of Fluid Mechanics 45, 203-208.

78. Vickery, B.J. (1966); Fluctuating lift and drag on a long cylinder of square section in a smooth and in a turbulent stream; Journal of Fluid Mechanics 25, part 3, 481-494.

79. WILLE, R. (1960); Karman vortex streets; Advances in Applied Mechanics 6, 273-287.

80. WILLE, R. (1966); On unsteady flows and transient motions; Progress in Aeronautical Sciences 7, 195-207.

81. WOOD, C.J. (1970); An examination of vortex street formation by particle tracers; Paper at Euromech 17, Cambridge, U.K., 1-3 July 1970.

82. GOLDSTEIN, S. editor, Modern Developments in Fluid Mechanics, Volumes I & II, Dover edition.

83. HINZE, J.O.; Turbulence; McGraw-Hill, New York, 1959.

84. LAMB, H. Sir; Hydrodynamics; Dover edition

85. Engineering Sciences Data Item. No. 71016, July 1973.

86. AGARD CP 4; Separated flows - 2 parts; Rhode-Saint Genese, Belgium, 1969.

87. AGARD CP 48; Aerodynamics of atmospheric shear flows; Munich, W.Germany, 1969

88. Proceedings of the wind effects on buildings and structures Conference; NPL Teddington, U.K, June 1963

89. Proceedings of the international research seminar - wind effects on buildings and structures; Ottawa, Canada, September 1967.

90. Proceedings of Symposium on wind effects on buildings and structures; Loughborough, U.K, April 1968.

91. Proceedings of the 3rd International Conference on wind effects on buildings and structures; Tokyo, Japan, September 1971.

92. Proceedings of the 4th International Conference on wind effects on buildings and structures; Heathrow, England, U.K, September 1974.

GEOMETRICAL CHARACTERISTICS OF GRIDS

Grid Number	Bar size b mm	Mesh size M mm	Solidity	Type of Flow	Comments
GRO	NO GRID PRESENT			Smooth flow	Blowdown tunnel
GR1	28	152	0.28	Turbulent	Flat bars. gap of ½ M between wall and first horizontal bar. Blowdown tunnel.
GR2	53	203	0.36	Turbulent	Flat bars. gap of ½ M between wall and first horizontal bar. Blowdown tunnel.
GR3	80	300	0.32	Turbulent	Flat bars. gap M between wall and first horizontal bar. Blowdown tunnel.
SH1	5	-	0.28	Shear	Circular bars. Blowdown tunnel.
SH2	3.2	-	0.24	Shear	Circular bars. No.4 Closed return tunnel.
SH3	3.2	-	0.24	Shear	Circular bars. No.4 Closed return tunnel.

TABLE 1

MODEL CONFIGURATIONS FOR CIRCUMFERENTIAL SURFACE

MEAN PRESSURES

	MODEL CONFIGURATIONS AND TEST CONDITIONS	
Model width (D mm)	48	48
H/D Z/H	16.04 0.5	11.67 0.5
Finite Cylinders H/D Z/H	 - -	
Flow Incidences (Degrees)	0.5,7,11,14, 20,30,40,45	0 45
Flow Types	GR0,GR1 GR2	GR0,GR1 GR2,SH1
Comments	No End Plates	Both End Plates for model spanning tunnel.

TABLE 2

MODEL CONFIGURATIONS FOR SPANWISE SURFACE MEAN PRESSURES

	MODEL CONFIGURATIONS AND TEST CONDITIONS		
Model width (D mm)	48	48	24
Model Spans Tunnel Span/D	16.04	11.67	22
Finite Cylinders H/D	-	2,3,4,5,6, 7,8,9,10,11	-
Flow Incidence	0°	0° 45°	0°
Types of Flows	GR0,GR1, GR2	GR0,GR1, GR2,SH1	SH2,SH3
Comments	No end plates present	Both End Plates for model spanning tunnel. Only roof end plate for finite Cylinders	No End Plates Present.

TABLE 3

MODEL CONFIGURATIONS FOR POWER SPECTRAL DENSITY MEASUREMENTS

	MODEL CONFIGURATIONS AND TEST CONDITIONS	
Model width (D mm)	48	24
Model Spans Tunnel Span/D	11.67	22
Finite Cylinders H/D	2,4,6,7,8, 9,10,11	-
Flow Incidence (Degrees)	0	0
Types of Flow	GRO,GR1, GR2,SH1	SH2,SH3
Comments	Both end plates present for model spanning tunnel. Only roof end plate for finite Cylinders.	No end plates present.

TABLE 4

FLOW PROPERTIES

Grid Number	Grid Distance x(m)	Grid Distance / Bar Size $x/_b$	Grid Distance / Mesh Length $x/_M$	Turbulence Intensity %	L(x,u) mm	L(z,u) mm	L(z,u) / L(x,u)	Flow Type
GRO	2.55	NO GRID		0.4	SMOOTH FLOW			Uniform
GR1	2.55	91.1	16.9	5.7	63	28	0.44	Uniform
GR2	2.55	48.1	12.6	9.1	84	42	0.50	Uniform
SH1	2.55	510	-	1.7	32	17	0.53	Linear Shear
SH2	0.86	271	-	2.0	NOT MEASURED			Linear Shear
SH3	0.86	271	-	1.7	NOT MEASURED			1/6th power law shear

TABLE 5

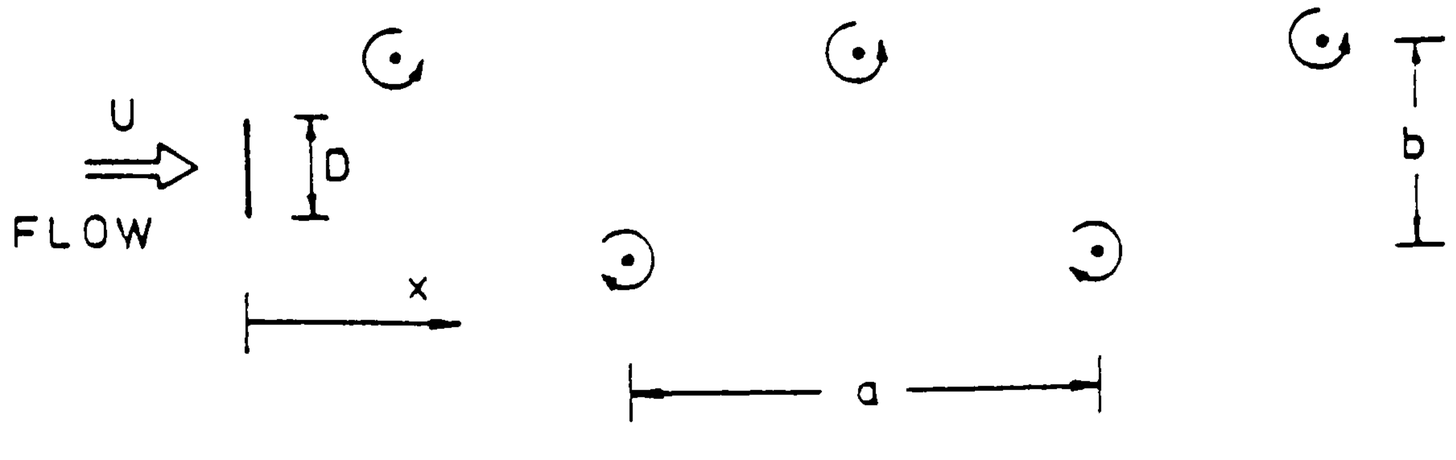

a) KÁRMÁN VORTEX STREET

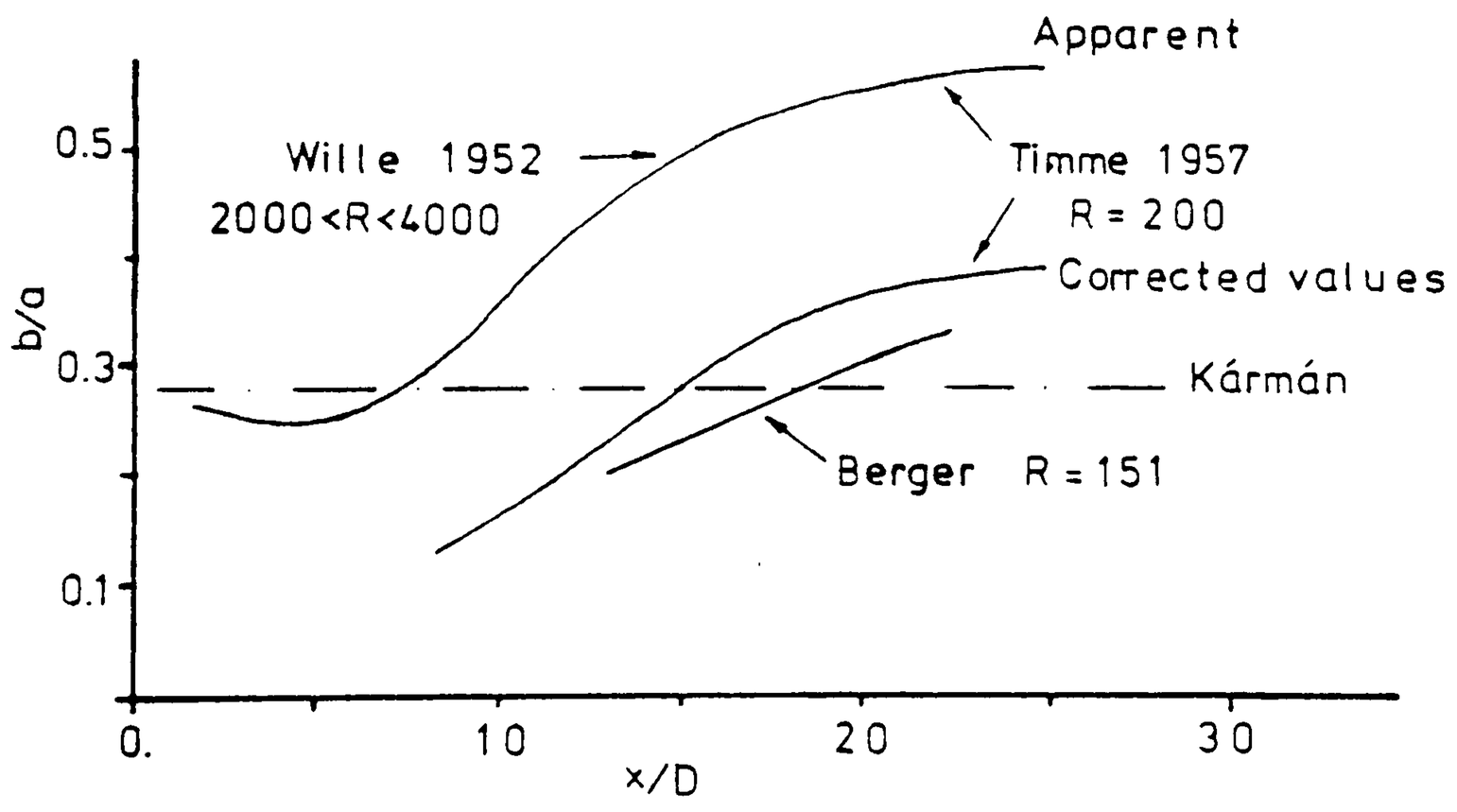

b) SPACING RATIO OF A KÁRMÁN VORTEX STREET AS A FUNCTION OF DISTANCE DOWNSTREAM FROM CYLINDER. (Wille, 1966)

FIGURE 1

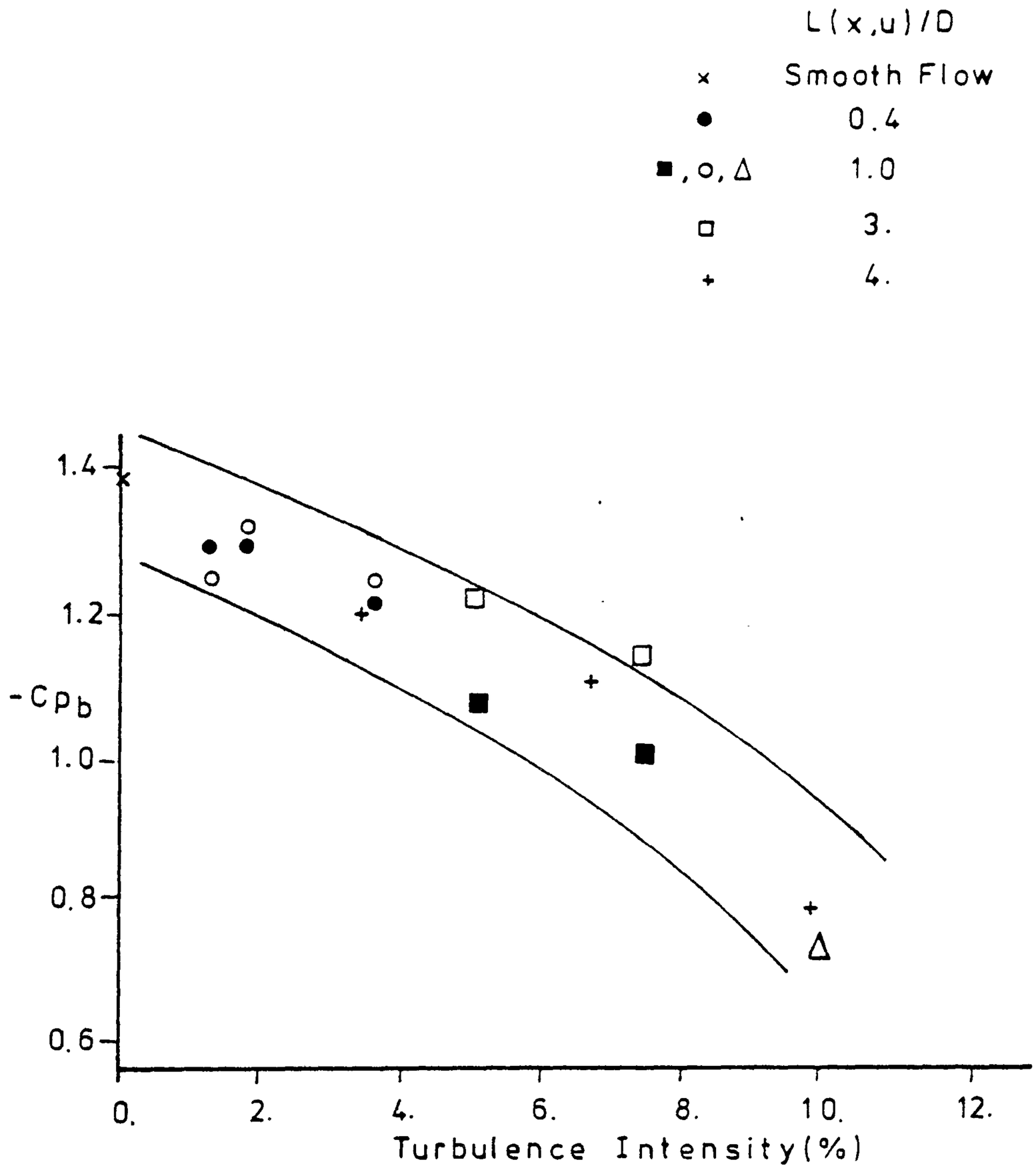

VARIATION OF BASE PRESSURE WITH TURBULENCE INTENSITY FOR A SQUARE SECTION CYLINDER AT ZERO INCIDENCE (Bearman, 1972)

FIGURE 2

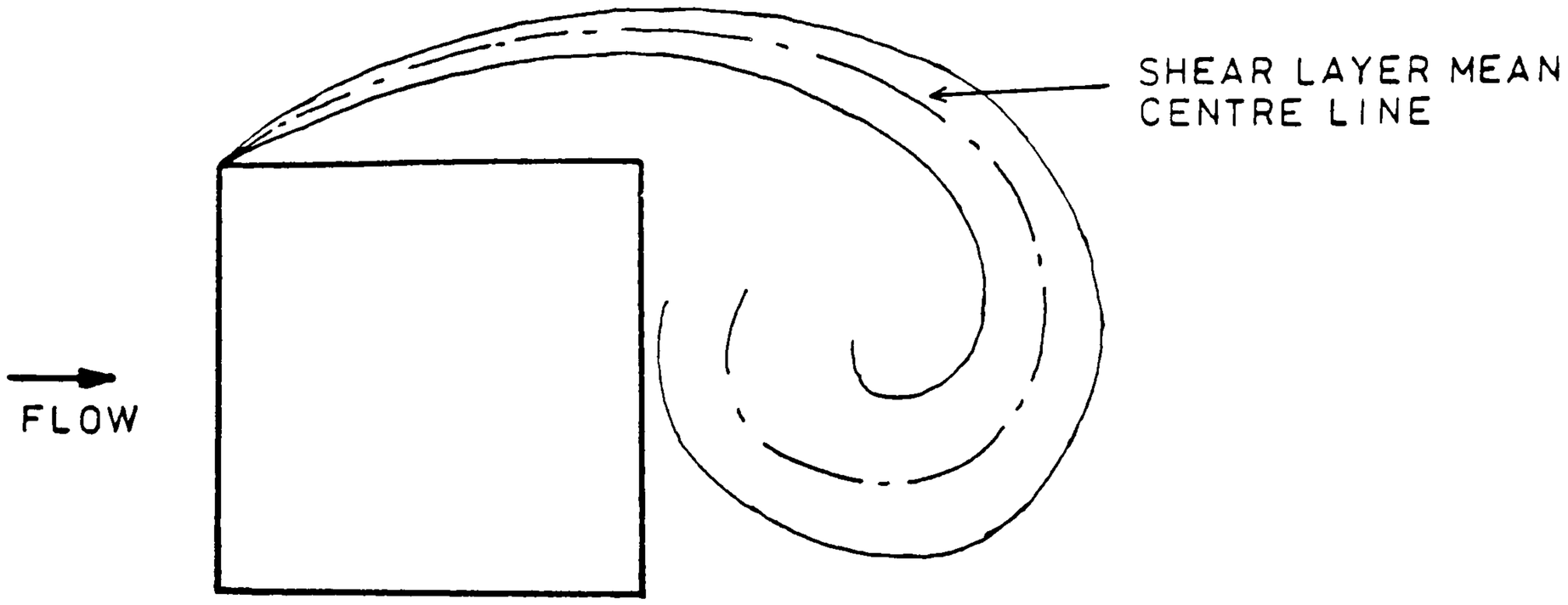

(a) UNIFORM FLOW

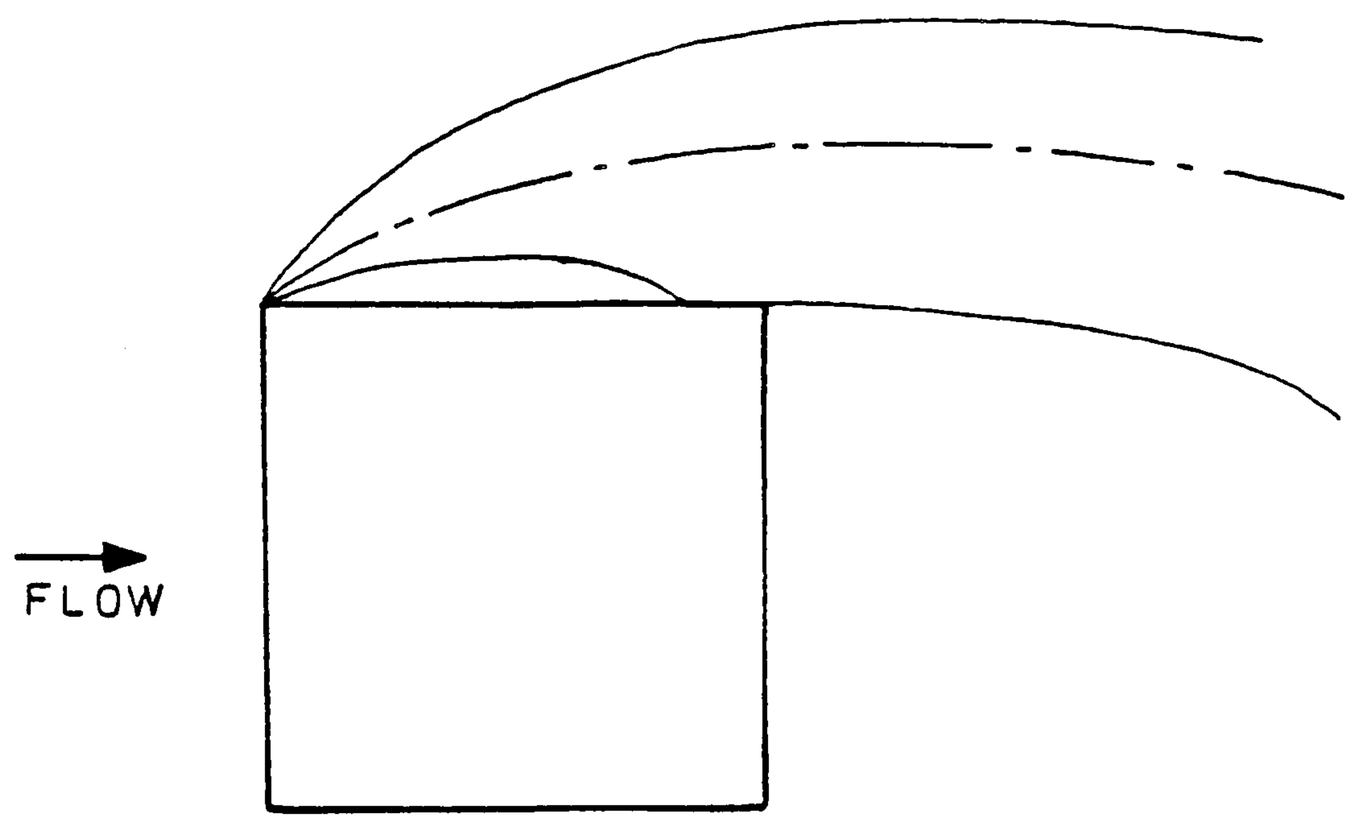

(b) TURBULENT FLOW. INCREASED ENTRAINMENT ONLY

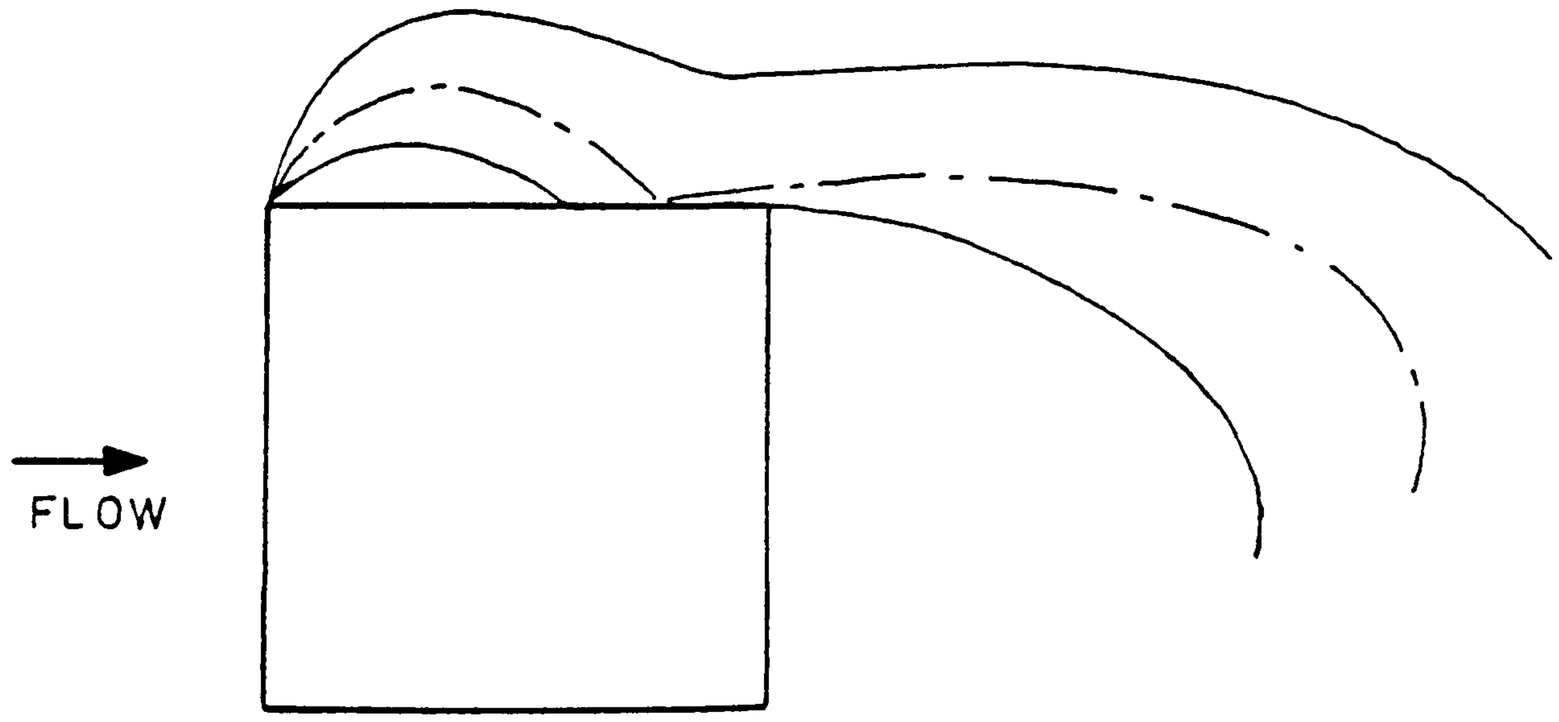

(c) TURBULENT FLOW. INCREASED ENTRAINMENT COMBINED WITH MEAN CENTRE LINE PATH DISTORTION

THE EFFECT OF INCIDENT FLOW TURBULENCE ON SHEAR LAYER GROWTH AND VORTEX FORMATION

(after LEE, 1974)

FIGURE 3

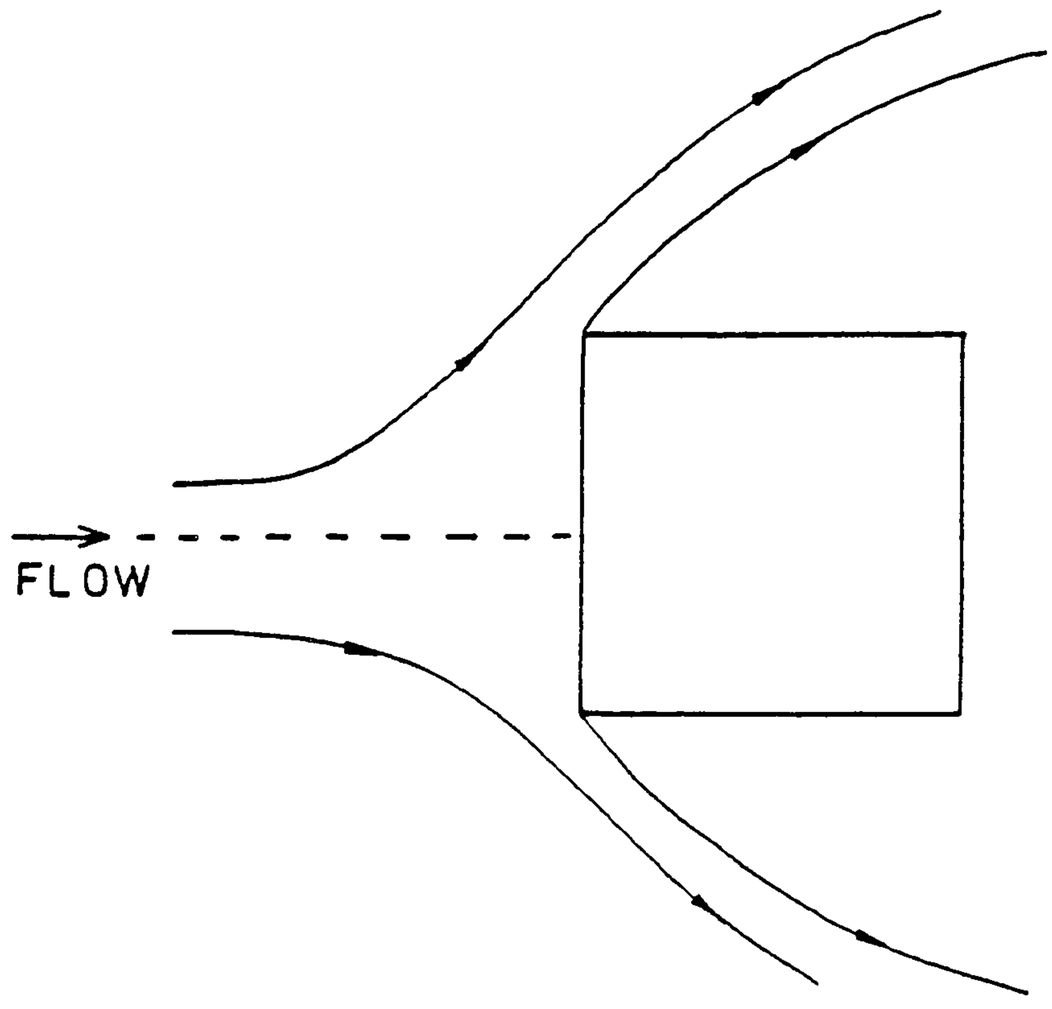

a) ZERO INCIDENCE

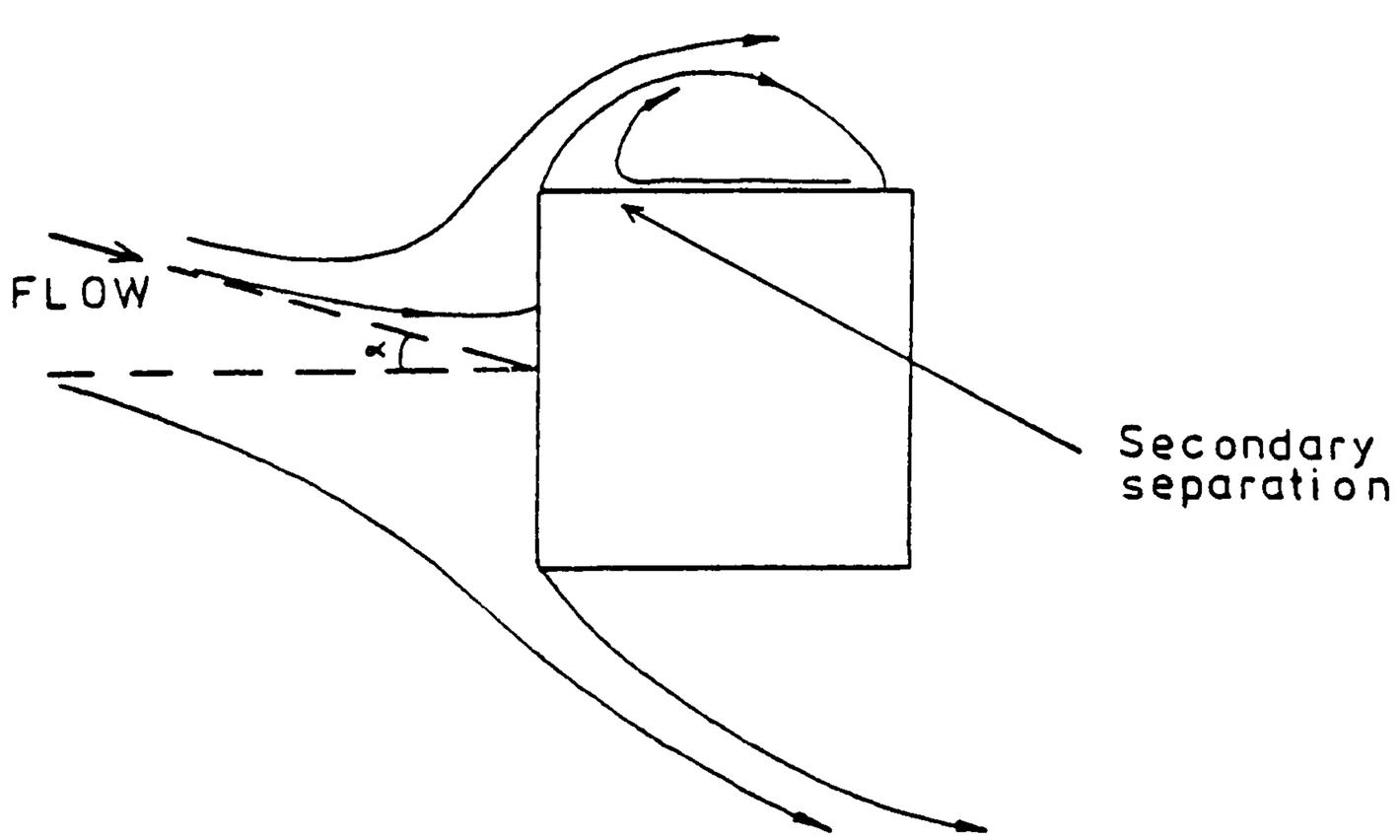

b) REATTACHMENT INCIDENCE

EFFECT OF INCIDENCE ON THE FLOW
AROUND A SQUARE CYLINDER (after Mulhearn, 1973)

FIGURE 4

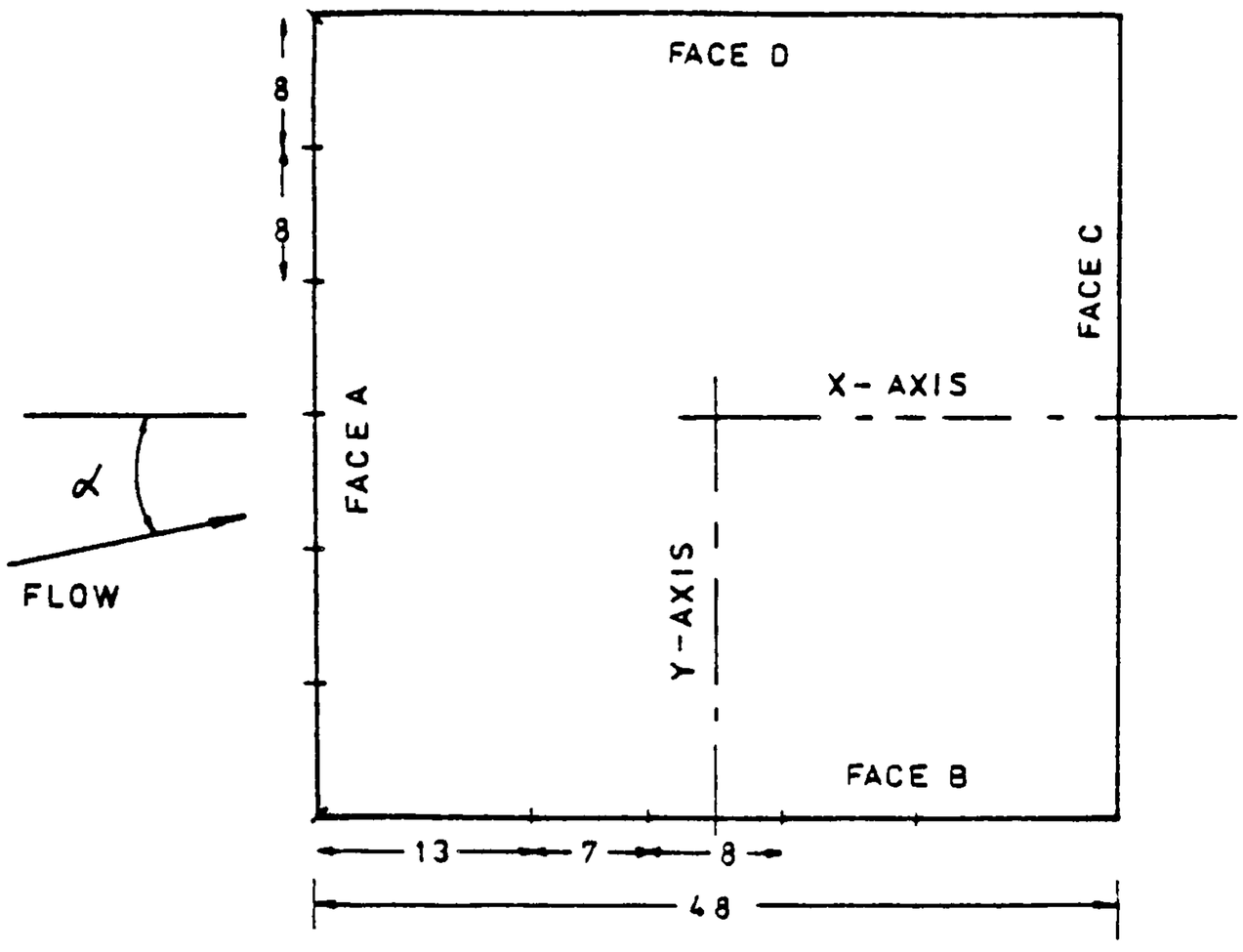

DIMENSIONS IN MM TAP DIAMETER = 0.762 mm

a) CIRCUMFERENTIAL PRESSURE TAP DISTRIBUTION ON 48mm MODEL

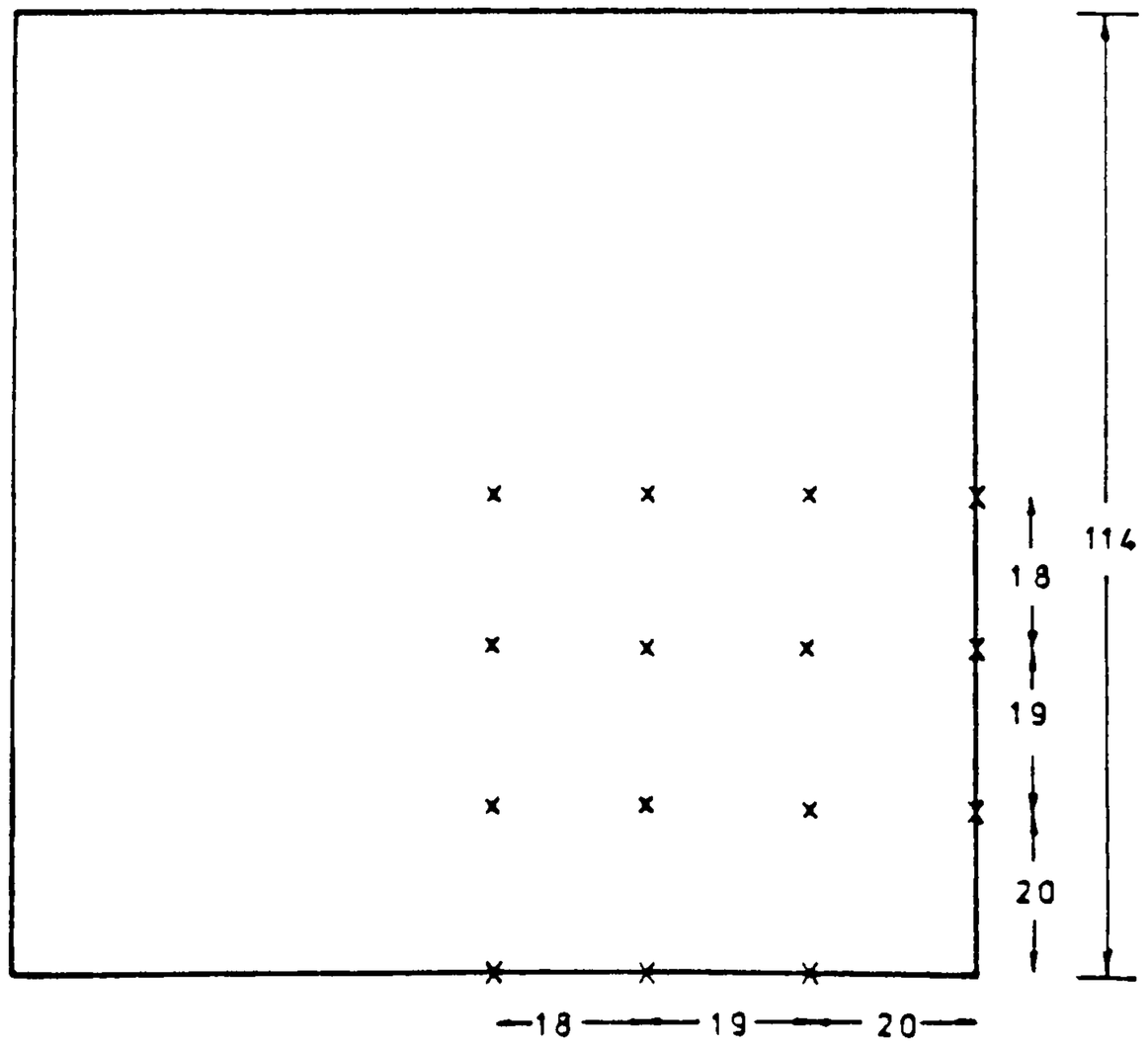

DIMENSIONS IN MM TAP DIAMETER = 1·524 mm

b) PRESSURE TAP DISTRIBUTION ON TOP SURFACE OF 114 mm MODEL

FIGURE 5

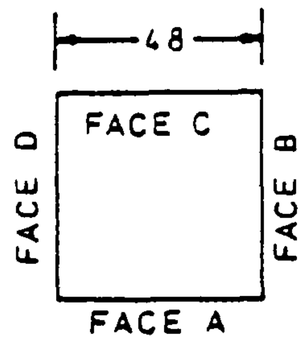

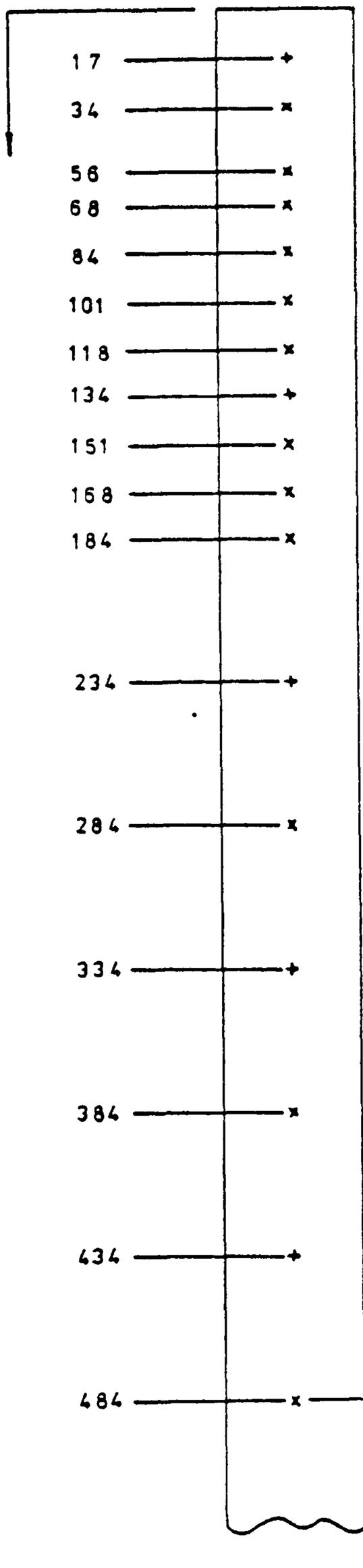

\+ ALSO PRESENT ON FACE B AND FACE D

TAP DIAMETER = 0.762 mm

DIMENSIONS IN MM

SPANWISE PRESSURE TAP DISTRIBUTION

FIGURE 6

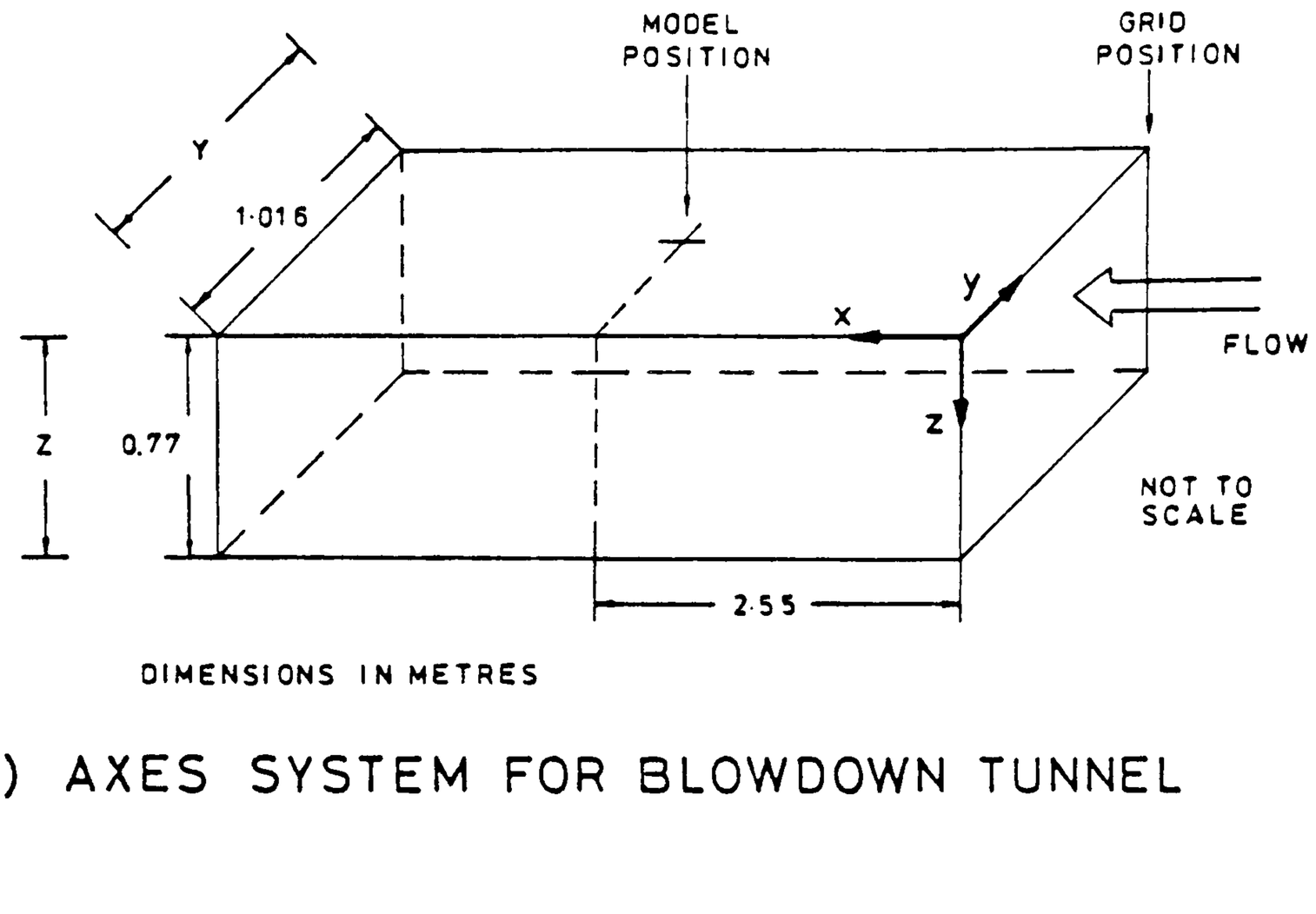

a) AXES SYSTEM FOR BLOWDOWN TUNNEL

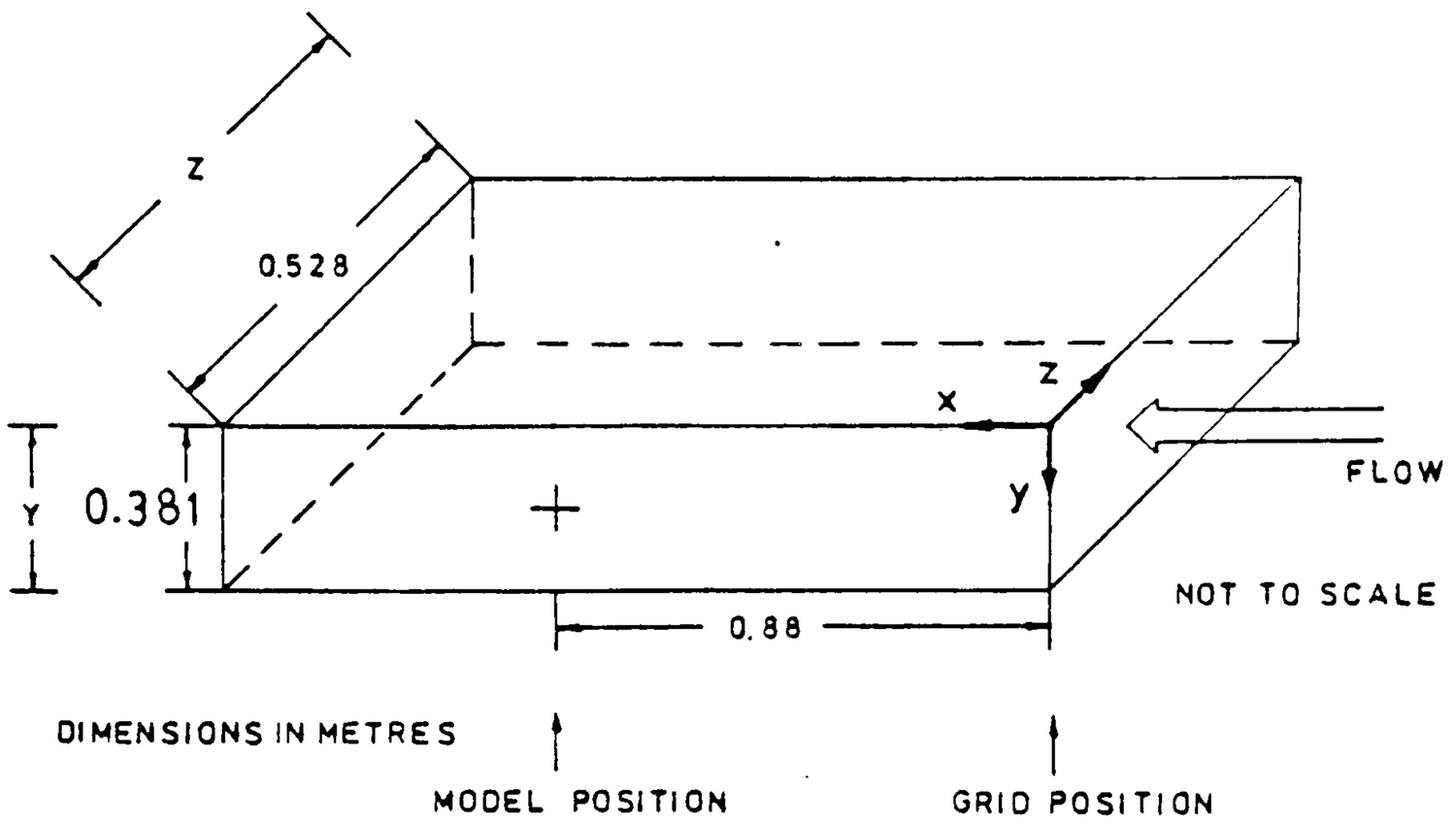

b) AXES SYSTEM FOR No 4 CLOSED RETURN TUNNEL

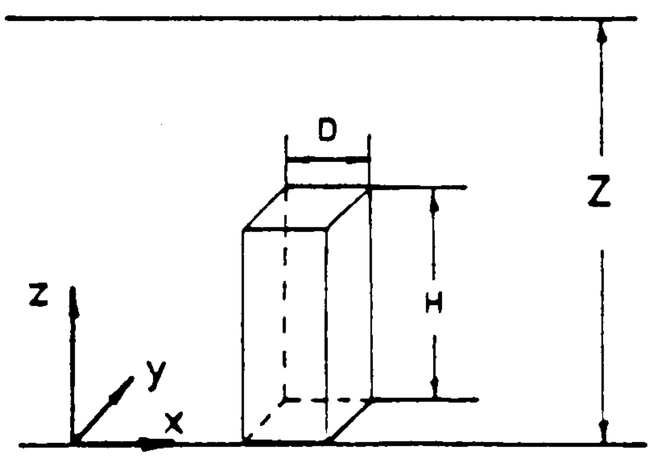

c) AXES SYSTEM FOR MODEL

AXES SYSTEMS

FIGURE 7

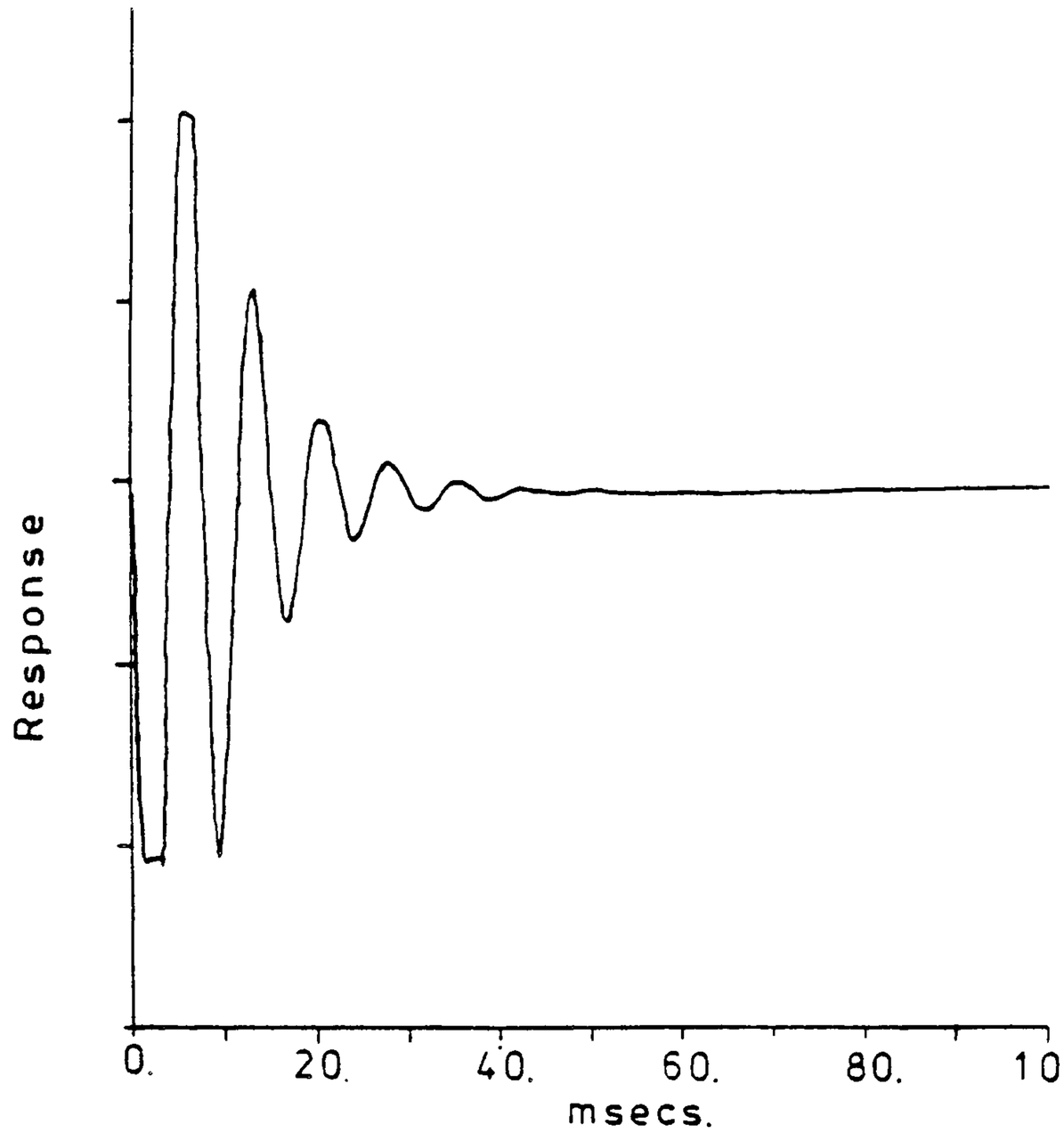

Transducer System response to step input

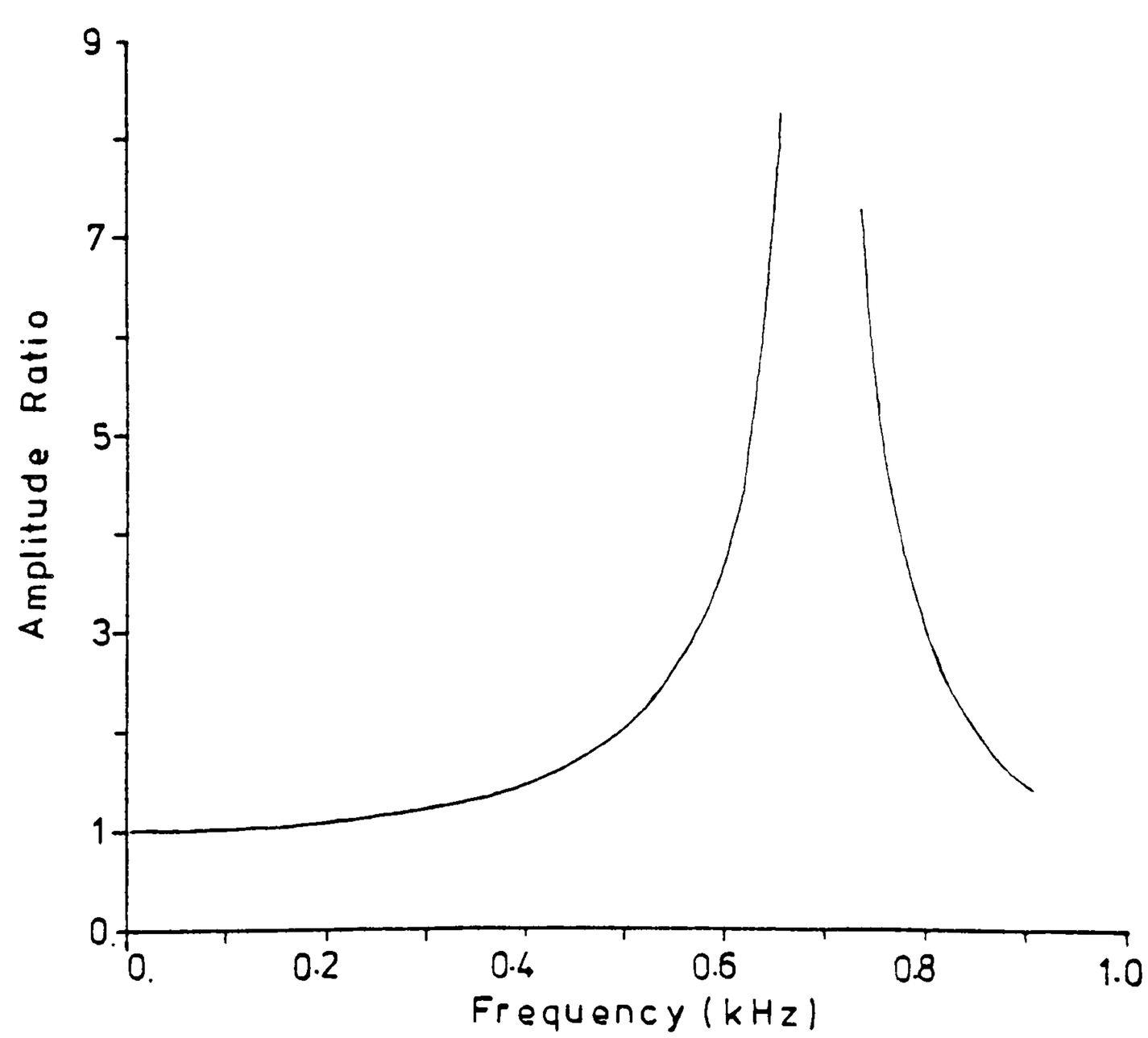

Transducer System frequency response

TRANSDUCER SYSTEM CHARACTERISTICS

FIGURE 8

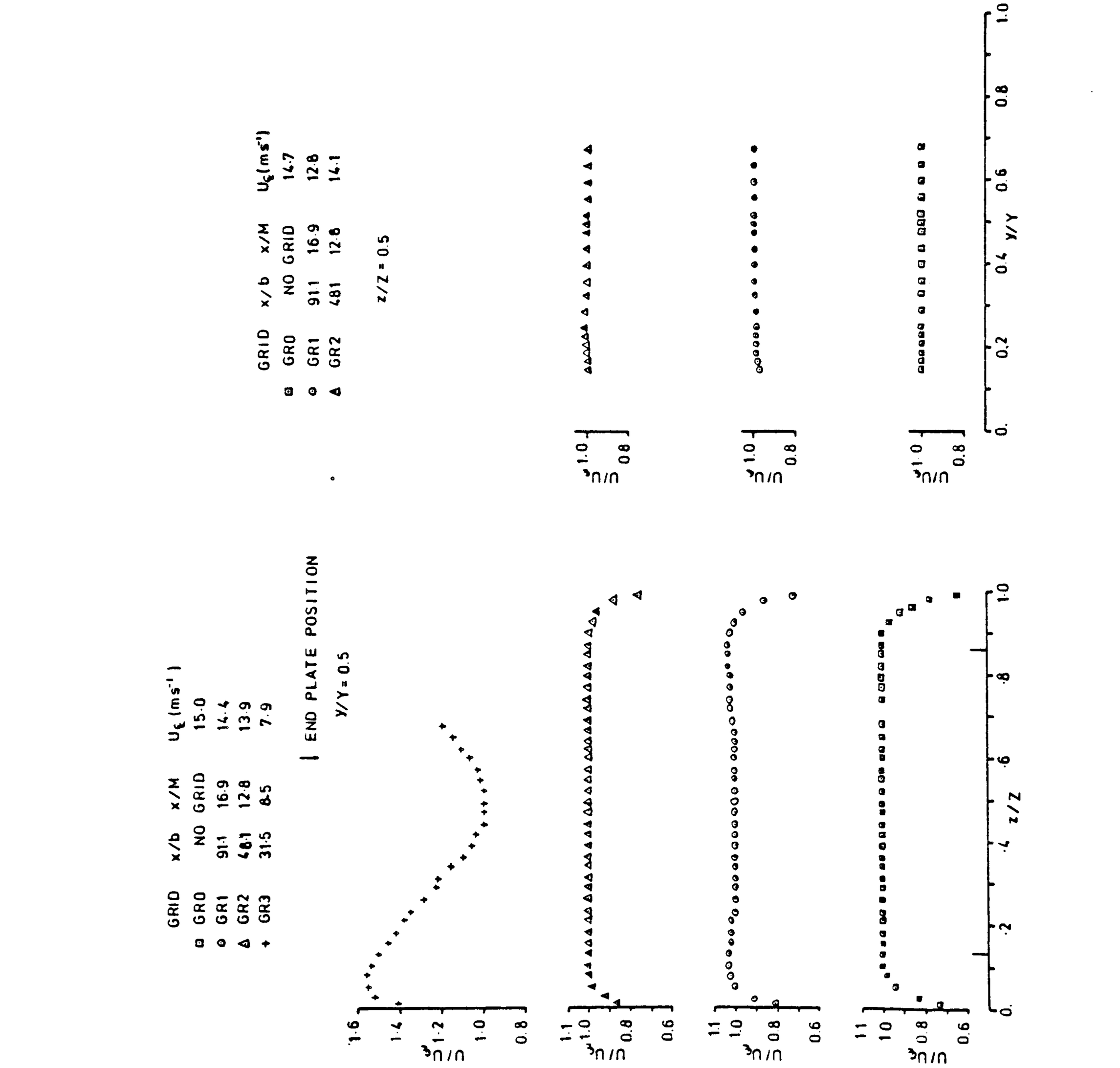

MEAN VELOCITY PROFILES FOR TURBULENCE GRIDS

FIGURE 9

	GRID	x(m)	x/b	U ($m\,s^{-1}$)	
⊙	SH1	2·55	510.	11·9	
△	SH1	2·55	510.	14·4	HOT WIRE
⊡	SH2	0.86	271.	14.3	
+	SH3	0.86	271.	14.3	

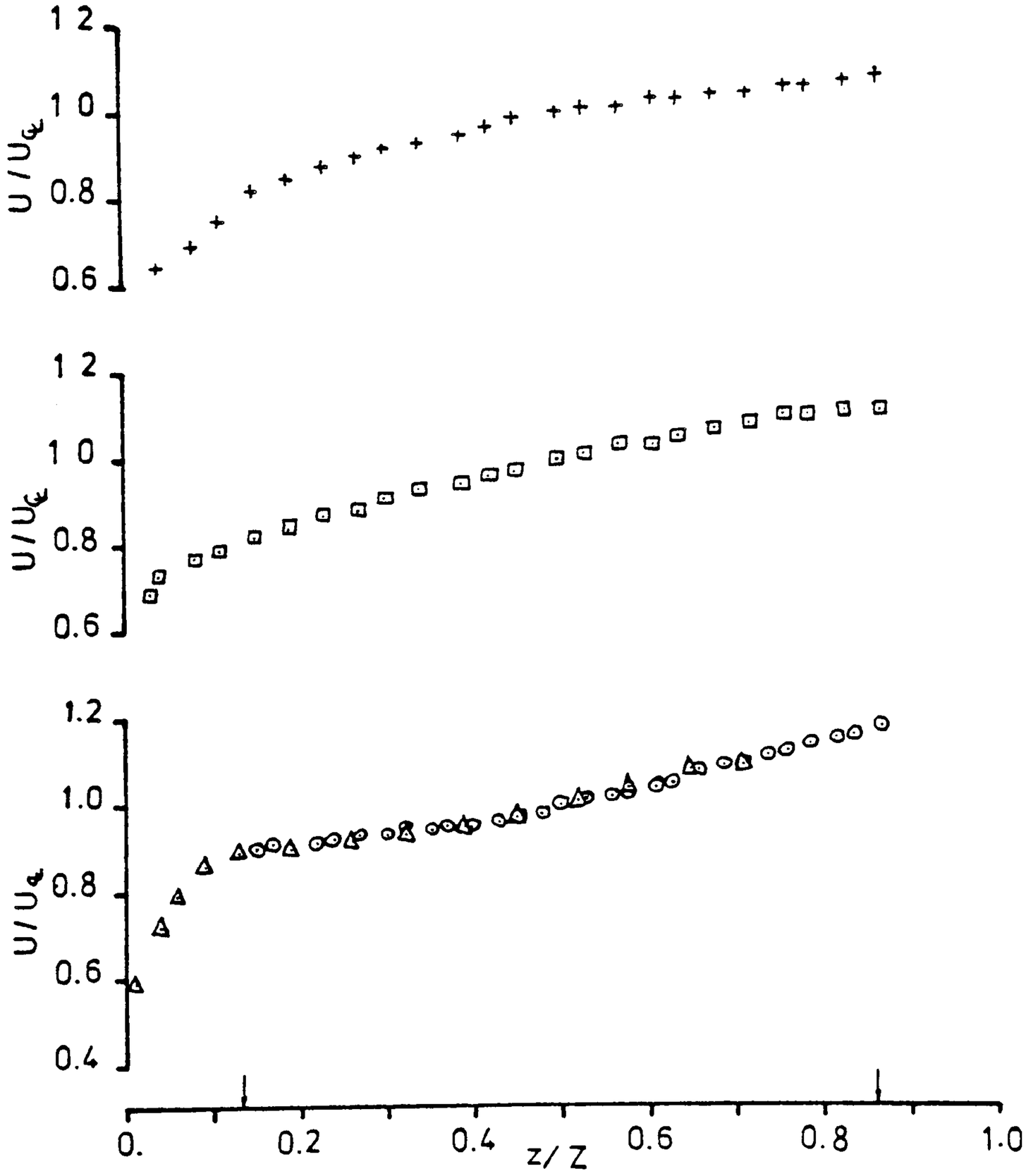

MEAN VELOCITY PROFILES DOWNSTREAM OF SHEAR GRIDS

FIGURE 10

	GRID	x(m)	x/b	x/M
+	GR0	2.55	NO GRID	
□	GR1	2.55	91.1	16.9
△	GR2	2.55	48.1	12.8
○	SH1	2.55	510.	-
▽	SH2	0.86	271.	-
×	SH3	0.86	271.	-

$y/Y = 0.5$

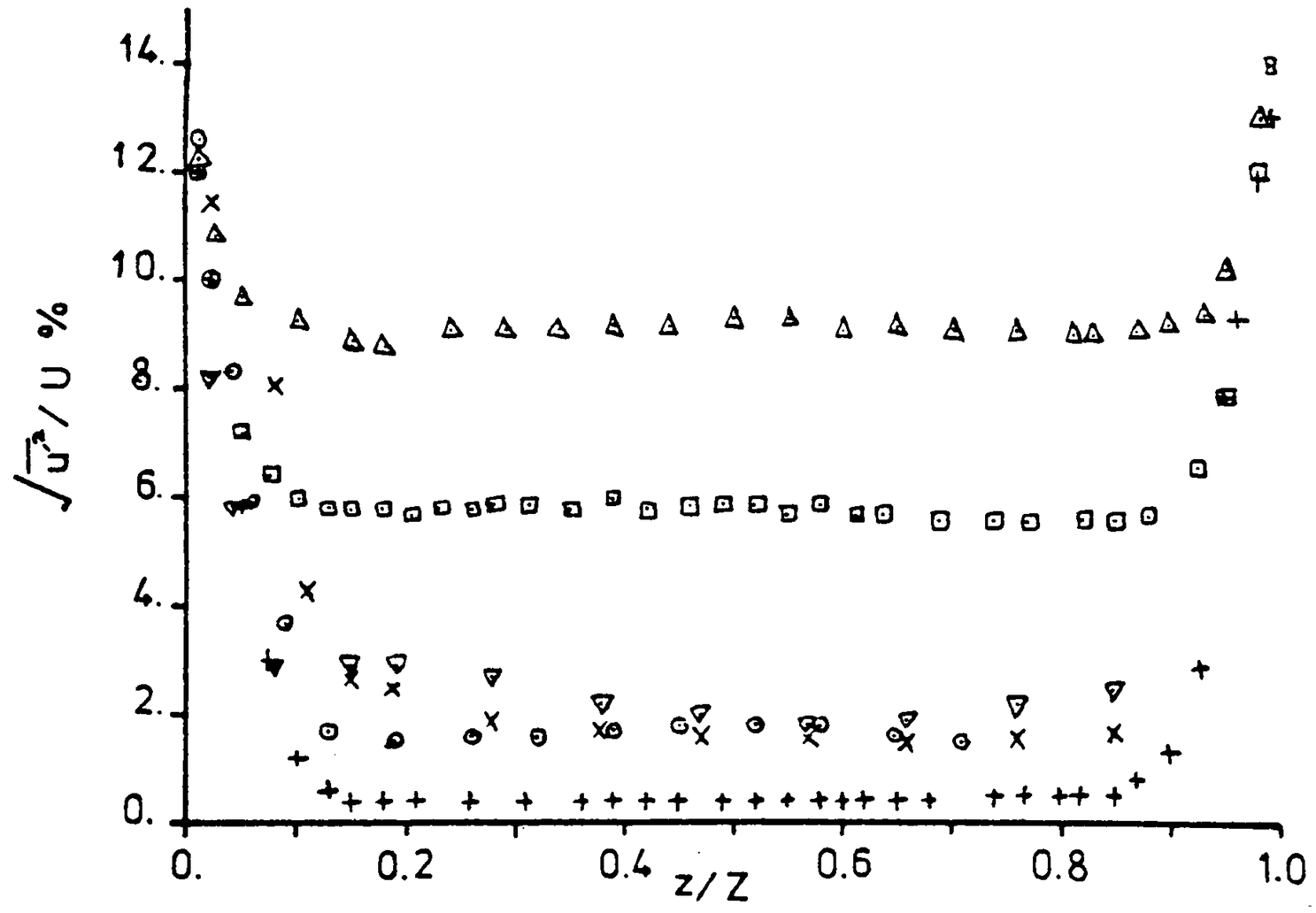

TURBULENCE INTENSITY PROFILES
DOWNSTREAM OF GRIDS

FIGURE 11

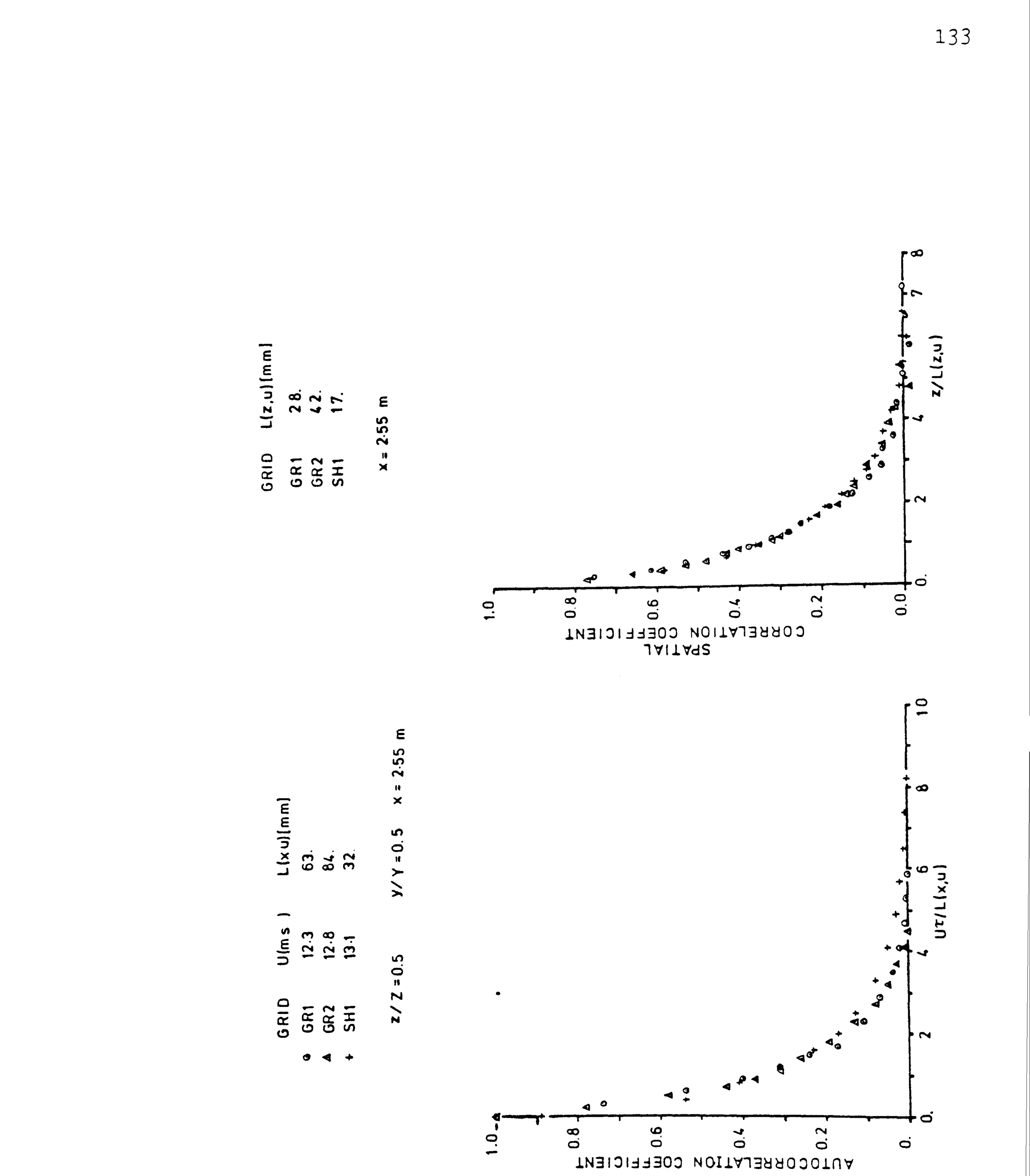

CORRELATION FUNCTIONS FOR TURBULENCE AND SHEAR GRID FLOWS

FIGURE 12

	R×E04	L(x,u)/D	L(z,u)/D	TURB%	FLOW
A	4.9	SMOOTH FLOW		0.4	GR0
B	4.9	1.31	0.58	5.7	GR1
C	4.9	1.75	0.88	9.1	GR2

D = 48 mm

Z = 770 mm

$\alpha = 0°$

○ WITHOUT END PLATES

△ WITH END PLATES (↓)

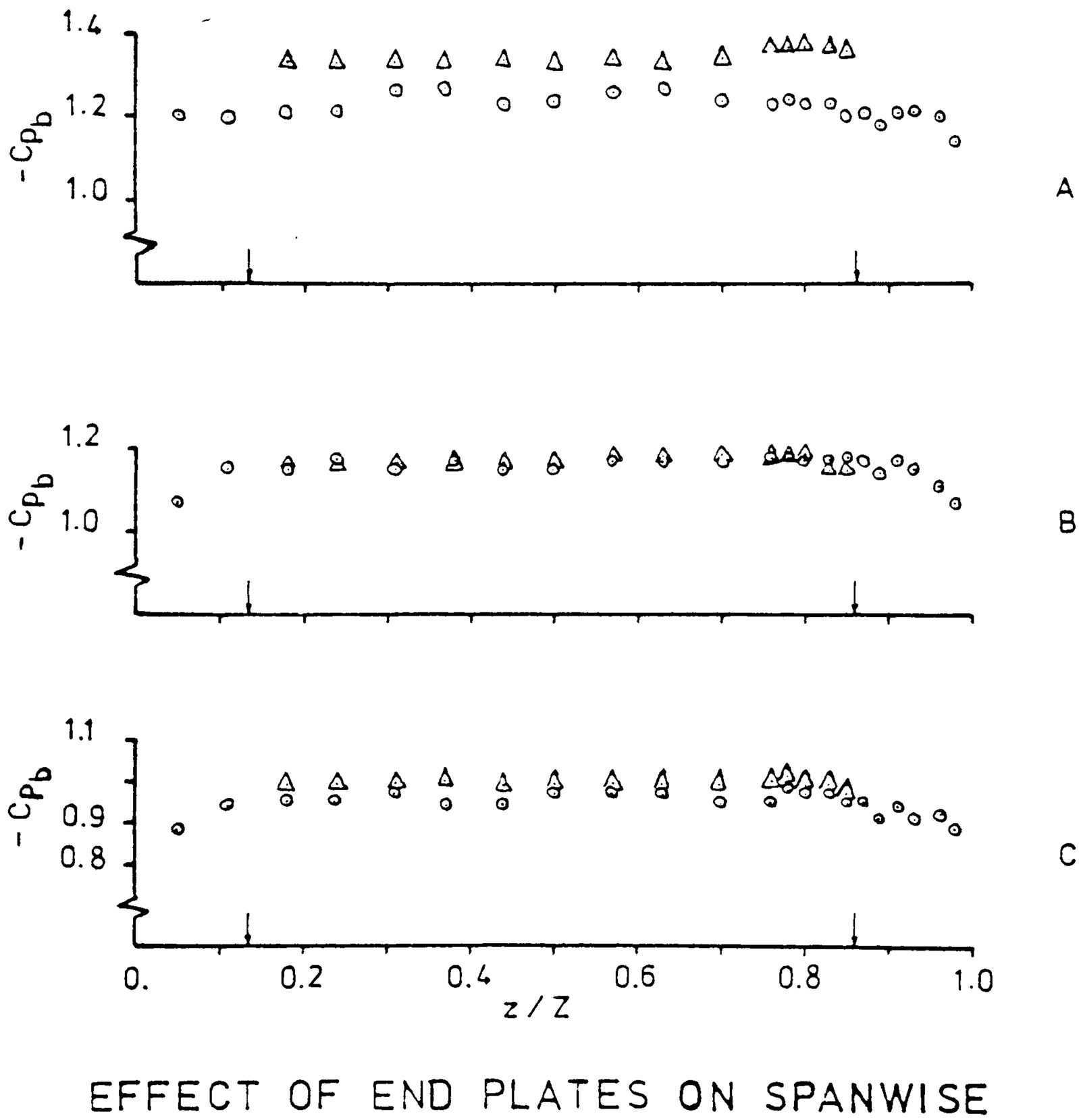

EFFECT OF END PLATES ON SPANWISE MEAN Cp IN UNIFORM FLOWS

FIGURE 13

R*E04	L(x,u)/D	L(z,u)/D	TURB %	FLOW
4.8	SMOOTH FLOW		0.4	GR0
4.8	1.31	0.58	5.7	GR1
4.8	1.75	0.88	9.1	GR2

SPANWISE MEAN Cp IN UNIFORM FLOWS
ON 48mm MODEL SPANNING TUNNEL
END PLATES PRESENT

FIGURE 14

	RxE04	L(x,u)/D	L(z,u)/D	TURB%	FLOW
⊡	4.8	SMOOTH	FLOW	0.4	GR0
⊙	4.8	1.31	0.58	5.7	GR1
△	4.8	1.75	0.88	9.1	GR2

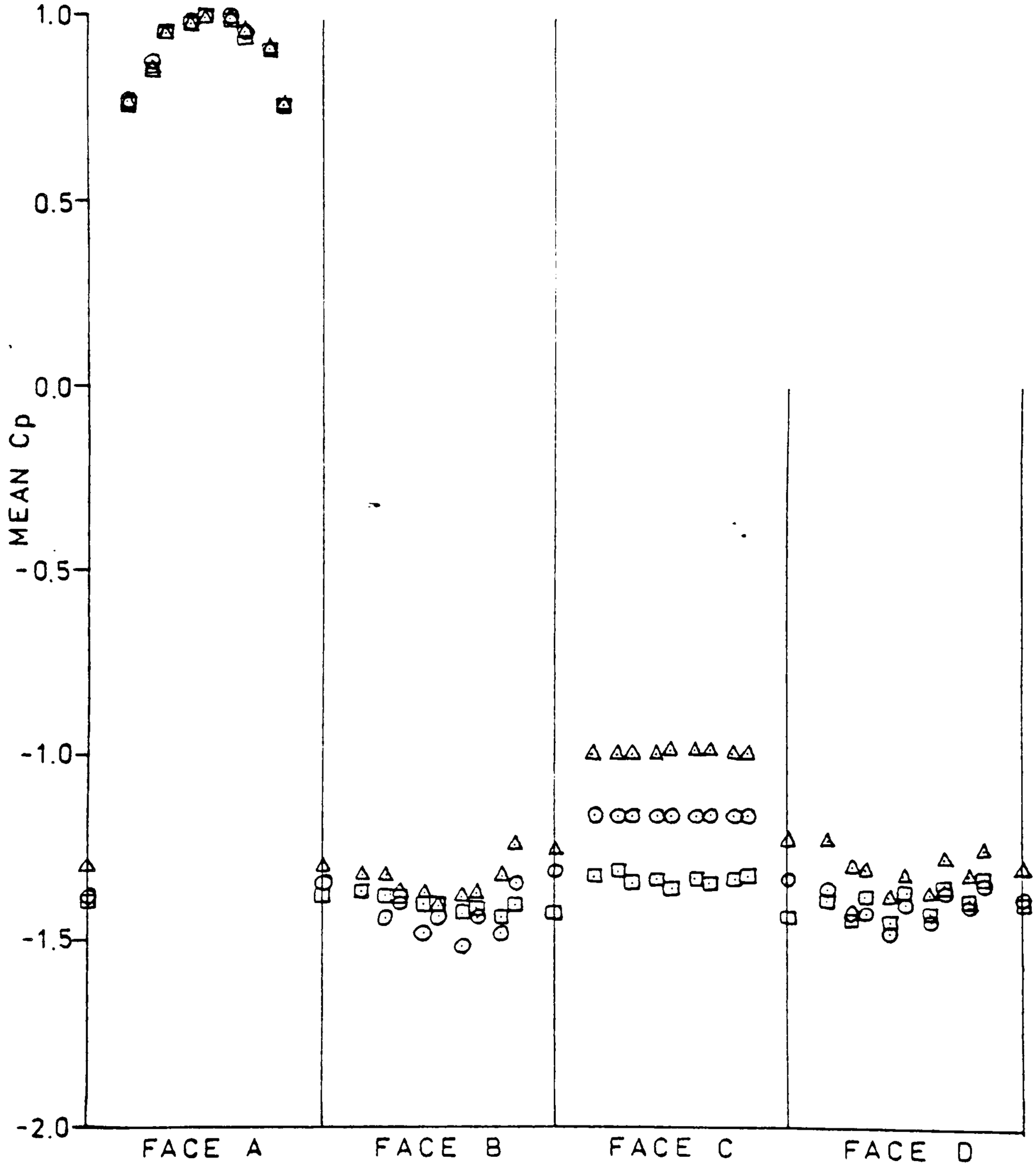

CIRCUMFERENTIAL Cp IN UNIFORM FLOWS ON 48mm MODEL AT $\alpha = 0°$ AND SPANNING TUNNEL WITH NO END PLATES

FIGURE 15

	R×E04	L(x,u)/D	L(z,u)/D	TURB%	FLOW
□	4·8	SMOOTH FLOW		0.4	GR0
○	4·8	1.31	0.58	5.7	GR1
△	4·8	1.75	0.88	9.1	GR2

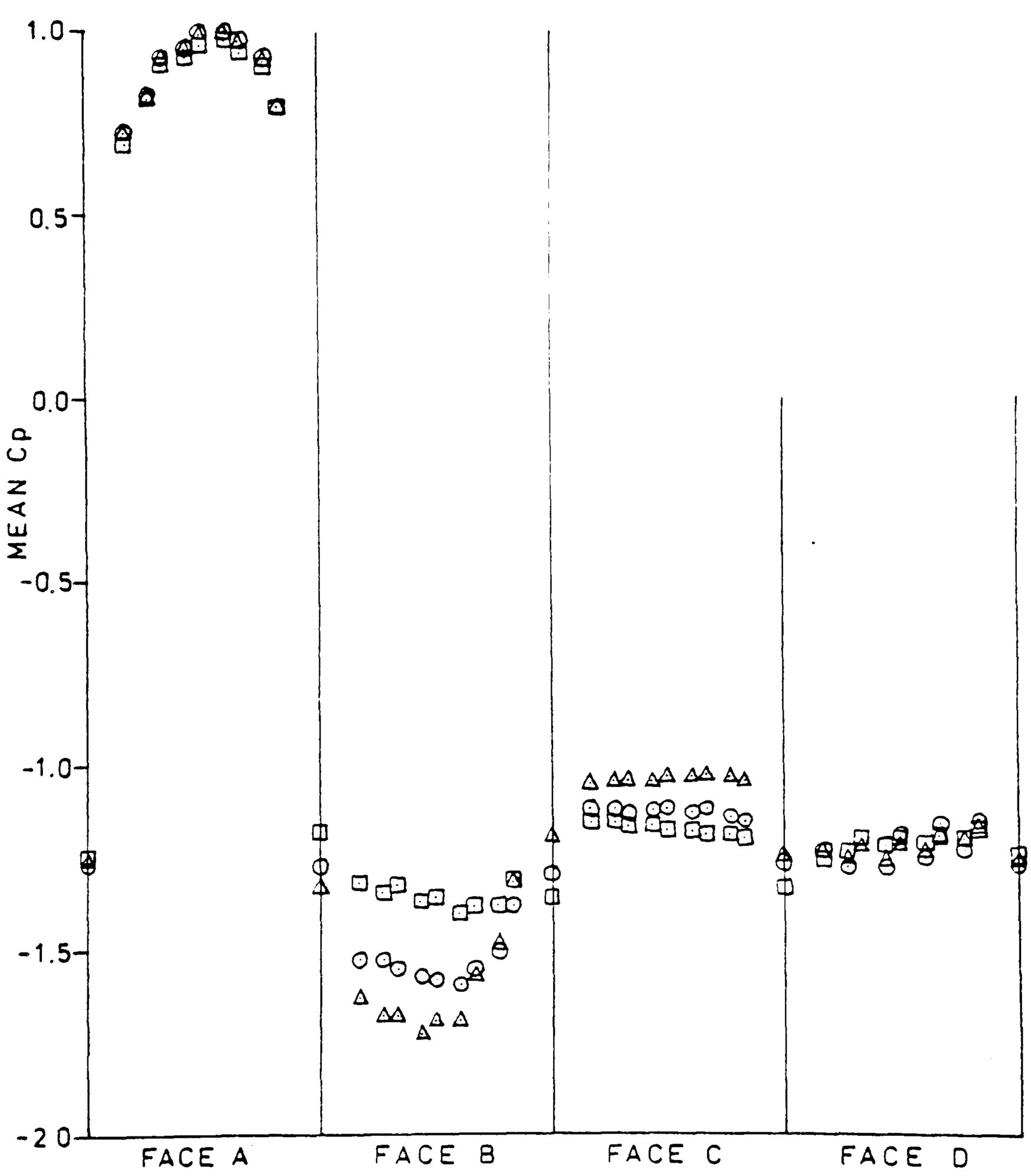

CIRCUMFERENTIAL Cp IN UNIFORM FLOWS ON 48mm MODEL AT $\alpha = 5°$ AND SPANNING TUNNEL WITH NO END PLATES

FIGURE 16

	RxE04	L(x,u)/D	L(z,u)/D	TURB%	FLOW
□	4.8	SMOOTH	FLOW	0.4	GR0
○	4.8	1.31	0.58	5.7	GR1
△	4.8	1.75	0.88	9.1	GR2

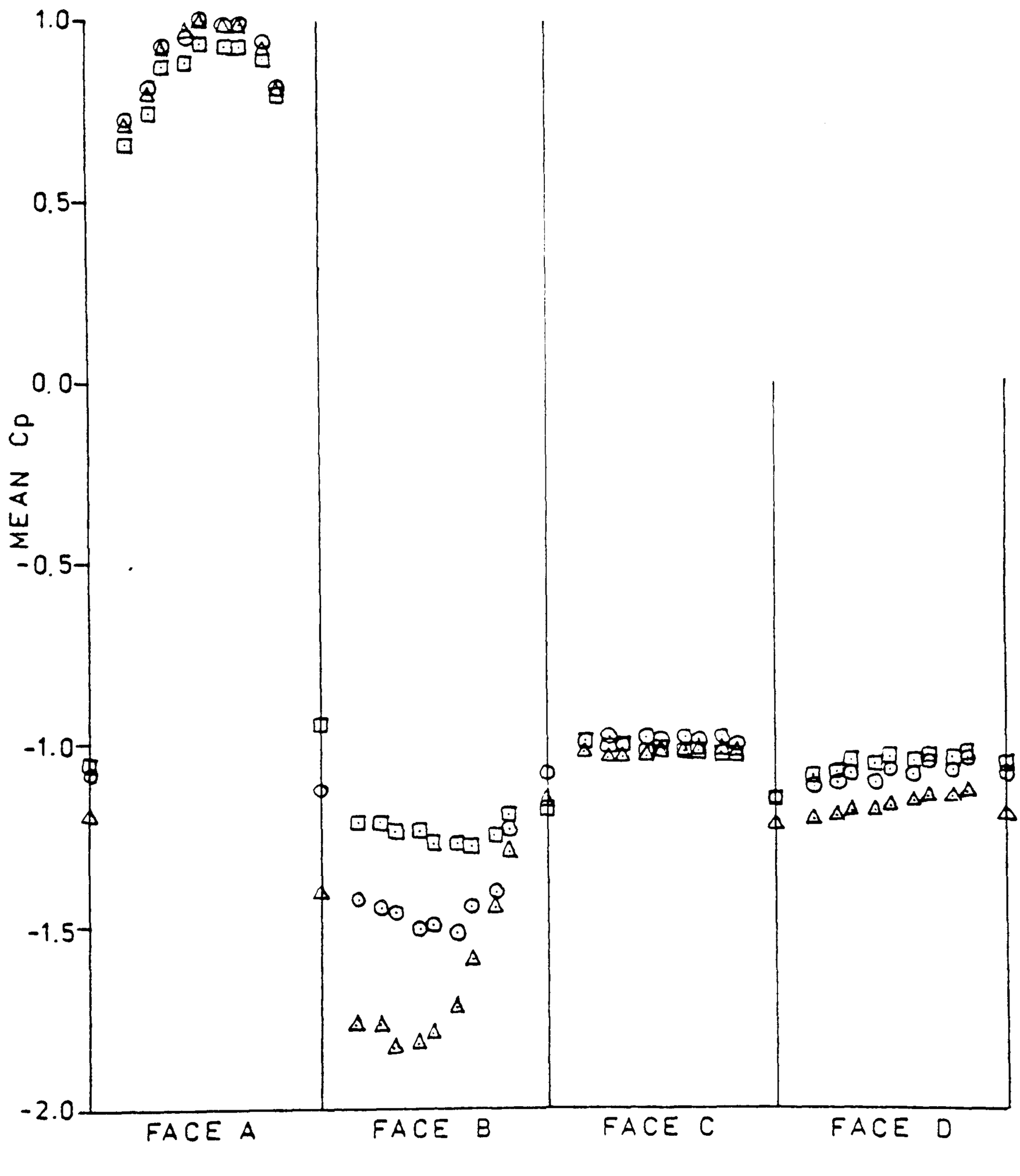

CIRCUMFERENTIAL Cp IN UNIFORM FLOWS ON 48mm MODEL AT $\alpha = 7°$ AND SPANNING TUNNEL WITH NO END PLATES

FIGURE 17

	R×E04	L(x,u)/D	L(z,u)/D	TURB %	FLOW
□	4.8	SMOOTH FLOW		0.4	GR0
○	4.8	1.31	0.58	5.7	GR1
△	4.8	1.75	0.88	9.1	GR2

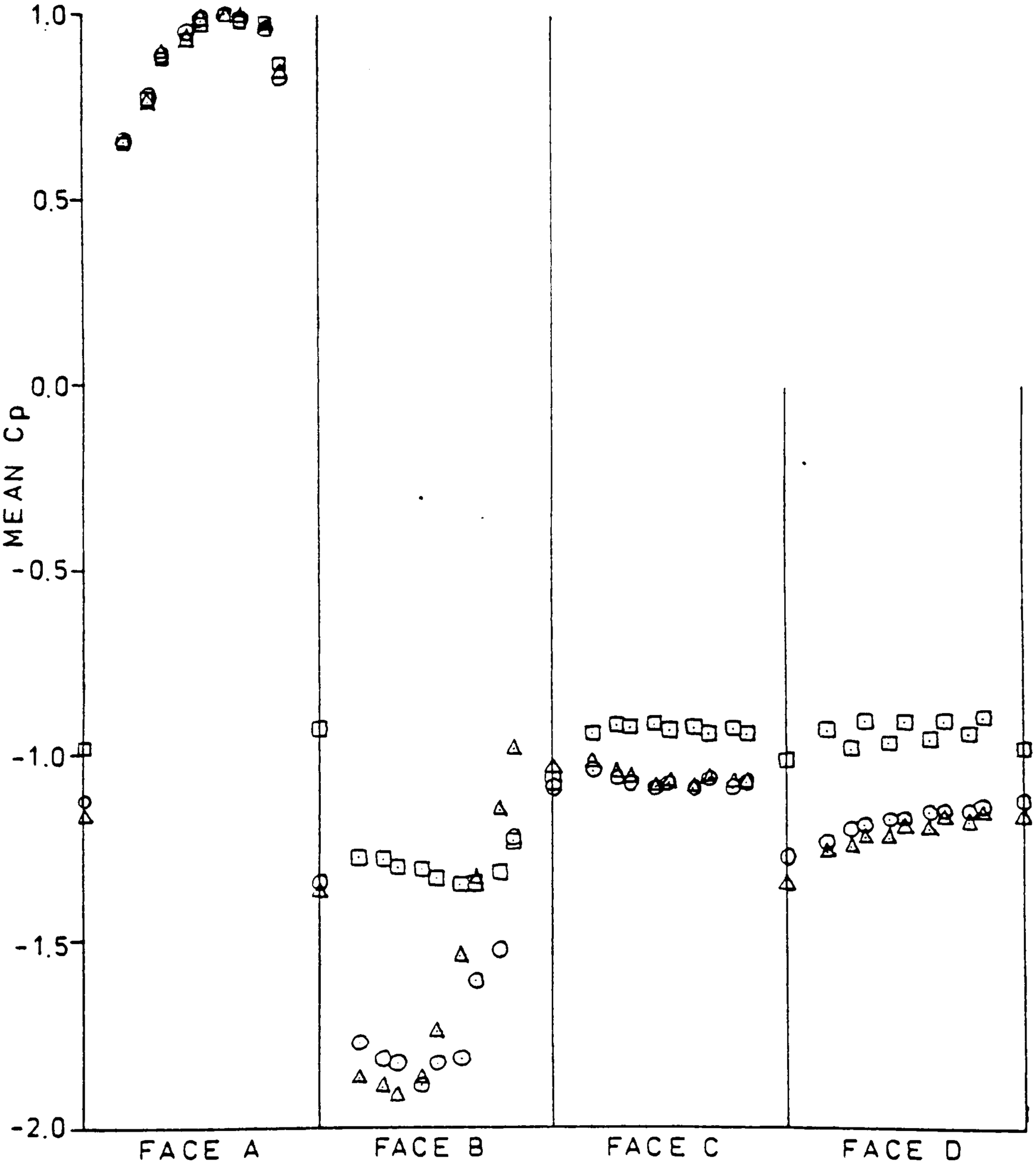

CIRCUMFERENTIAL Cp IN UNIFORM FLOWS ON 48mm MODEL AT $\alpha = 11°$ AND SPANNING TUNNEL WITH NO END PLATES

FIGURE 18

	R x E04	L(x,u)/D	L(z,u)/D	TURB %	FLOW
□	4.8	SMOOTH	FLOW	0.4	GR0
⊙	4.8	1.31	0.58	5.7	GR1
△	4.8	1.75	0.88	91	GR2

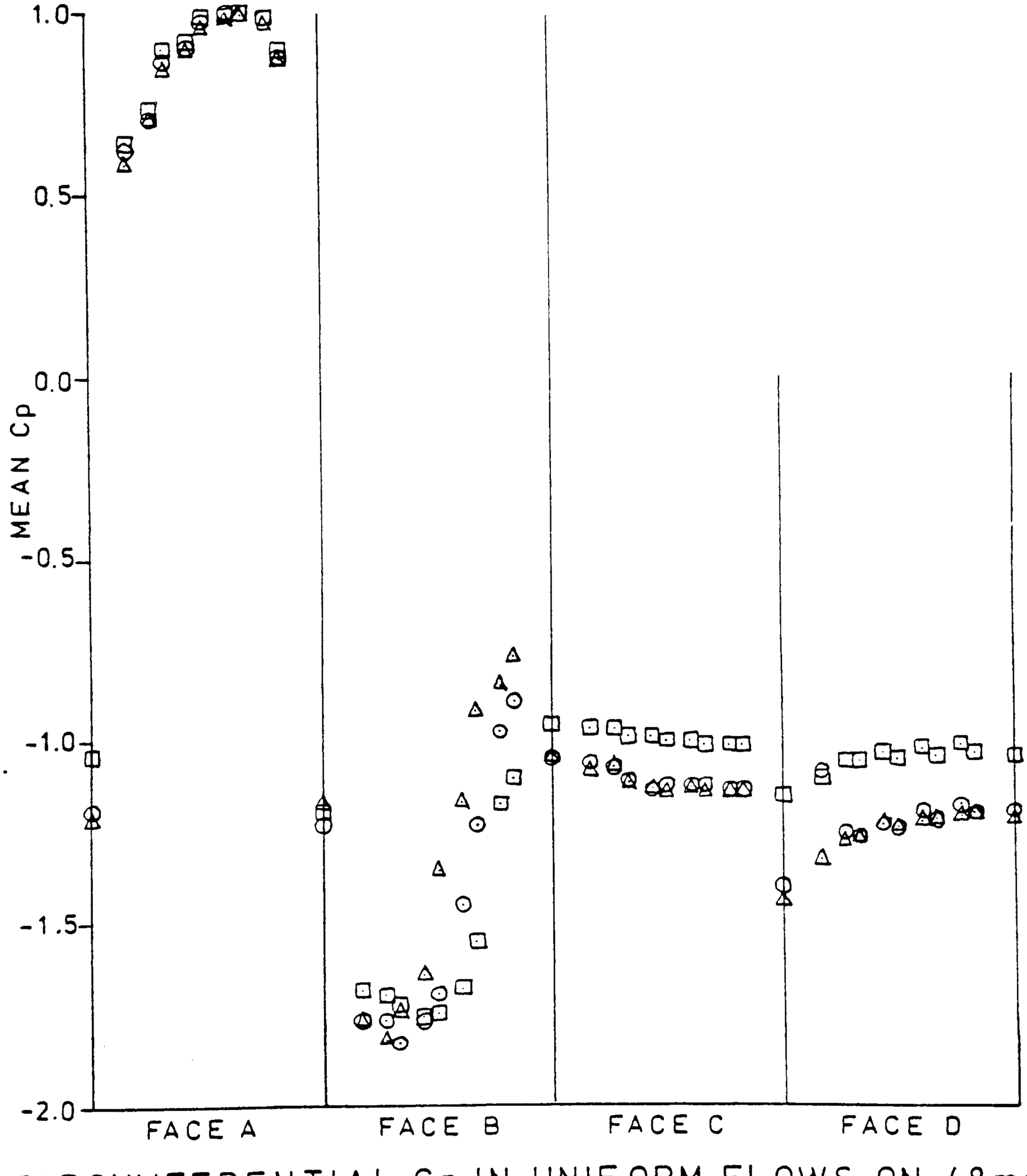

CIRCUMFERENTIAL Cp IN UNIFORM FLOWS ON 48mm MODEL AT $\alpha = 14°$ AND SPANNING TUNNEL WITH NO END PLATES

FIGURE 19

	R×E04	L(x,u)/D	L(z,u)/D	TURB%	FLOW
□	4.8	SMOOTH	FLOW	0.4	GR0
○	4.8	1.31	0.58	5.7	GR1
△	4.8	1.75	0.88	9.1	GR2

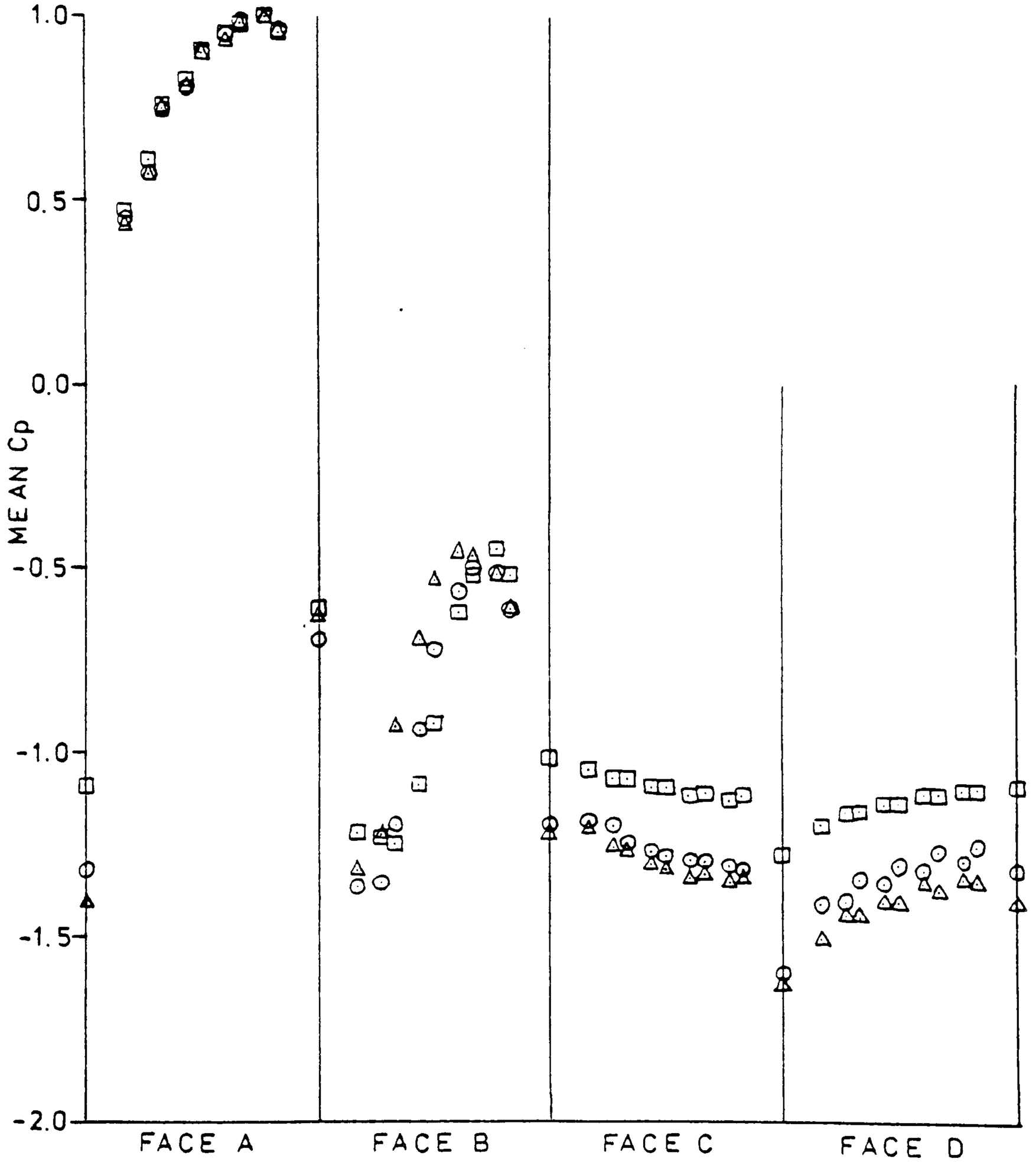

CIRCUMFERENTIAL Cp IN UNIFORM FLOWS ON 48mm MODEL AT $\alpha = 20°$ AND SPANNING TUNNEL WITH NO END PLATES

FIGURE 20

	RxE04	L(x,u)/D	L(z,u)/D	TURB%	FLOW
□	4.8	SMOOTH FLOW		0.4	GR0
○	4.8	1.31	0.58	5.7	GR1
△	4.8	1.75	0.88	9.1	GR2

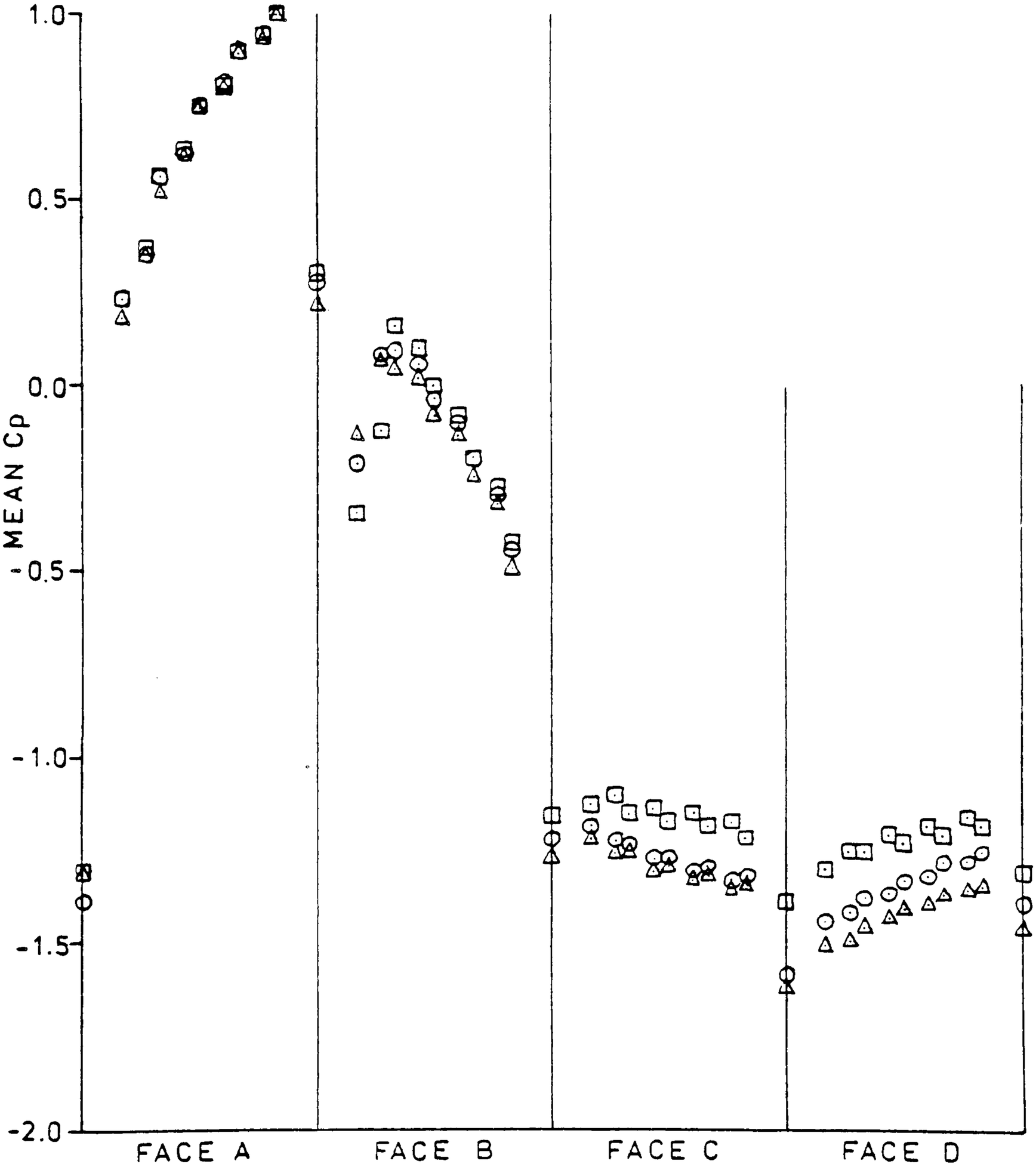

CIRCUMFERENTIAL Cp IN UNIFORM FLOWS ON 48mm MODEL AT $\alpha = 30°$ AND SPANNING TUNNEL WITH NO END PLATES

FIGURE 21

	RxE04	L(x,u)/D	L(z,u)/D	TURB%	FLOW
□	4.8	SMOOTH FLOW		0.4	GR0
○	4.8	1.31	0.58	5.7	GR1
△	4.8	1.75	0.88	9.1	GR2

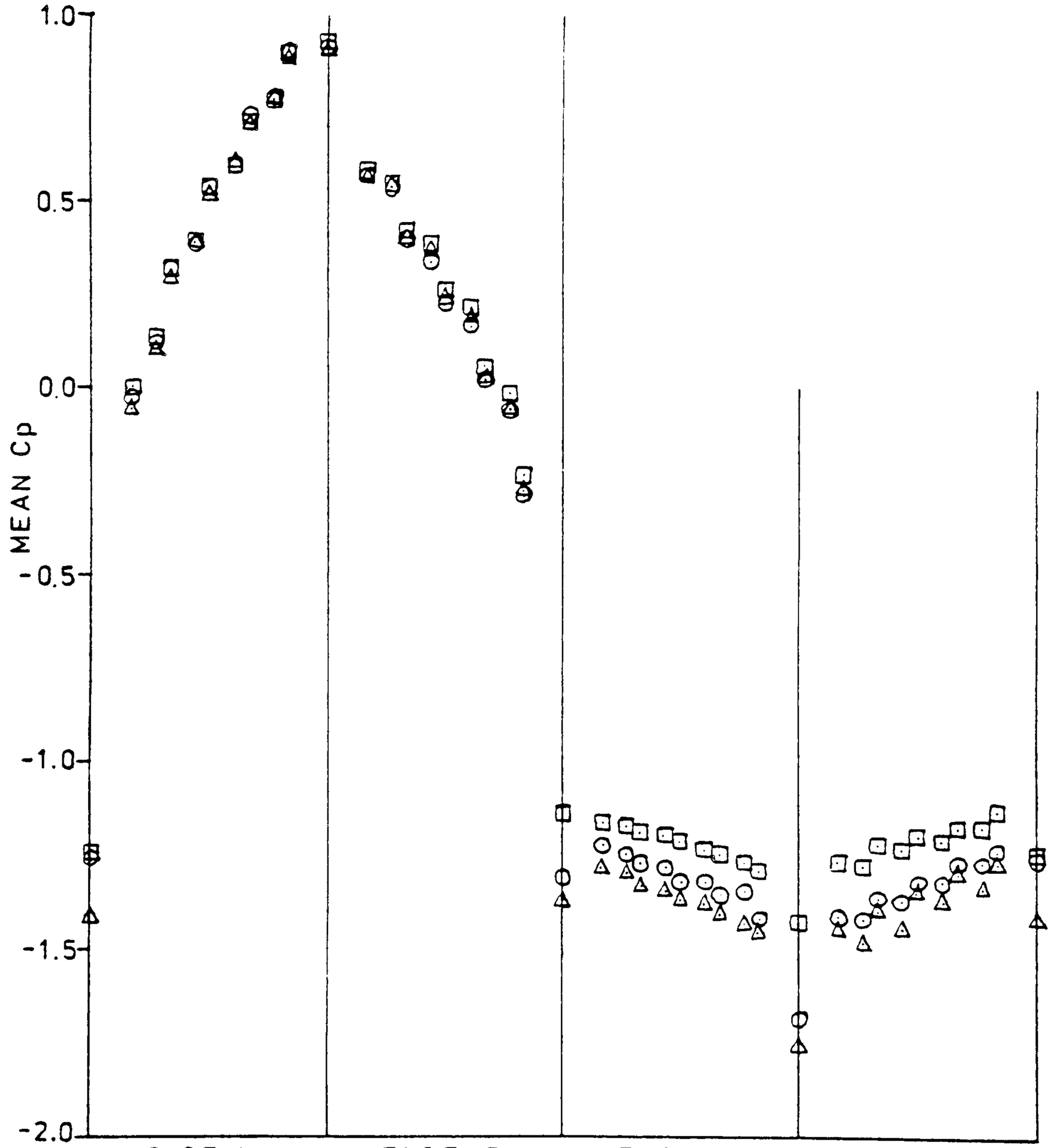

CIRCUMFERENTIAL Cp IN UNIFORM FLOWS ON 48mm MODEL AT $\alpha = 40°$ AND SPANNING TUNNEL WITH NO END PLATES

FIGURE 22

	RxE04	L(x,u)/D	L(z,u)/D	TURB%	FLOW
□	4.8	SMOOTH	FLOW	0.4	GR0
○	4.8	1.31	0.58	5.7	GR1
△	4.8	1.75	0.88	9.1	GR2

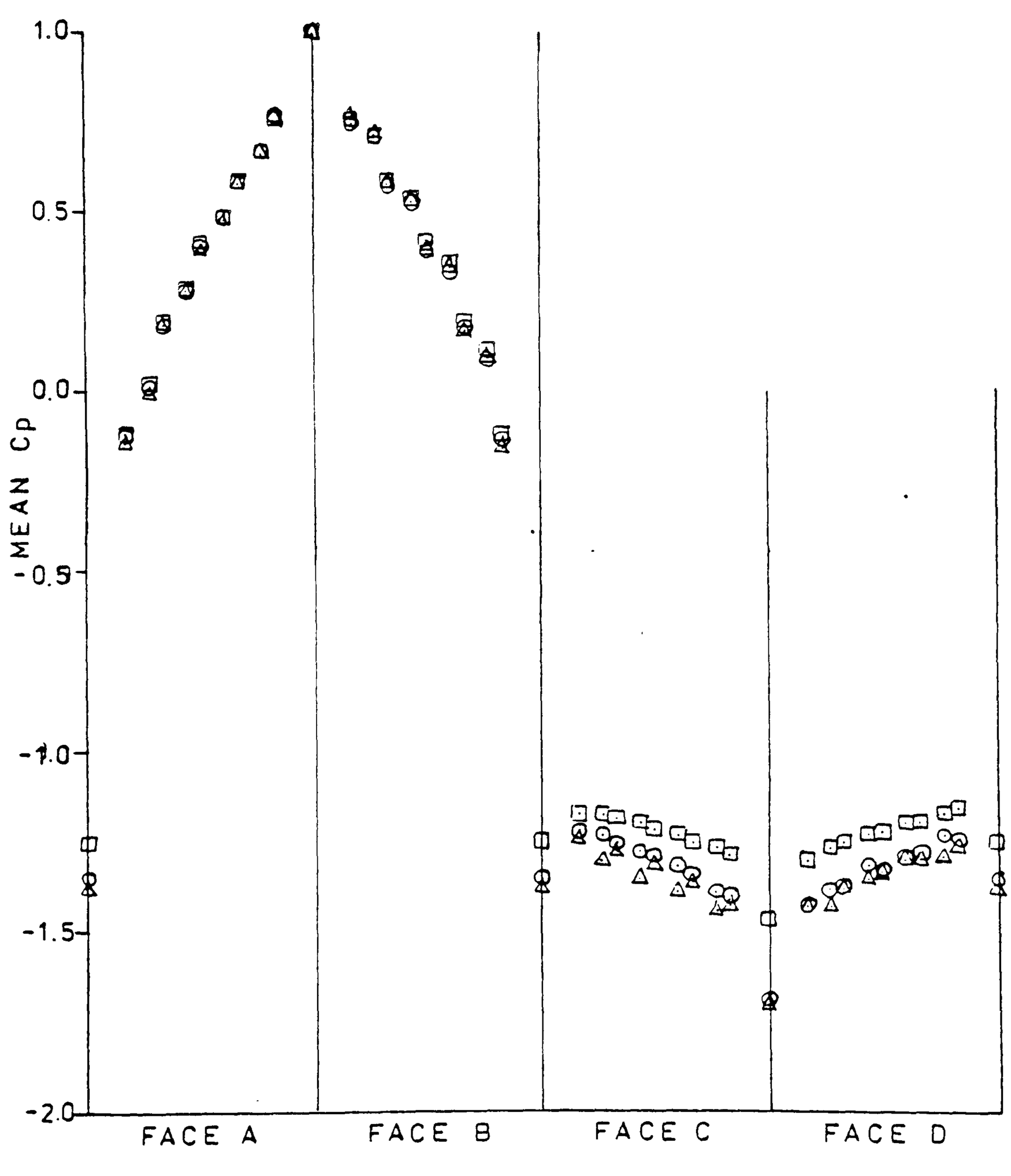

CIRCUMFERENTIAL Cp IN UNIFORM FLOWS ON 48mm MODEL AT $\alpha = 45°$ AND SPANNING TUNNEL WITH NO END PLATES

FIGURE 23

	R×E04	L(x,u)/D	L(z,u)/D	TURB %	FLOW
⊡	4·8	SMOOTH	FLOW	0.4	GR0
⊙	4·8	1 31	0 58	5.7	GR1
Δ	4·8	1 75	0.88	9.1	GR2
+	4·8	0.69	0.35	1.7	SH1

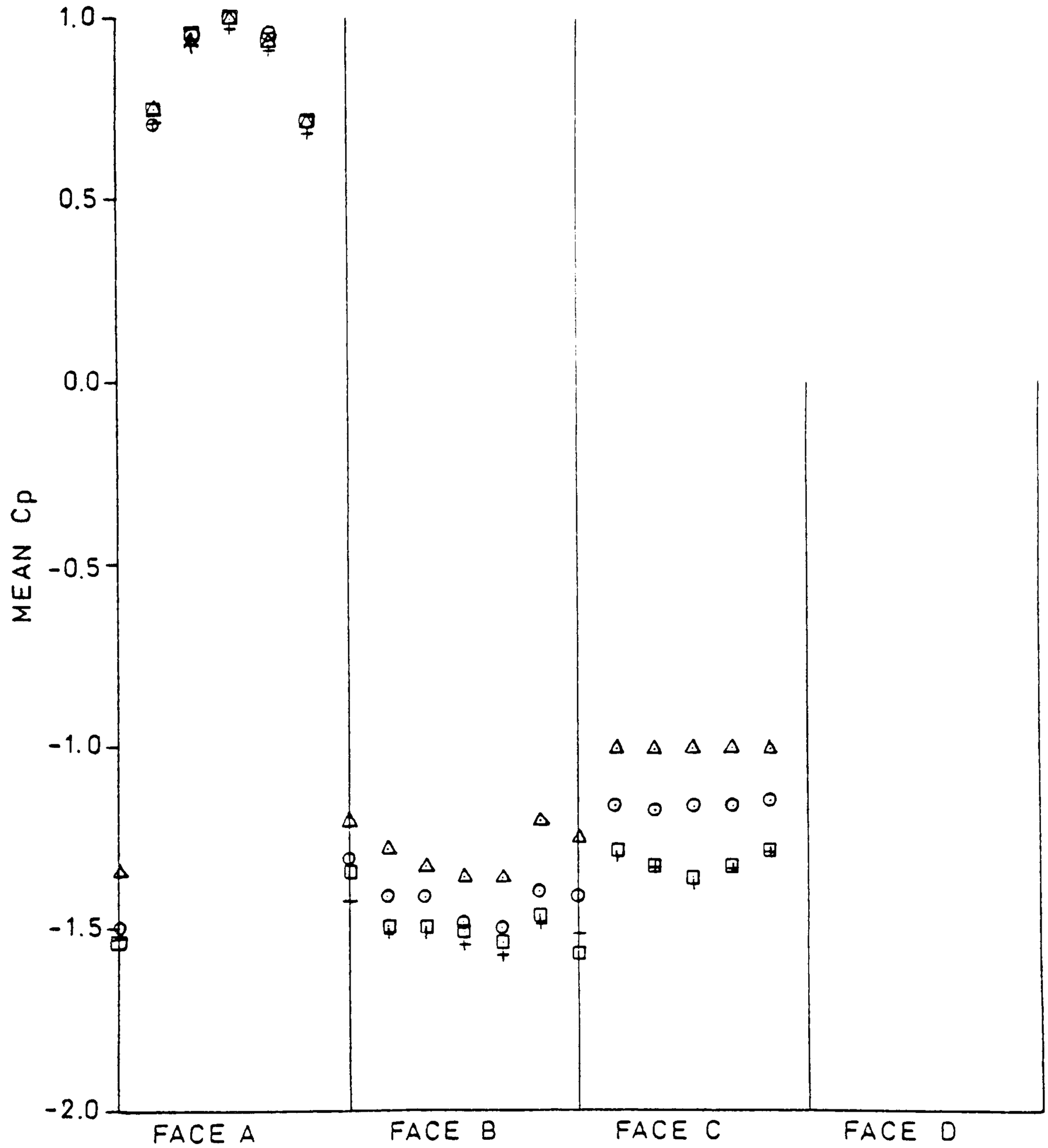

CIRCUMFERENTIAL Cp IN UNIFORM AND SHEAR FLOWS
FOR 48mm MODEL SPANNING TUNNEL. INCIDENCE = 0°
END PLATES PRESENT

FIGURE 24

	R x E04	L(x,u)/D	L(z,u)/D	TURB%	FLOW
⊡	4.8	SMOOTH	FLOW	0.4	GR0
⊙	4.8	1.31	0.58	5.7	GR1
Δ	4.8	1.75	0.88	9.1	GR2
+	4.8	0.69	0.35	1.7	SH1

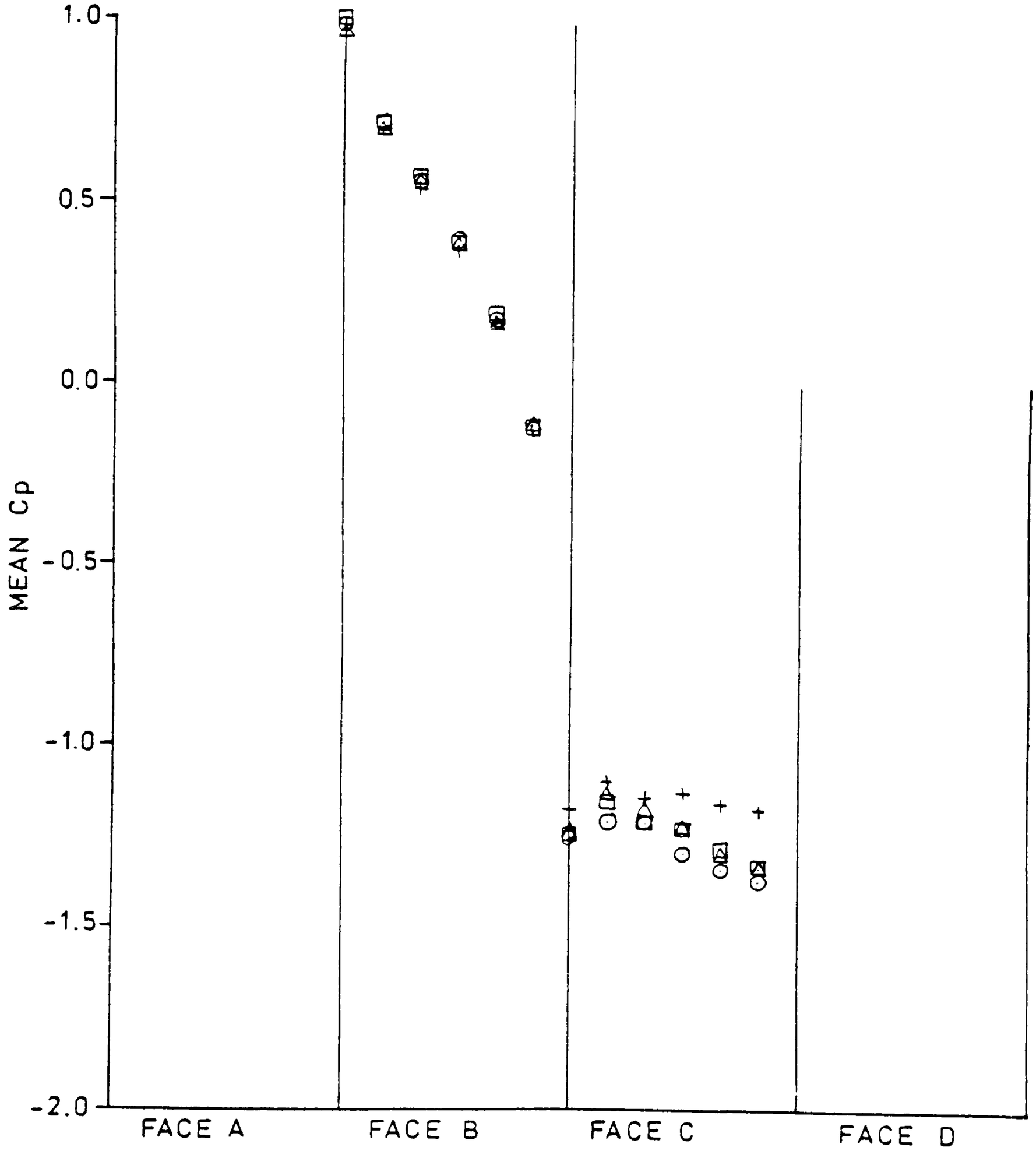

CIRCUMFERENTIAL Cp IN UNIFORM AND SHEAR FLOWS FOR 48mm MODEL SPANNING TUNNEL. INCIDENCE=45° END PLATES PRESENT

FIGURE 25

	R×E04	L(x,u)/D	L(z,u)/D	TURB%	FLOW
o	5.0	SMOOTH FLOW		0.4	GR0
Δ	4.9	1.31	0.58	5.7	GR1
+	4.9	1.75	0.88	9.1	GR2

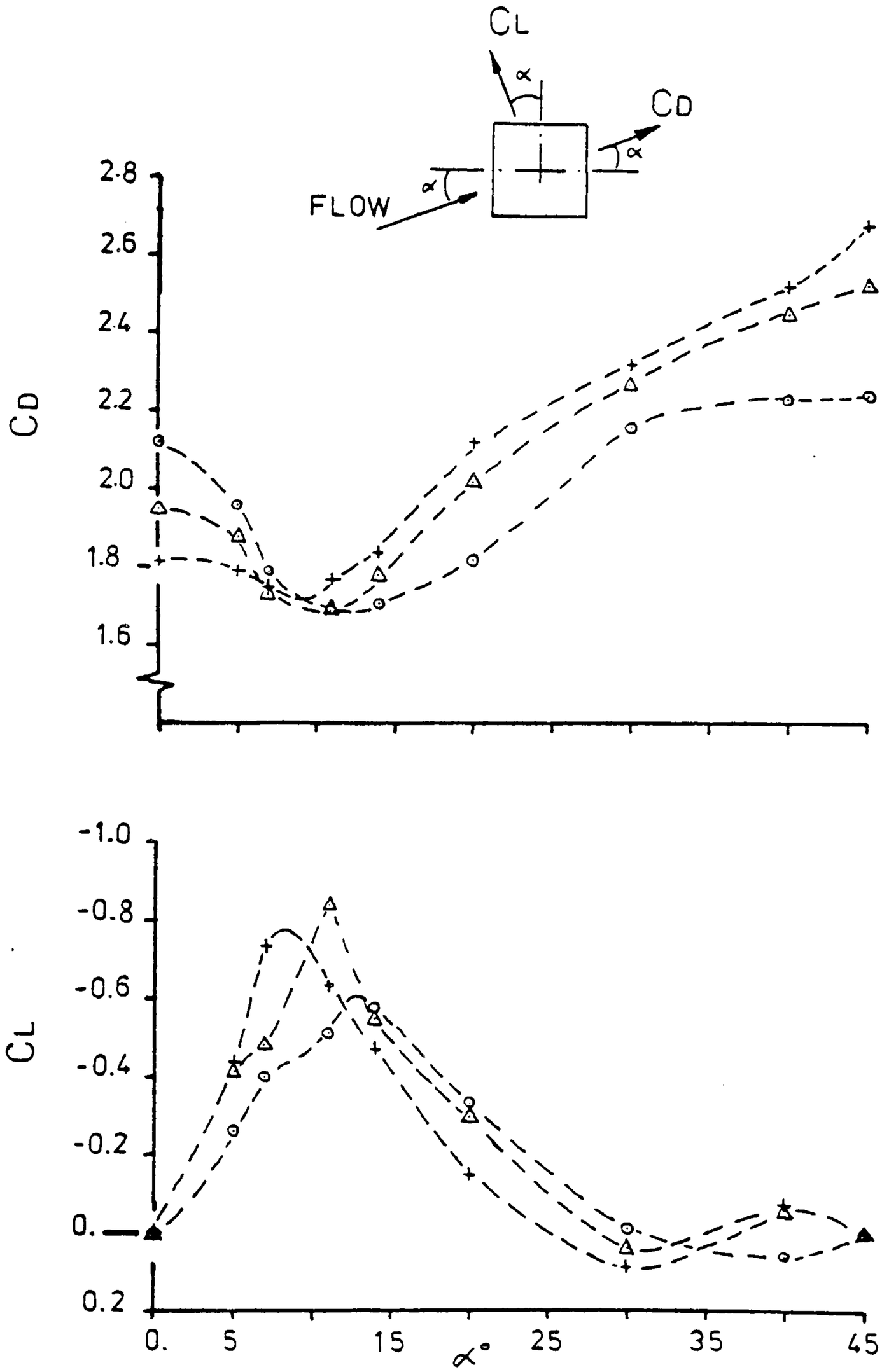

VARIATION OF C_D AND C_L WITH FLOW INCIDENCE IN UNIFORM FLOWS

FIGURE 26

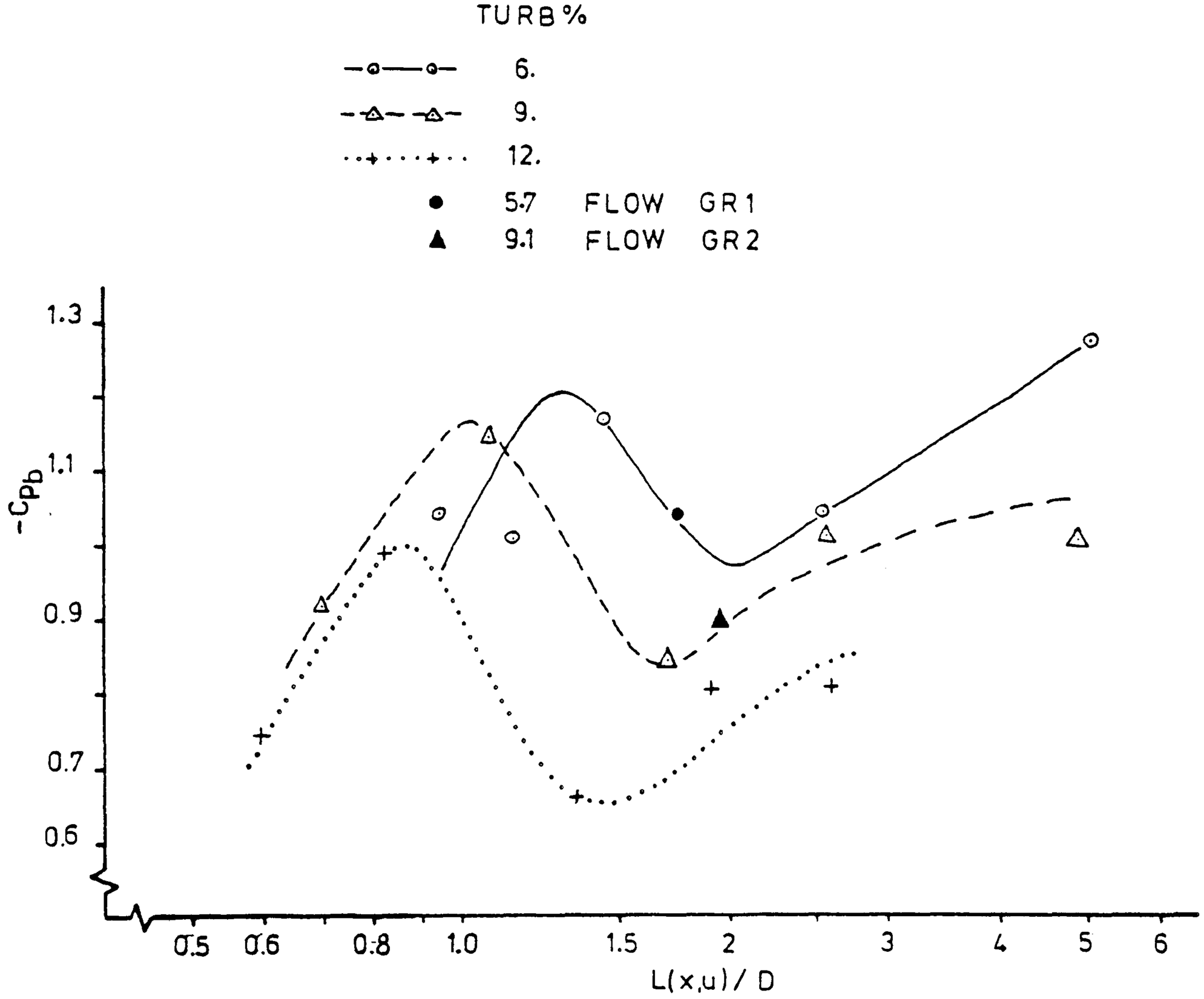

VARIATION OF BASE PRESSURE WITH LONGITUDINAL TURBULENCE LENGTH SCALE (after LEE, 1976)
INCIDENCE = 0°

FIGURE 27

	R×E04	L(x,u)/D	L(z,u)/D	TURB %	FLOW
□	4.8	SMOOTH FLOW		0.4	GR0
○	4.8	1·31	0.58	5.7	GR1
△	4·8	1·75	0.88	9.1	GR2

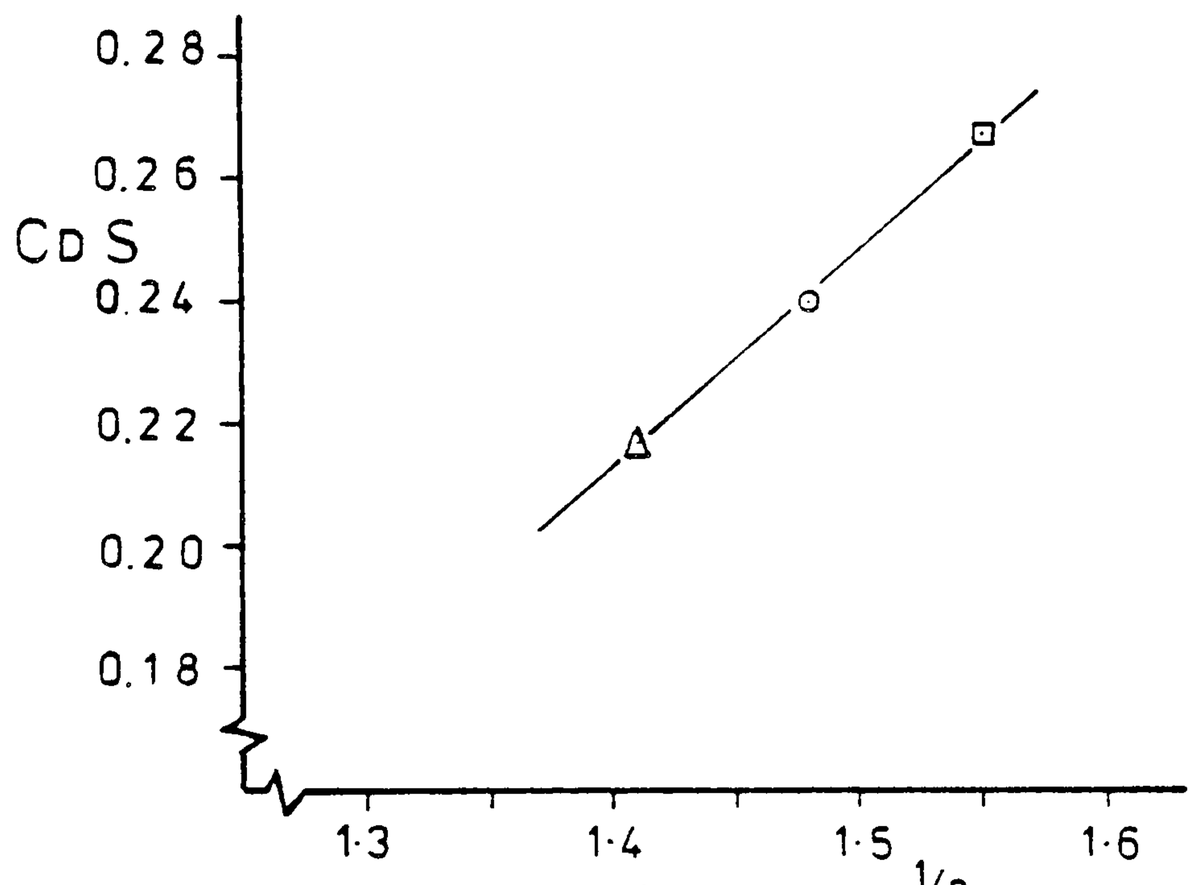

VARIATION OF C S WITH k IN UNIFORM FLOWS AT $\alpha = 0°$ FOR 48mm MODEL SPANNING TUNNEL

FIGURE 28

	R x E04	L(x,u)/D	L(z,u)/D	TURB%	FLOW
⊙	12.	SMOOTH	FLOW	0.4	GR0
△	12.	0.55	0.25	5.7	GR1
+	12.	0.74	0.37	9.1	GR2

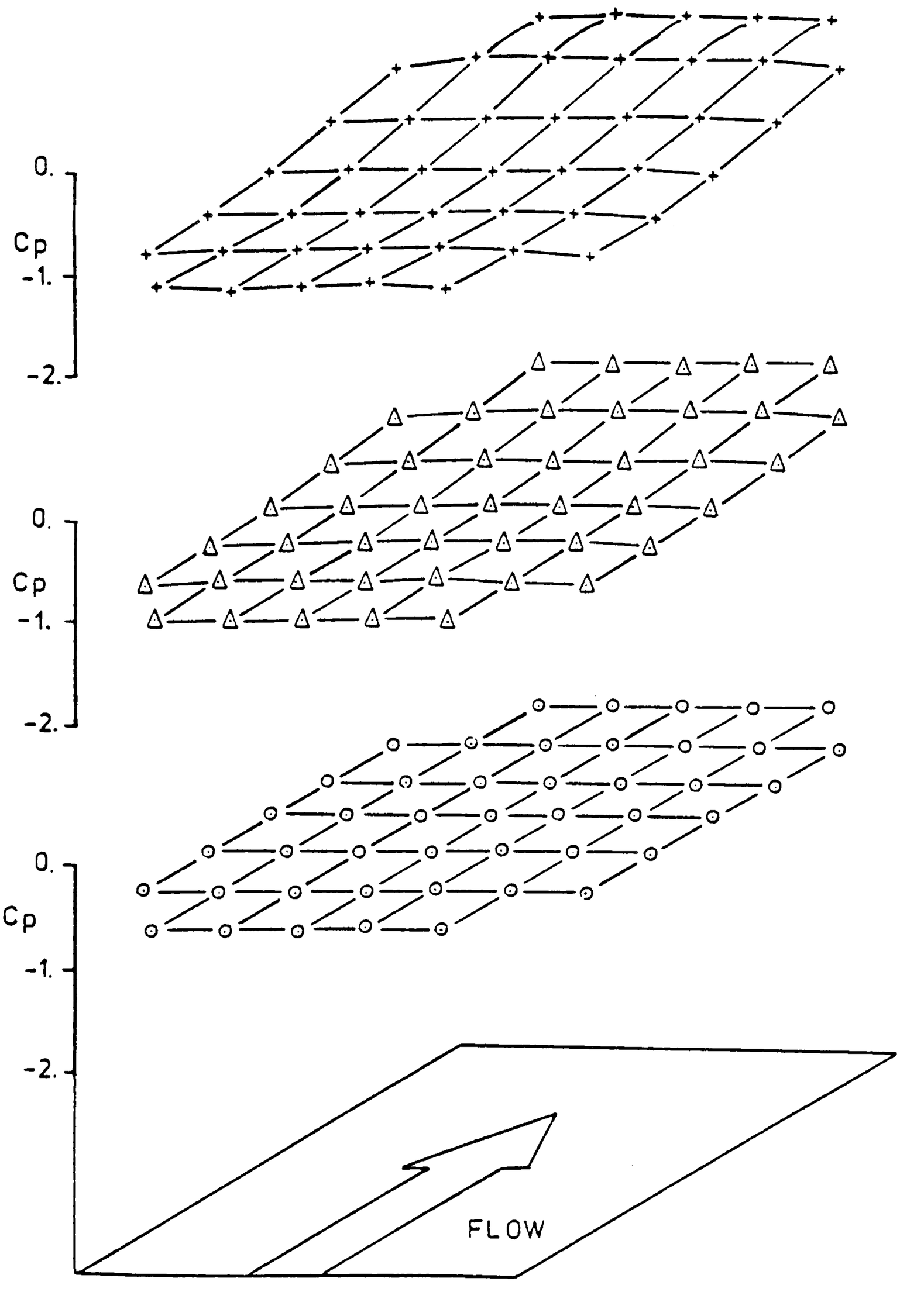

TOP SURFACE MEAN Cp IN UNIFORM FLOWS
ON 114mm MODEL AT $\alpha = 0°$ FOR H/D=3.3

FIGURE 29

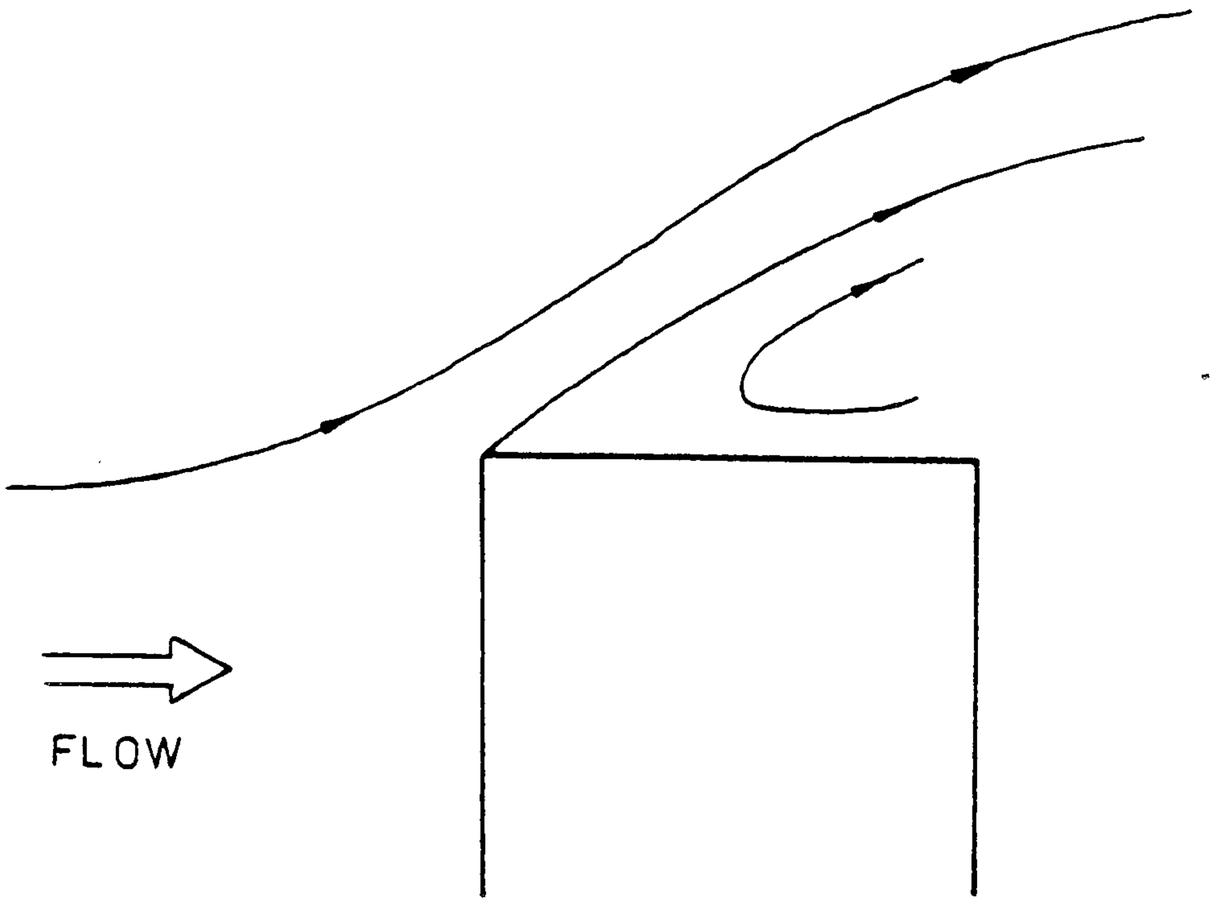

FLOW STREAMLINES OVER TOP SURFACE
IN SMOOTH FLOW FOR $\alpha = 0°$

FIGURE 30

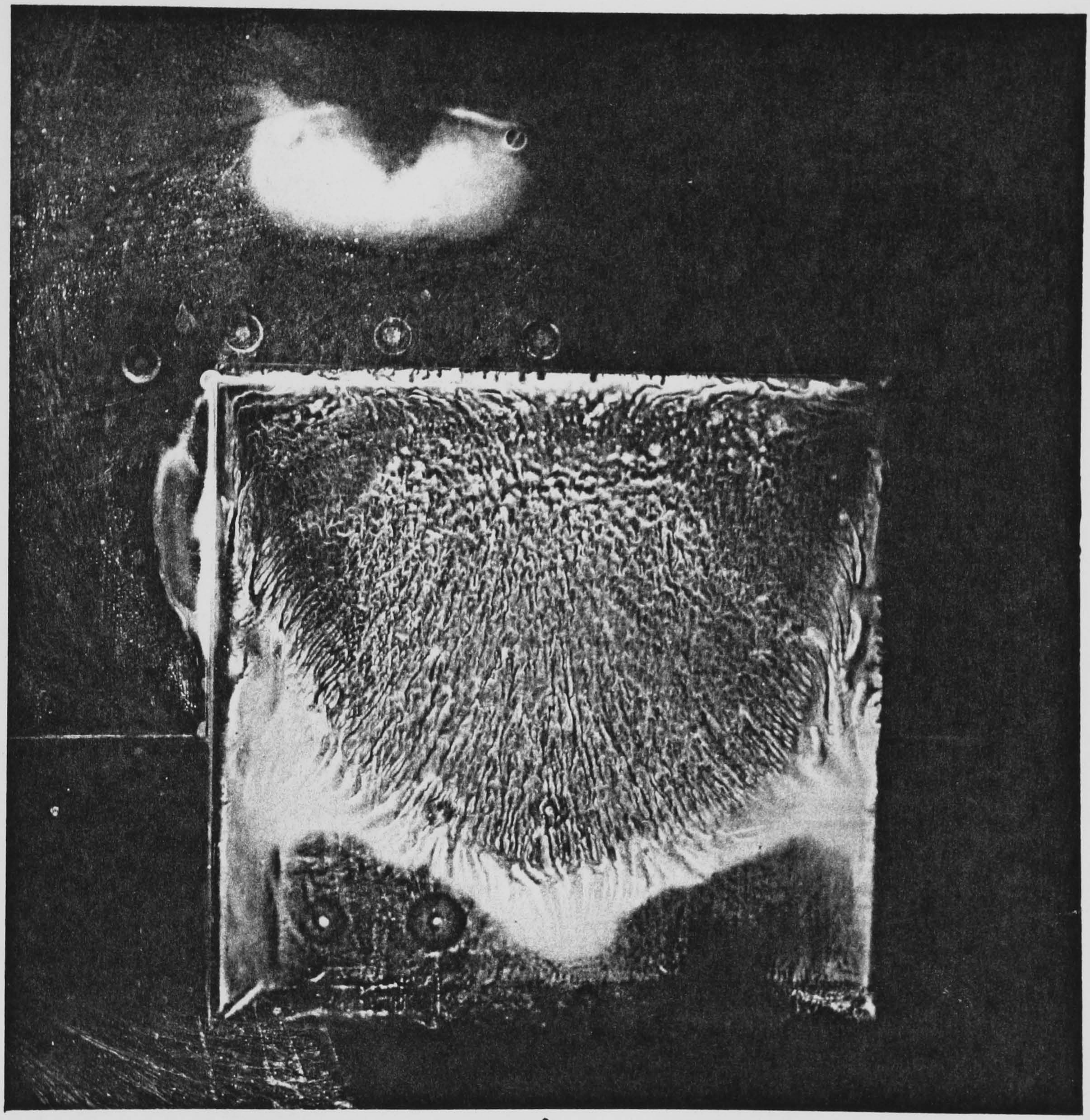

FLOW

TOP SURFACE FLOW PATTERN IN SMOOTH FLOW ON 114 mm MODEL AT α = 0° FOR H/D = 3.3

PLATE 1

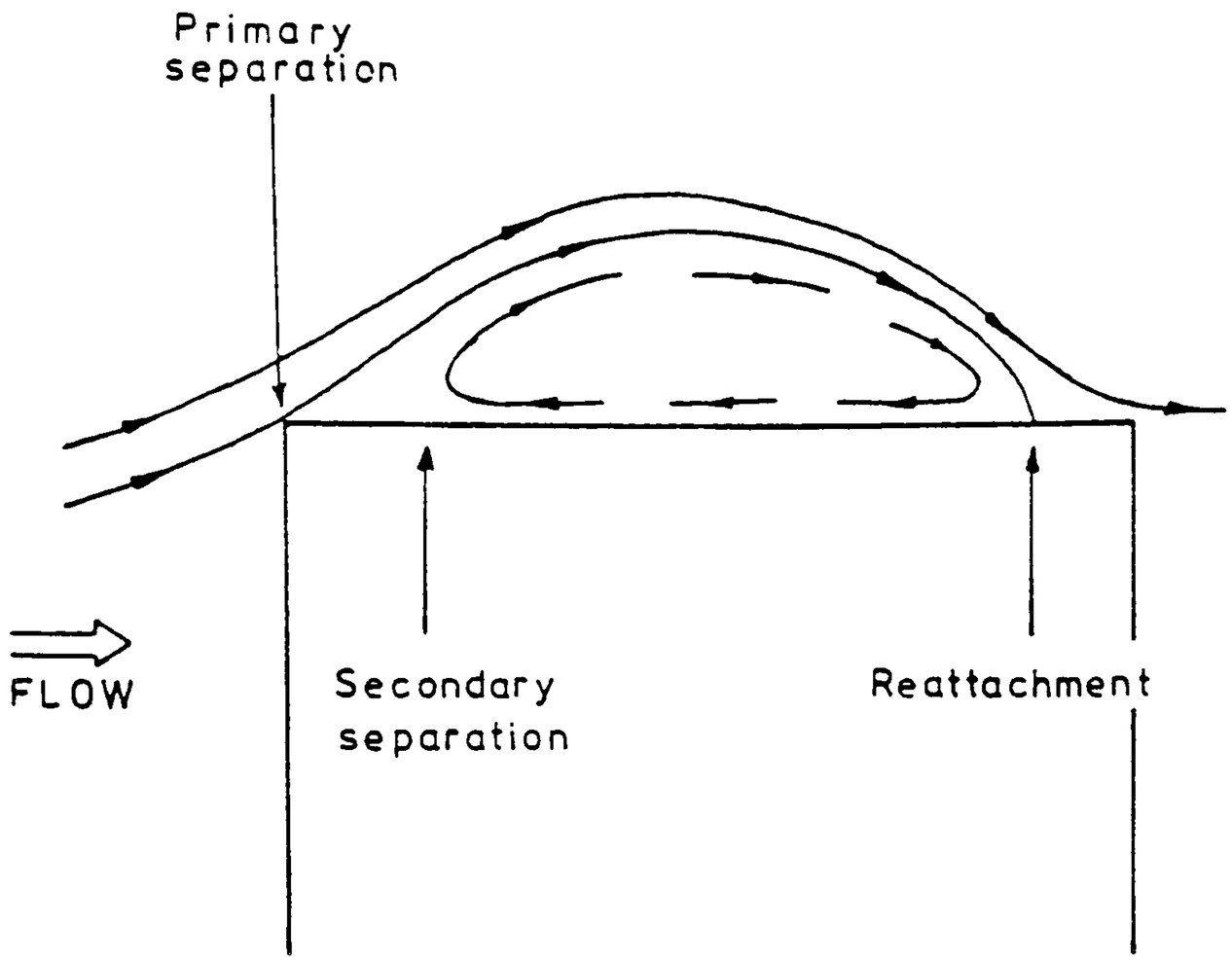

a) FLOW STREAMLINES OVER TOP SURFACE IN TURBULENT FLOW FOR $\alpha = 0°$

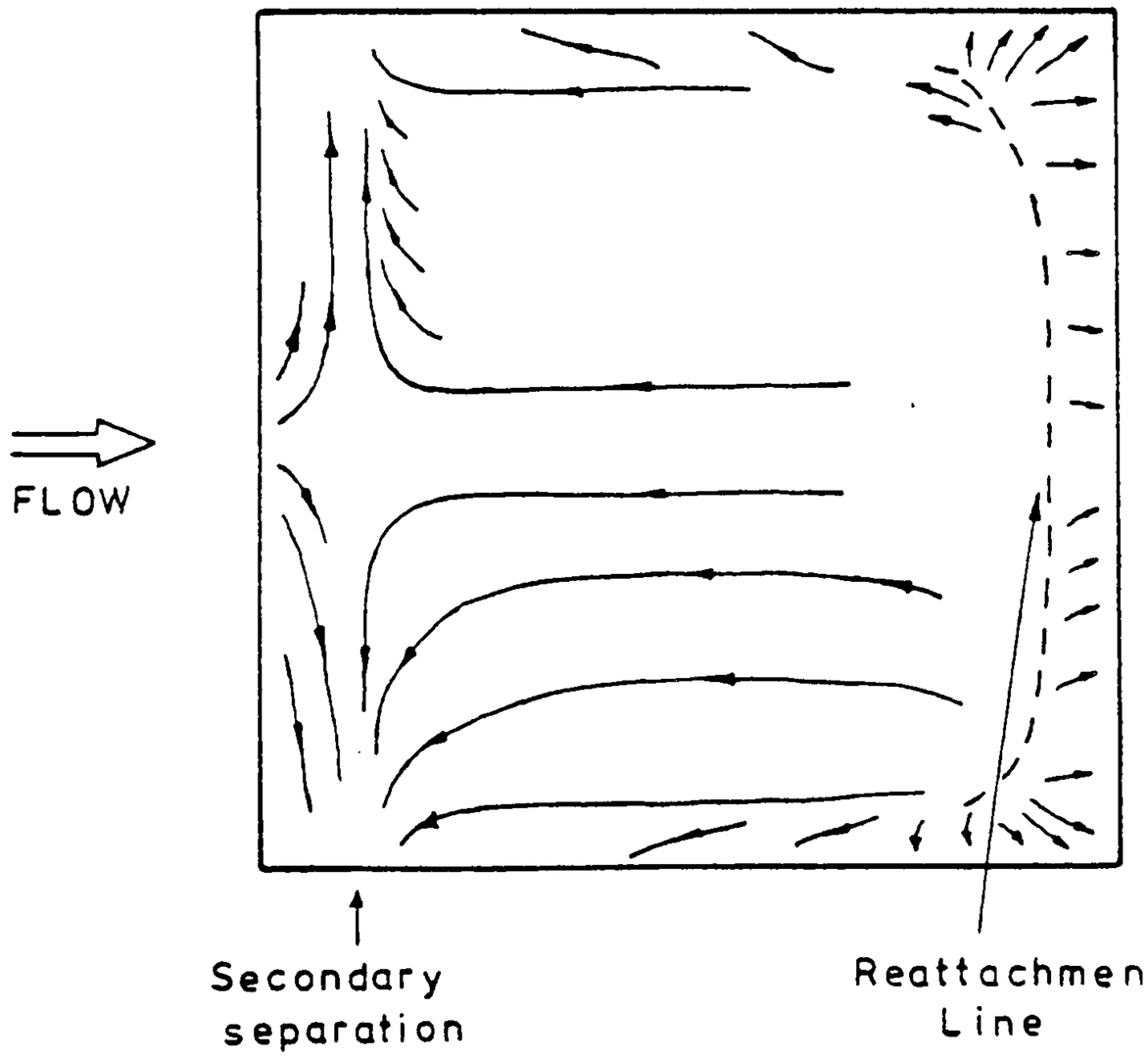

b) FLOW PATTERN ON TOP SURFACE IN TURBULENT FLOW FOR $\alpha = 0°$

FIGURE 31

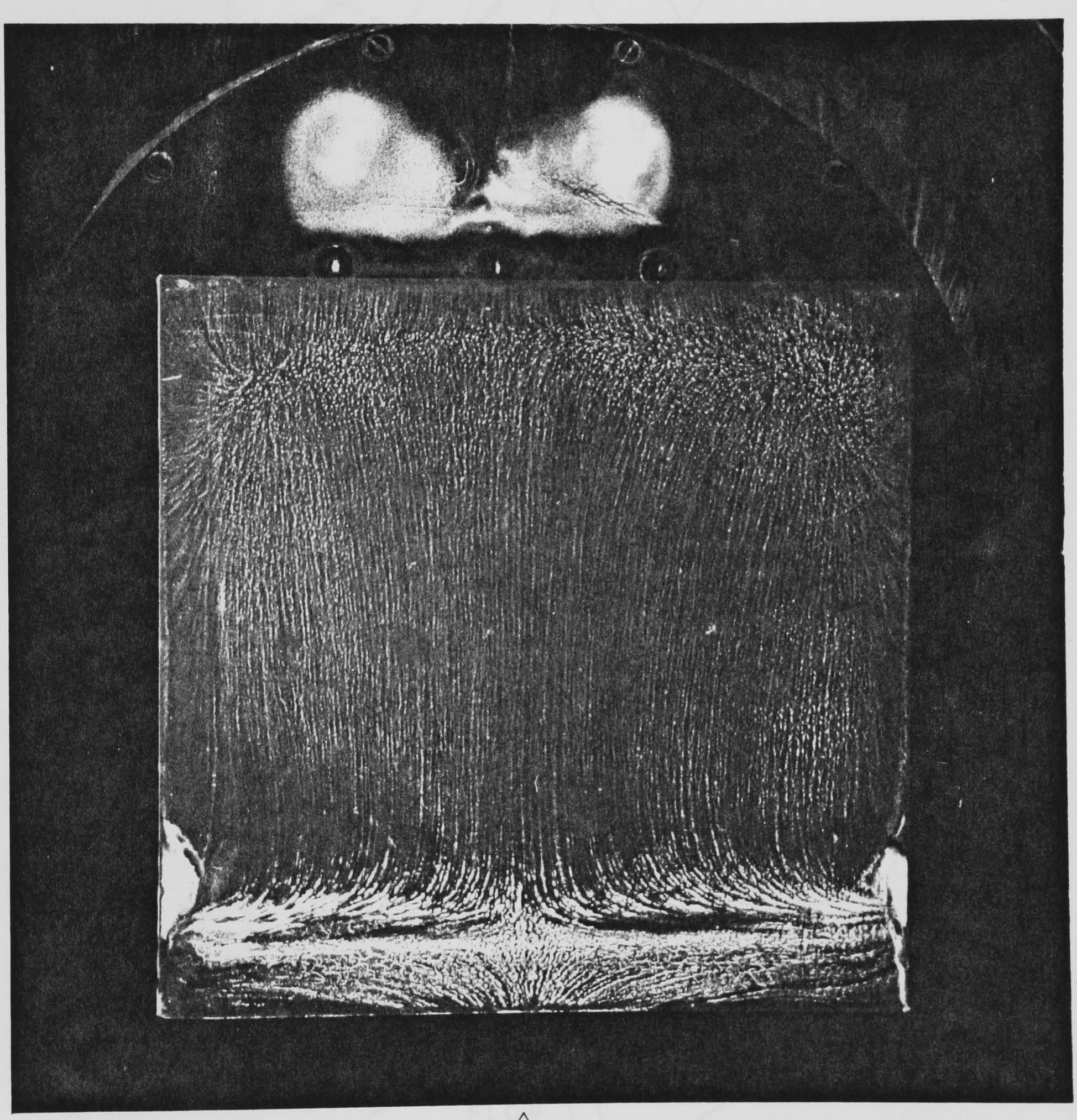

TOP SURFACE FLOW PATTERN IN TURBULENT FLOW ON 114mm MODEL AT $\alpha = 0°$ FOR H/D=3.3

PLATE 2

	R×E04	L(x,u)/D	L(z,u)/D	TURB%	FLOW
⊙	12.	SMOOTH FLOW		0.4	GR0
Δ	12.	0.55	0.25	5 7	GR1
+	12.	0.74	0.37	9.1	GR2

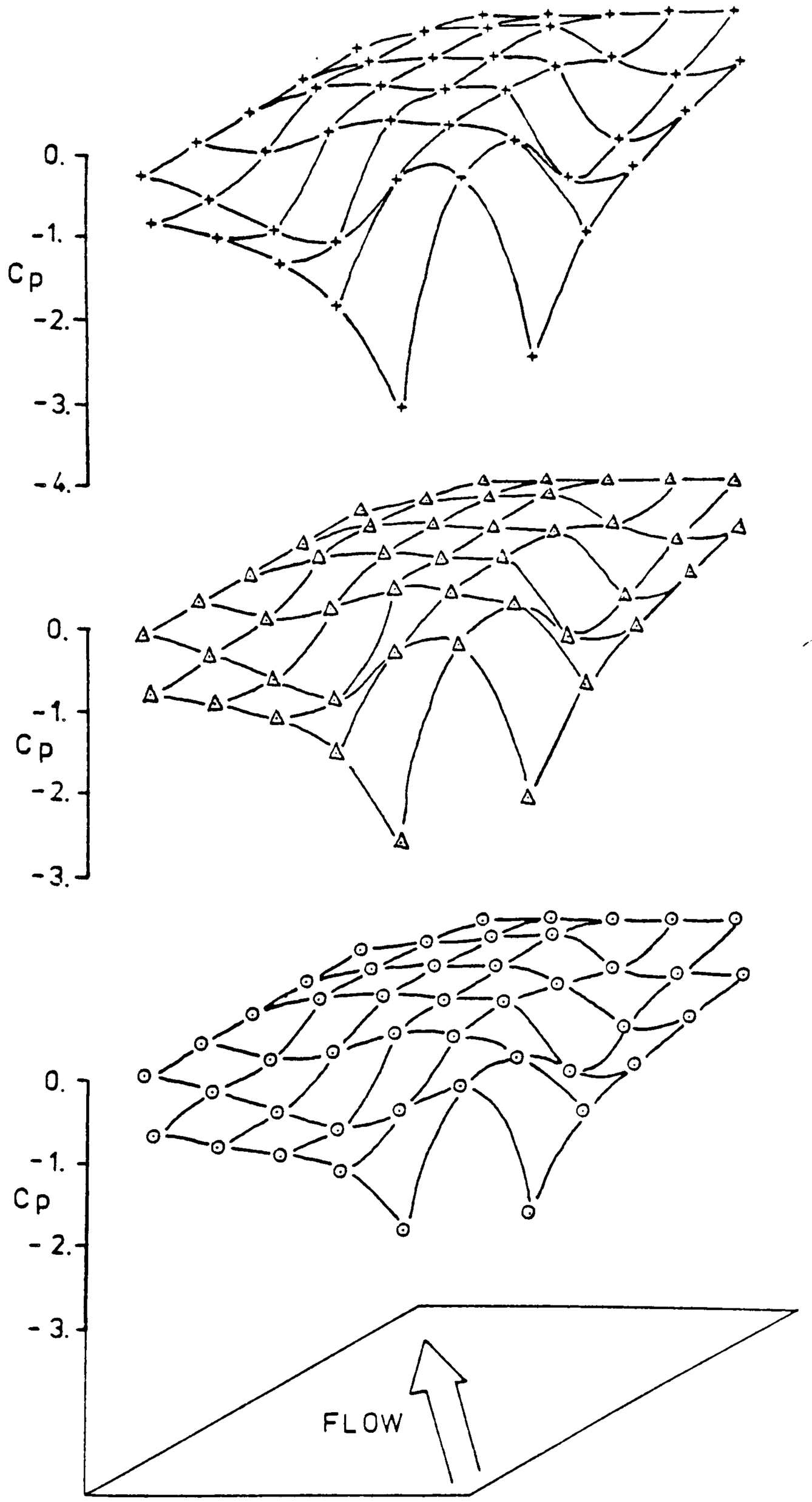

TOP SURFACE MEAN Cp IN UNIFORM FLOWS ON 114mm MODEL AT α =45° FOR H/D=3.3

FIGURE 32

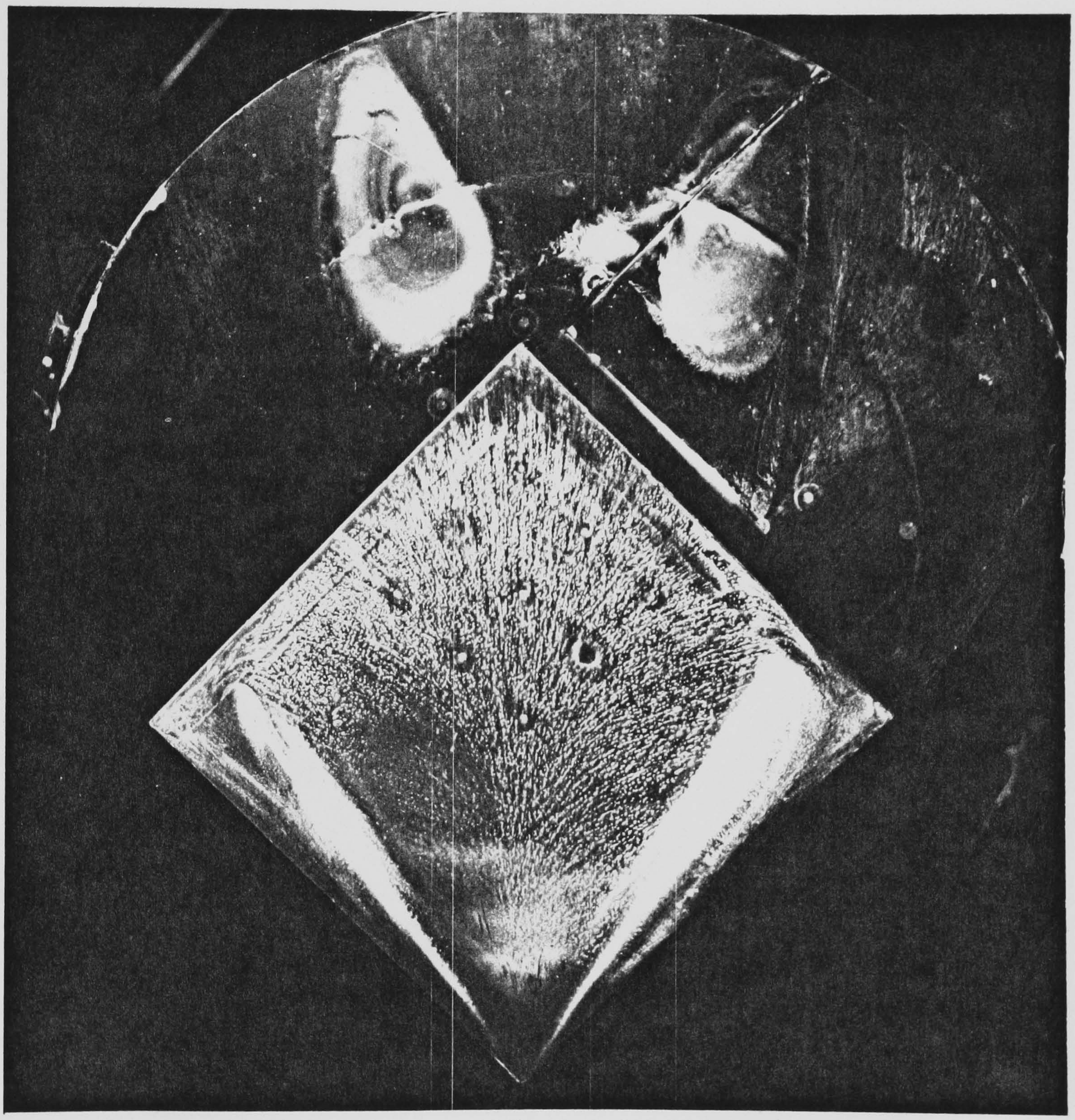

TOP SURFACE FLOW PATTERN IN SMOOTH FLOW ON
114mm MODEL AT $\alpha = 45^\circ$ FOR H/D = 3.3

PLATE 3

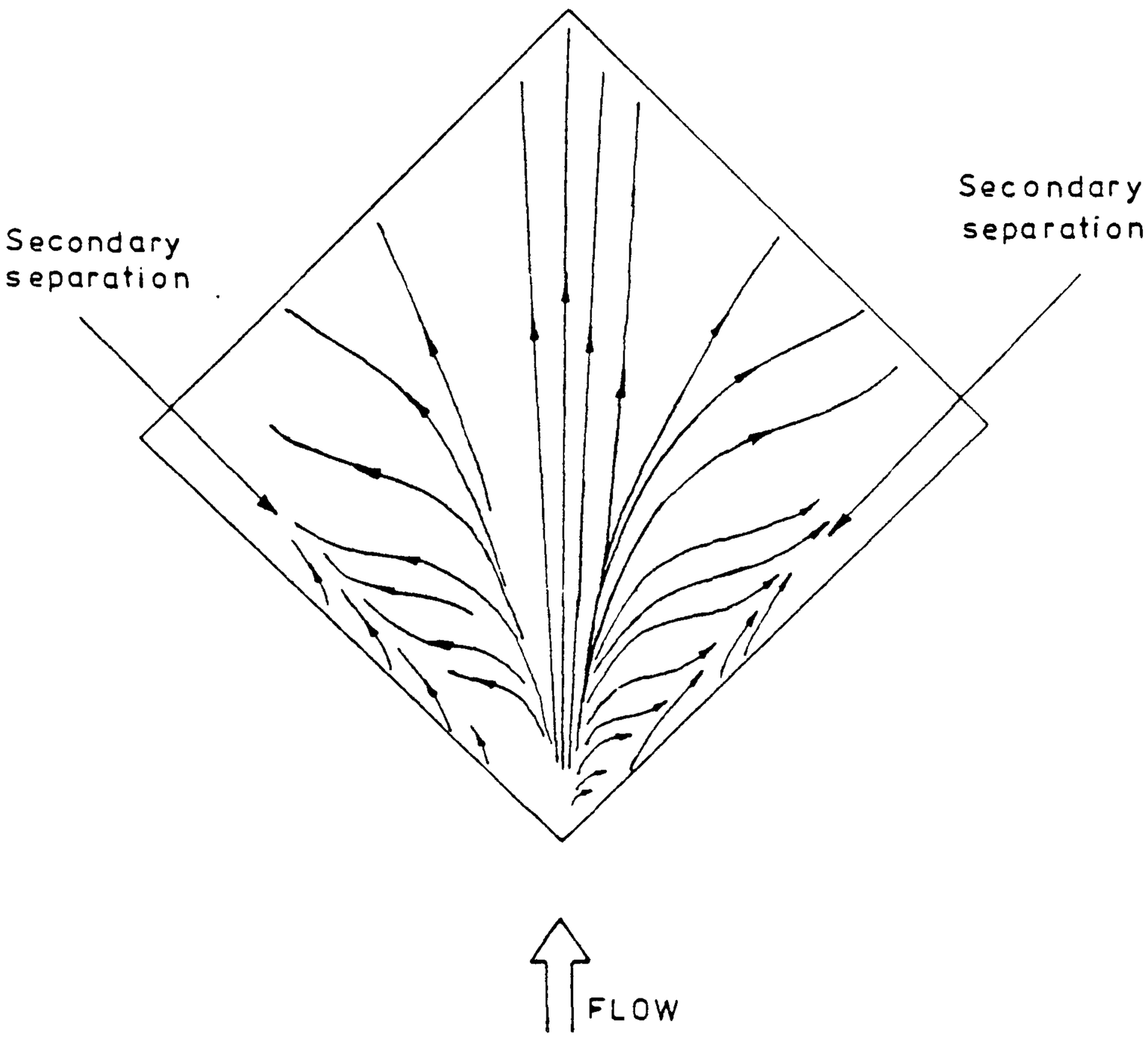

TOP SURFACE FLOW PATTERN FOR MODEL AT
$\alpha = 45°$

FIGURE 33

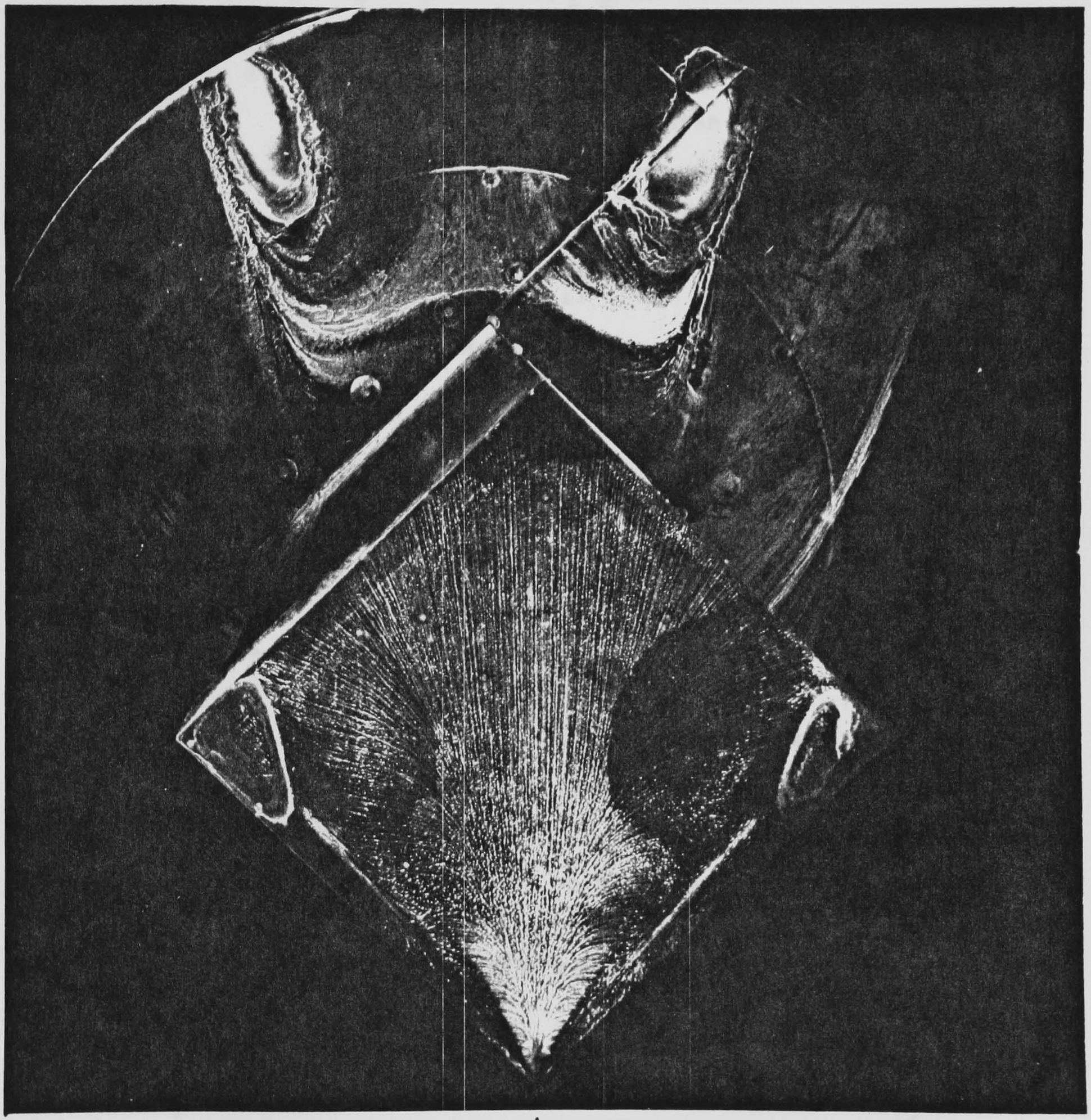

TOP SURFACE FLOW PATTERN IN TURBULENT FLOW ON 114mm MODEL AT $\alpha = 45°$ FOR H/D = 3.3

PLATE 4

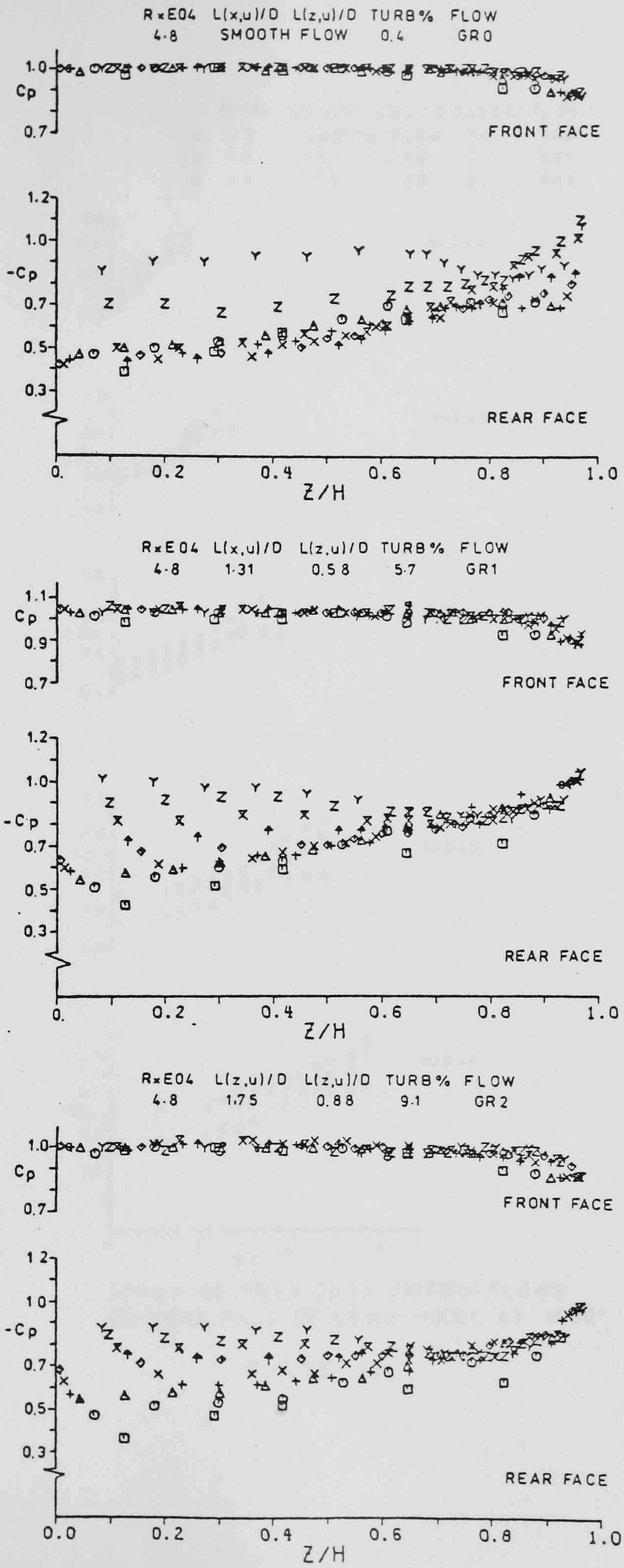

SPANWISE MEAN Cp IN UNIFORM FLOWS ON 48mm MODEL AT $\alpha = 0°$ FOR $2 \leq H/D \leq 11$

FIGURE 34

	R×E04	L(x u)/D	L(z u)/D	TURB%	FLOW
□	4 8	SMOOTH	FLOW	0.4	GR0
○	4 8	1 31	0.58	5 7	GR1
△	4 8	1 75	0.88	9 1	GR2

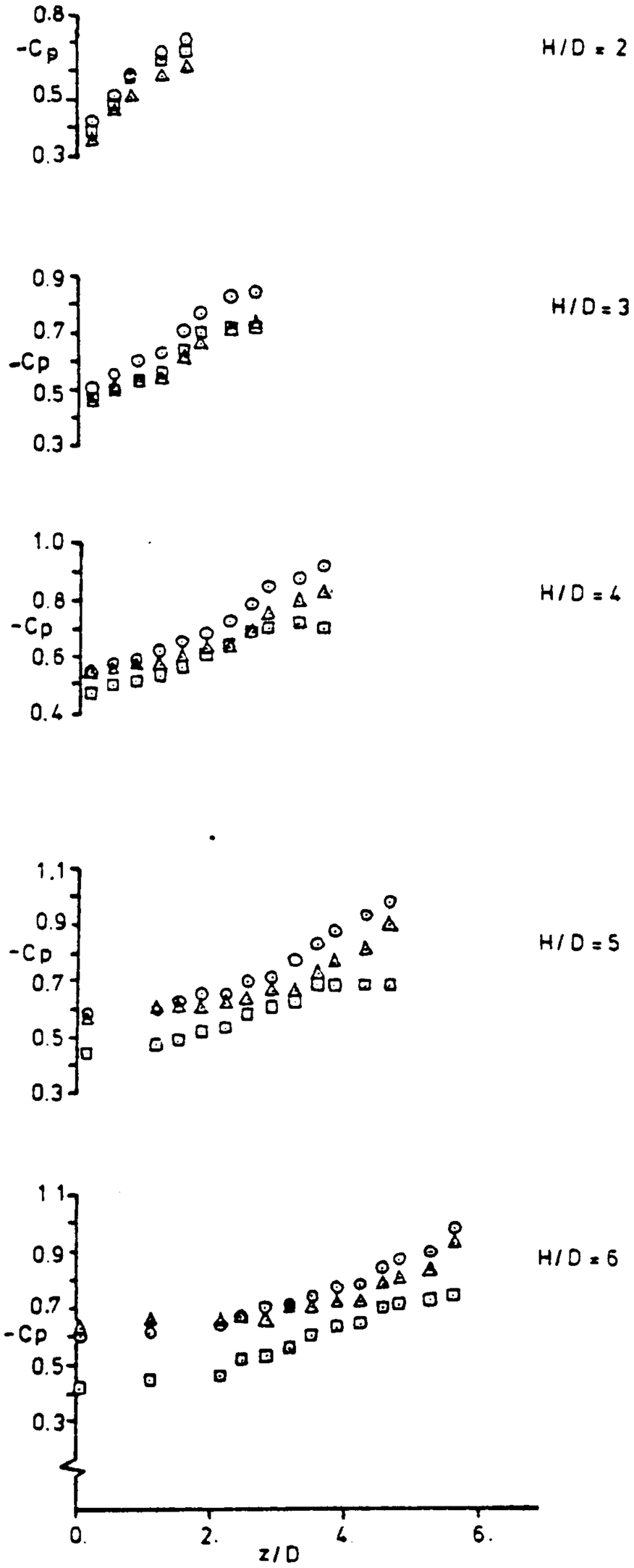

SPANWISE MEAN Cp IN UNIFORM FLOWS
ON REAR FACE OF 48 mm MODEL AT $\alpha = 0°$

FIGURE 35

	R×E04	L(x,u)/D	L(z,u)/D	TURB%	FLOW
□	4.8	SMOOTH FLOW		0.4	GR0
○	4.8	1.31	0.58	5.7	GR1
△	4.8	1.75	0.88	9.1	GR2

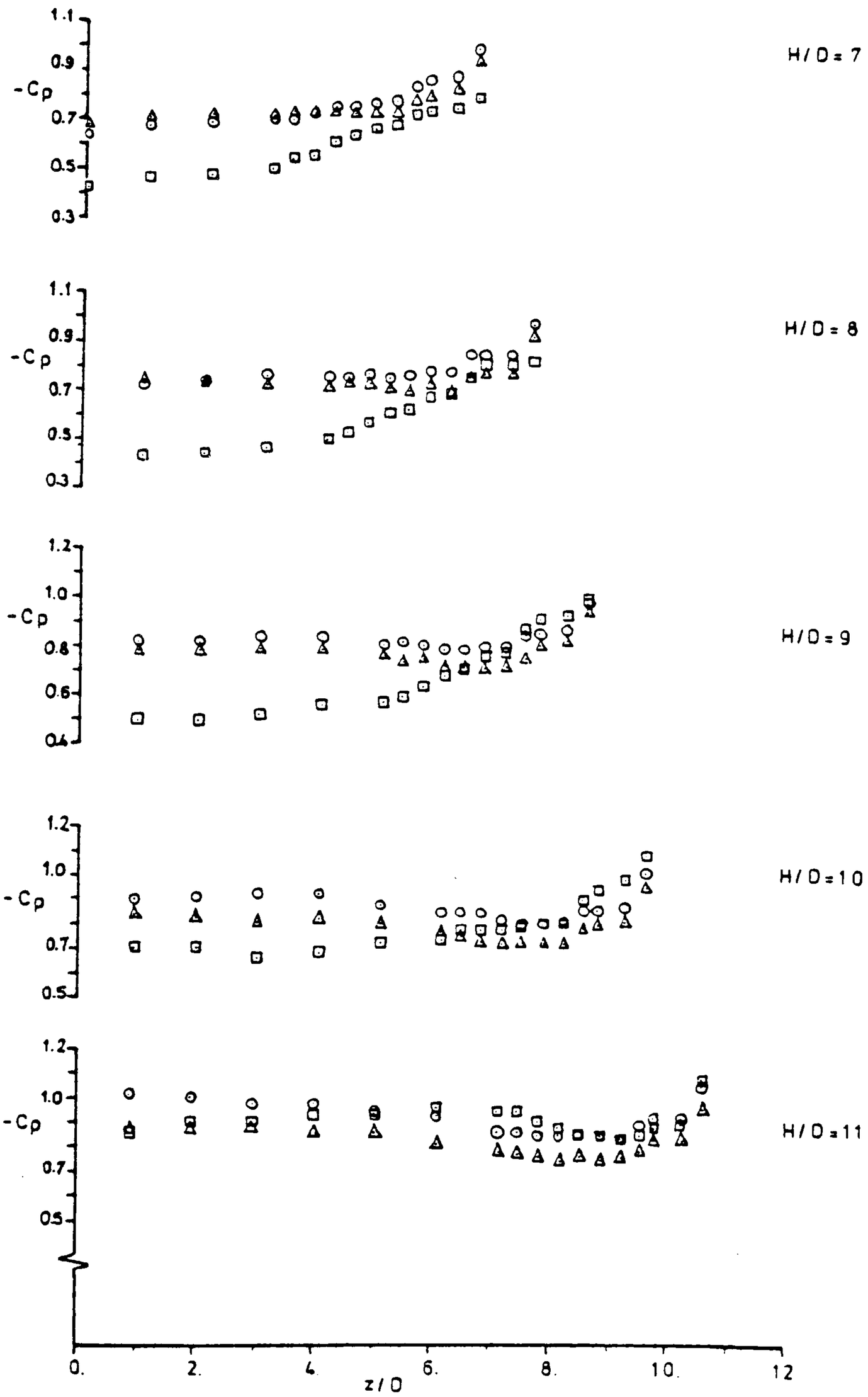

SPANWISE MEAN Cp IN UNIFORM FLOWS ON REAR FACE OF 48mm MODEL AT $\alpha = 0°$

FIGURE 36

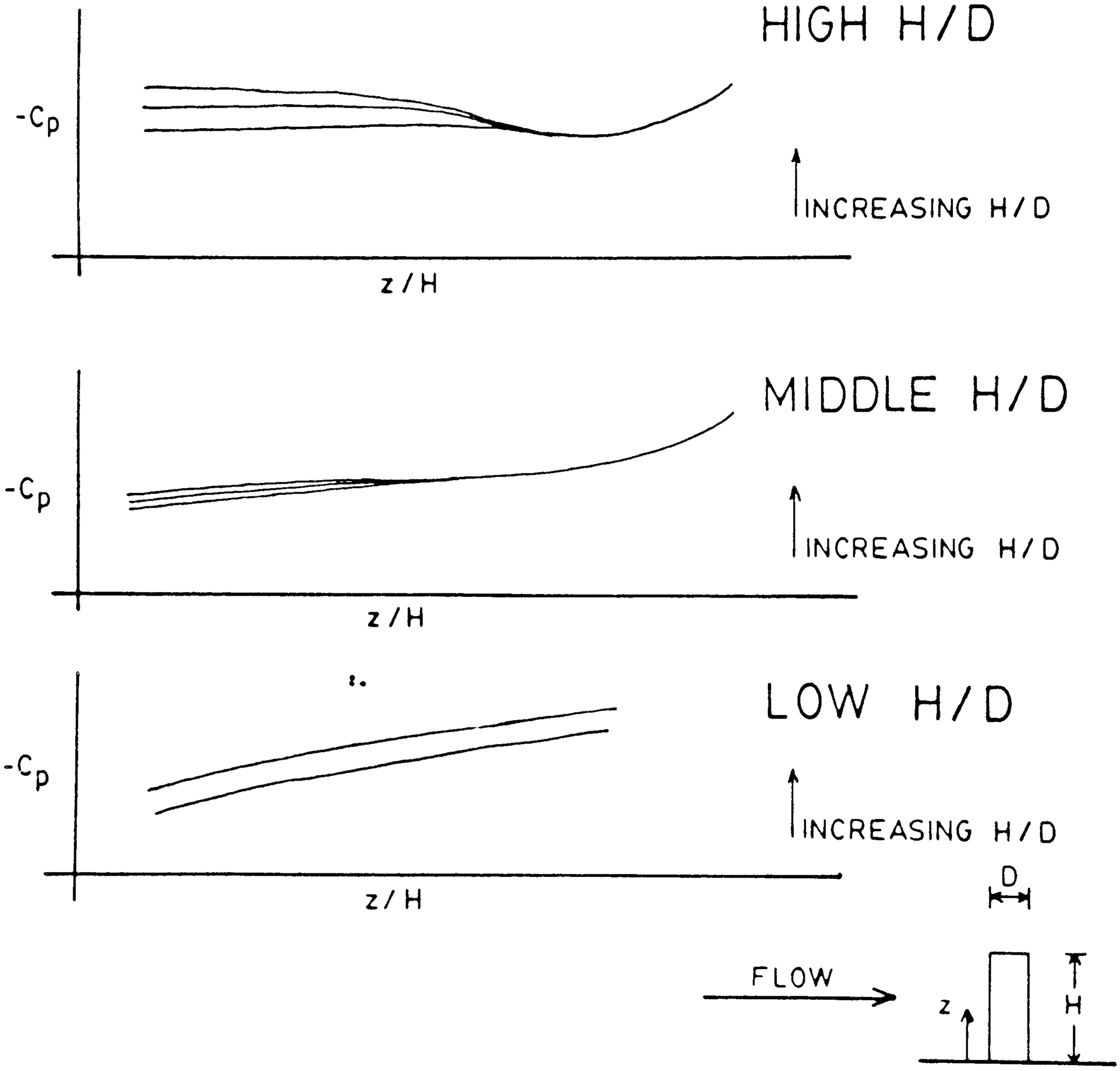

SCHEMATIC REPRESENTATION OF THE VARIATION OF SPANWISE REAR FACE C_p FOR FINITE SQUARE CYLINDERS AT ZERO INCIDENCE

FIGURE 37

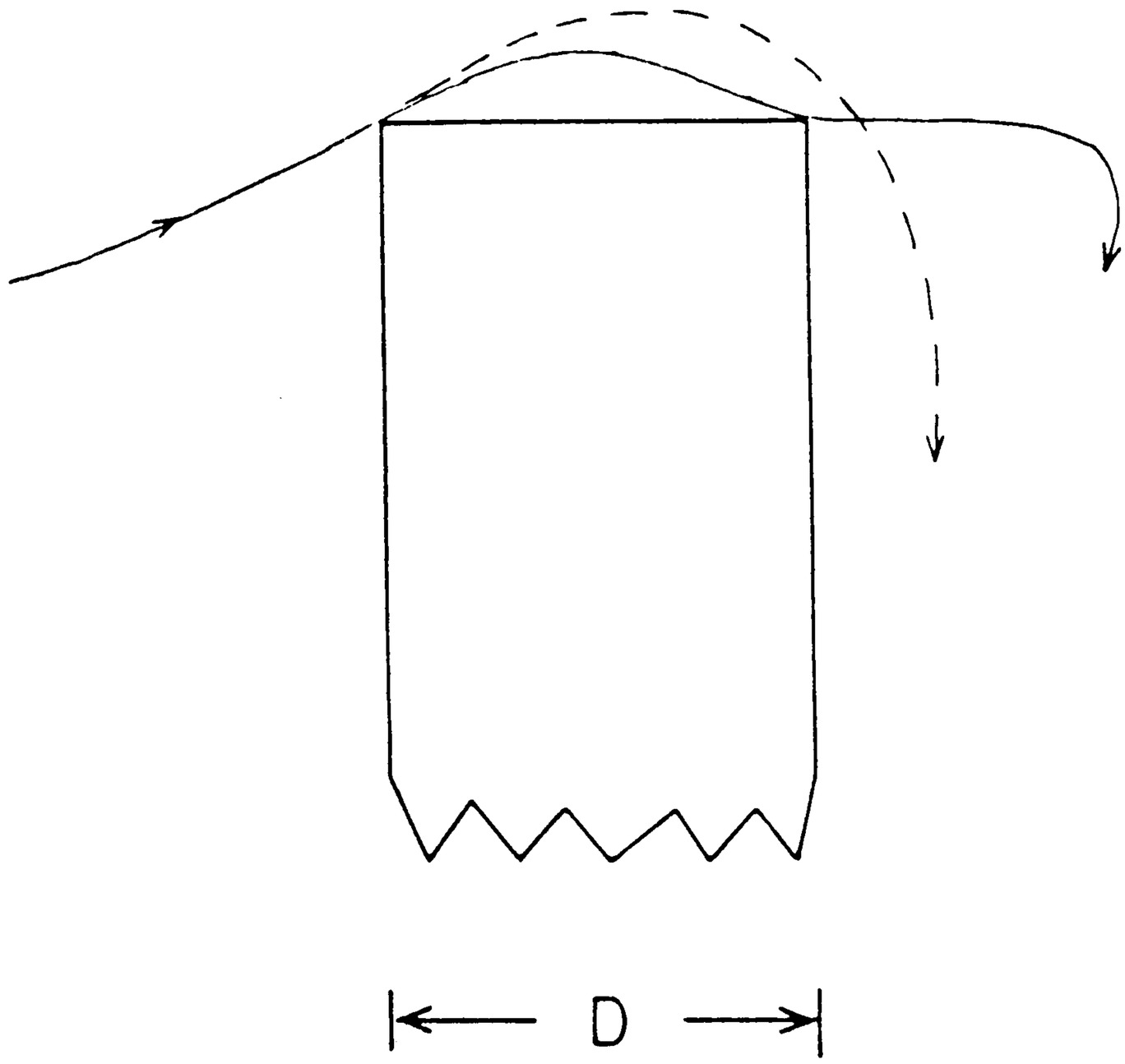

FLOW STREAMLINE OVER THE TOP SURFACE IN SMOOTH AND TURBULENT FLOWS FOR A FINITE SQUARE CYLINDER AT $\alpha = 0°$

FIGURE 38

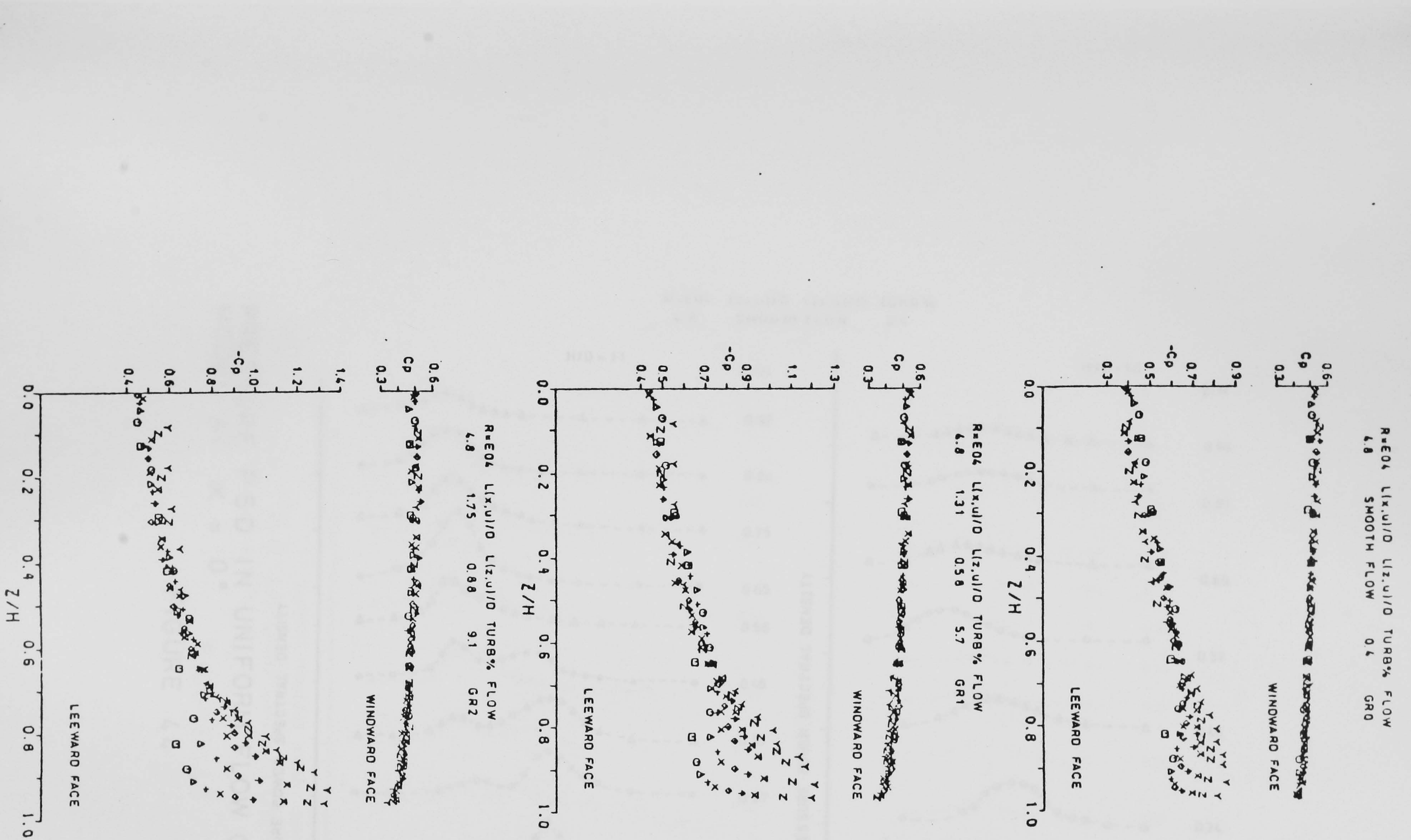

SPANWISE MEAN Cp IN UNIFORM FLOWS ON 48mm
MODEL AT $\alpha = 45°$ FOR $2 \leq H/D \leq 11$

FIGURE 39

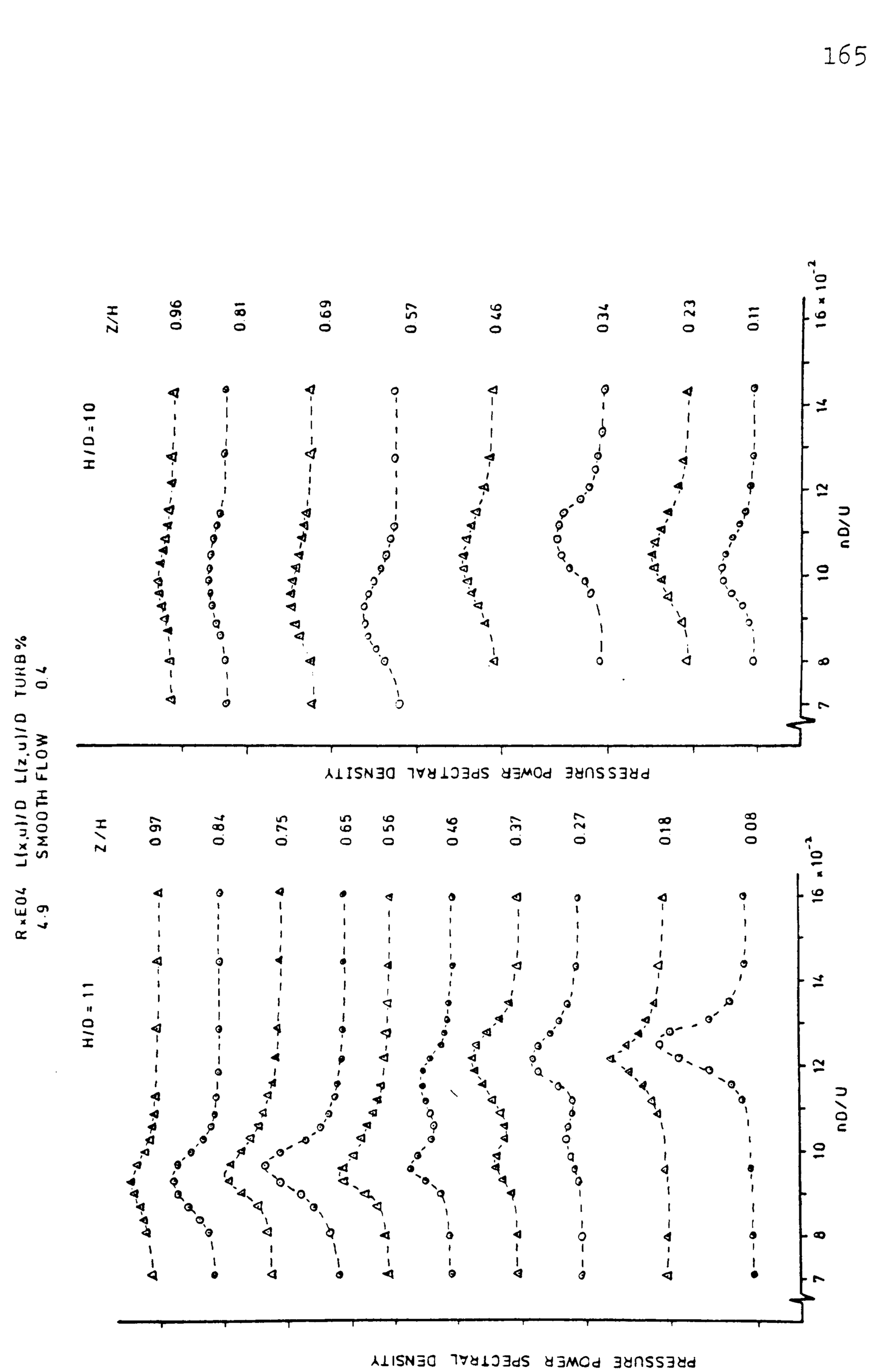

PRESSURE PSD IN UNIFORM FLOW GRO ON 48mm MODEL AT $\alpha = 0°$

FIGURE 44

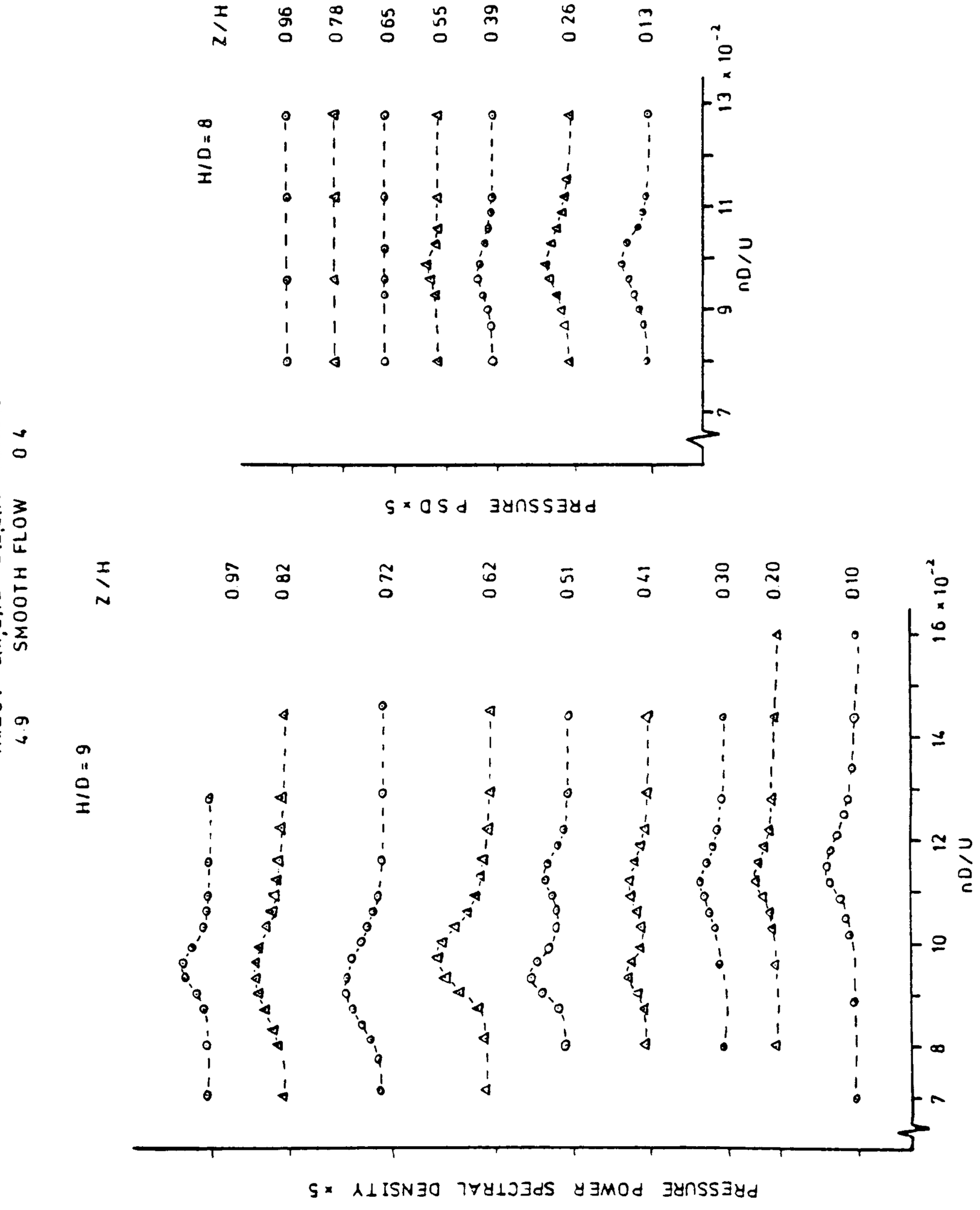

PRESSURE P S D IN UNIFORM FLOW GR0 ON 48mm MODEL AT $\alpha = 0°$

FIGURE 45

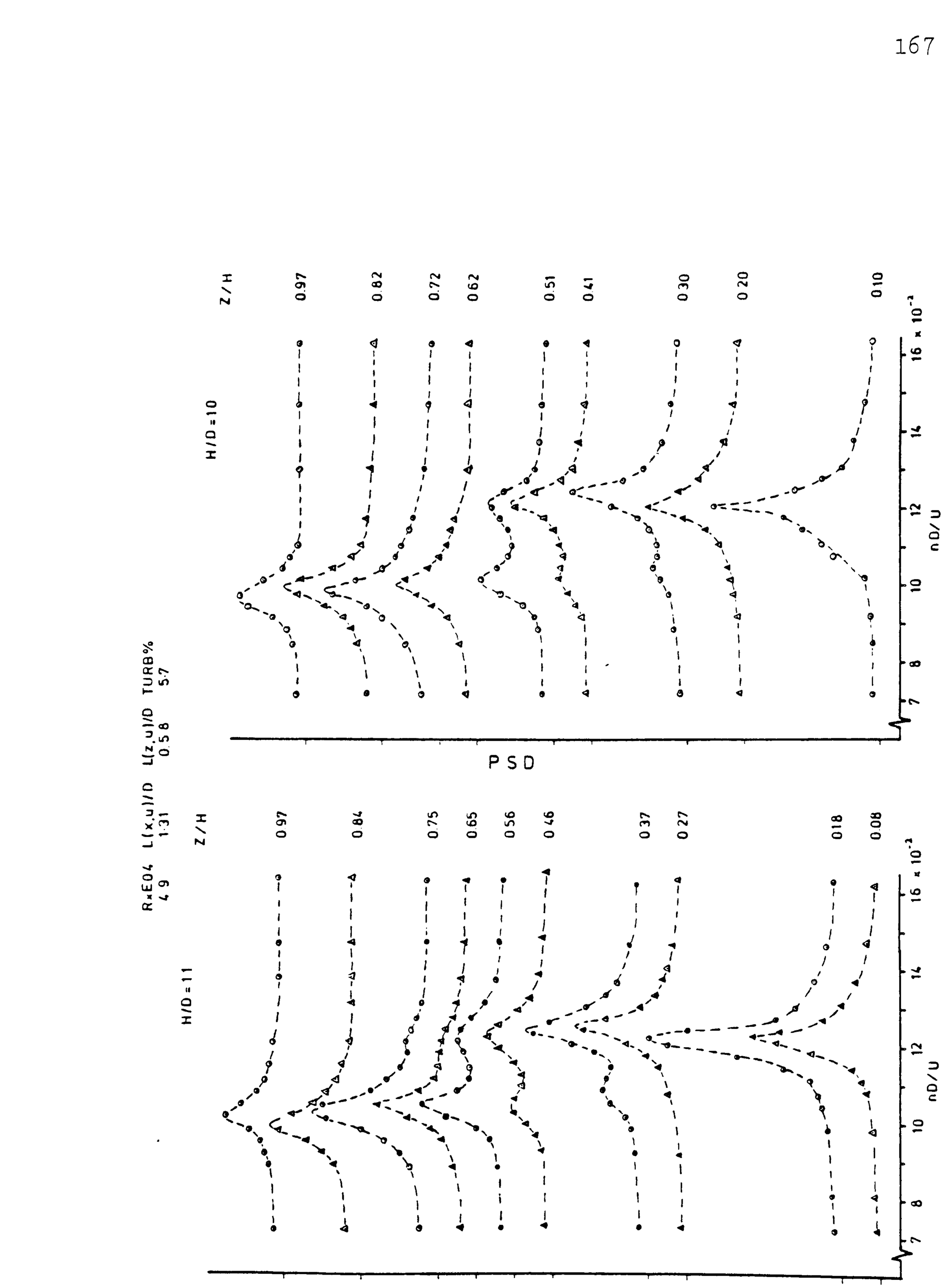

PRESSURE P S D IN UNIFORM FLOW GR1 ON 48mm MODEL AT $\alpha = 0°$

FIGURE 46

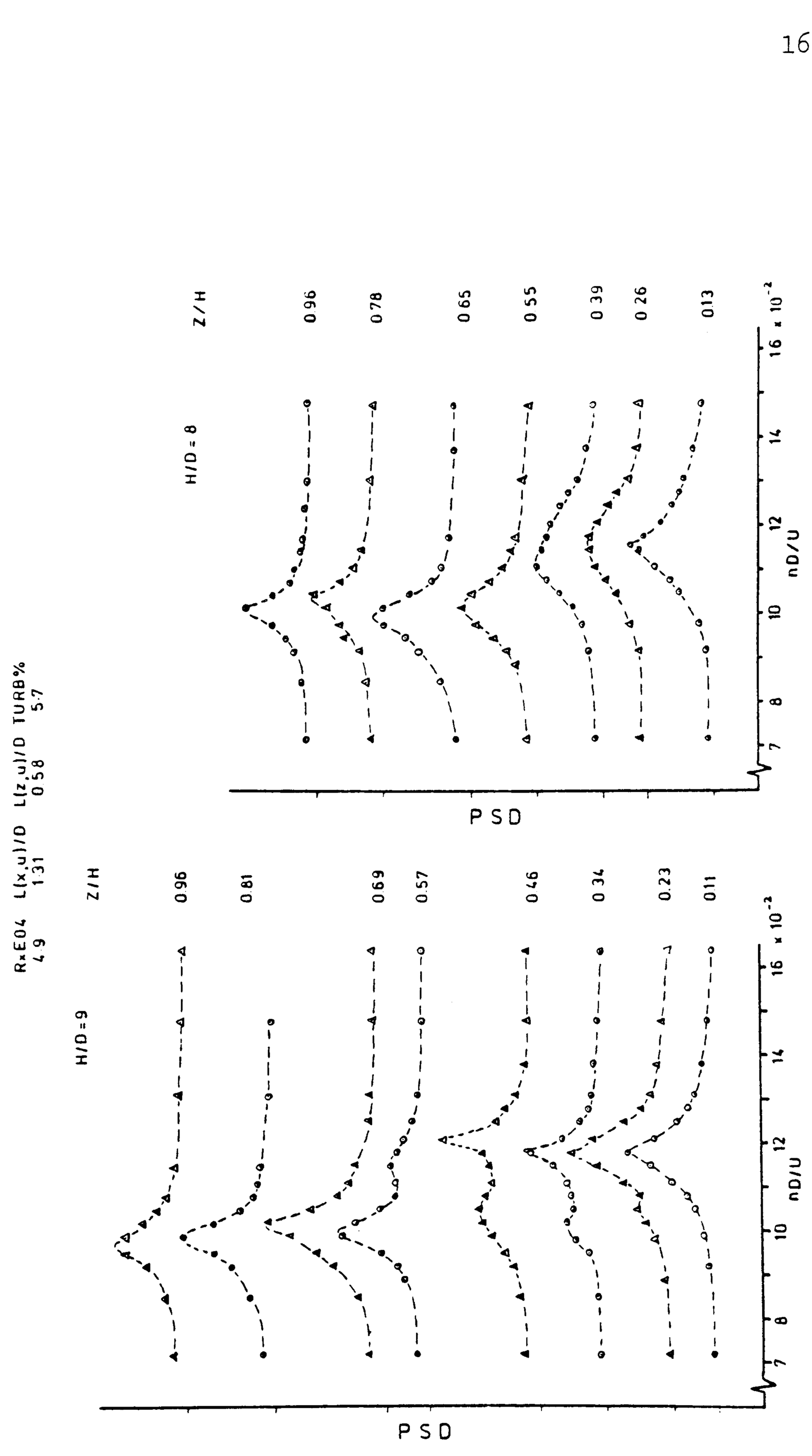

PRESSURE PSD IN UNIFORM FLOW GR1 ON 48mm MODEL AT $\alpha = 0°$

FIGURE 47

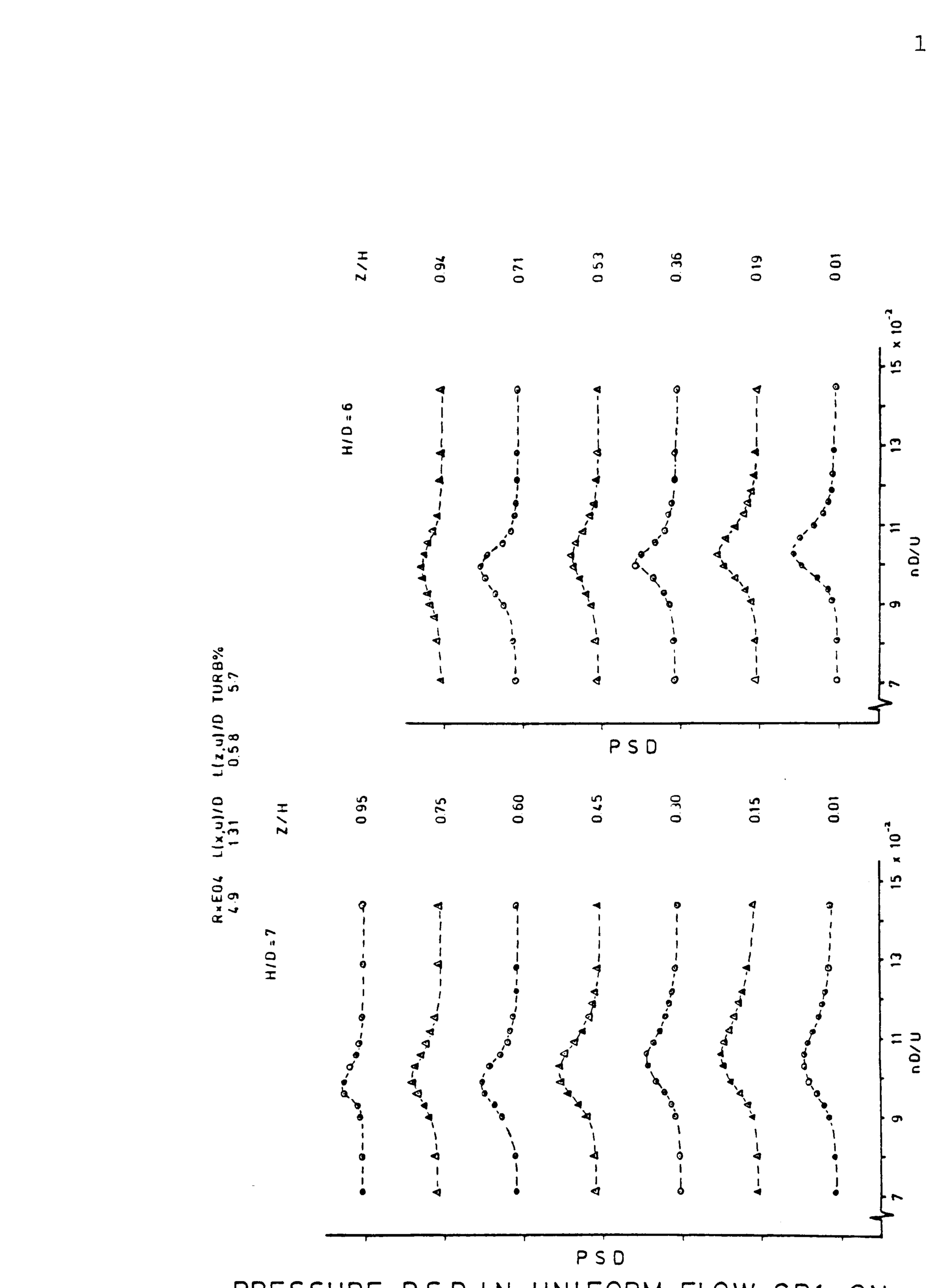

PRESSURE PSD IN UNIFORM FLOW GR1 ON 48mm MODEL AT $\alpha = 0°$

FIGURE 48

R×E04	L(x,u)/D	L(z,u)/D	TURB %
4.9	1·31	0·58	5·7

D = 48 mm

$\alpha = 0°$

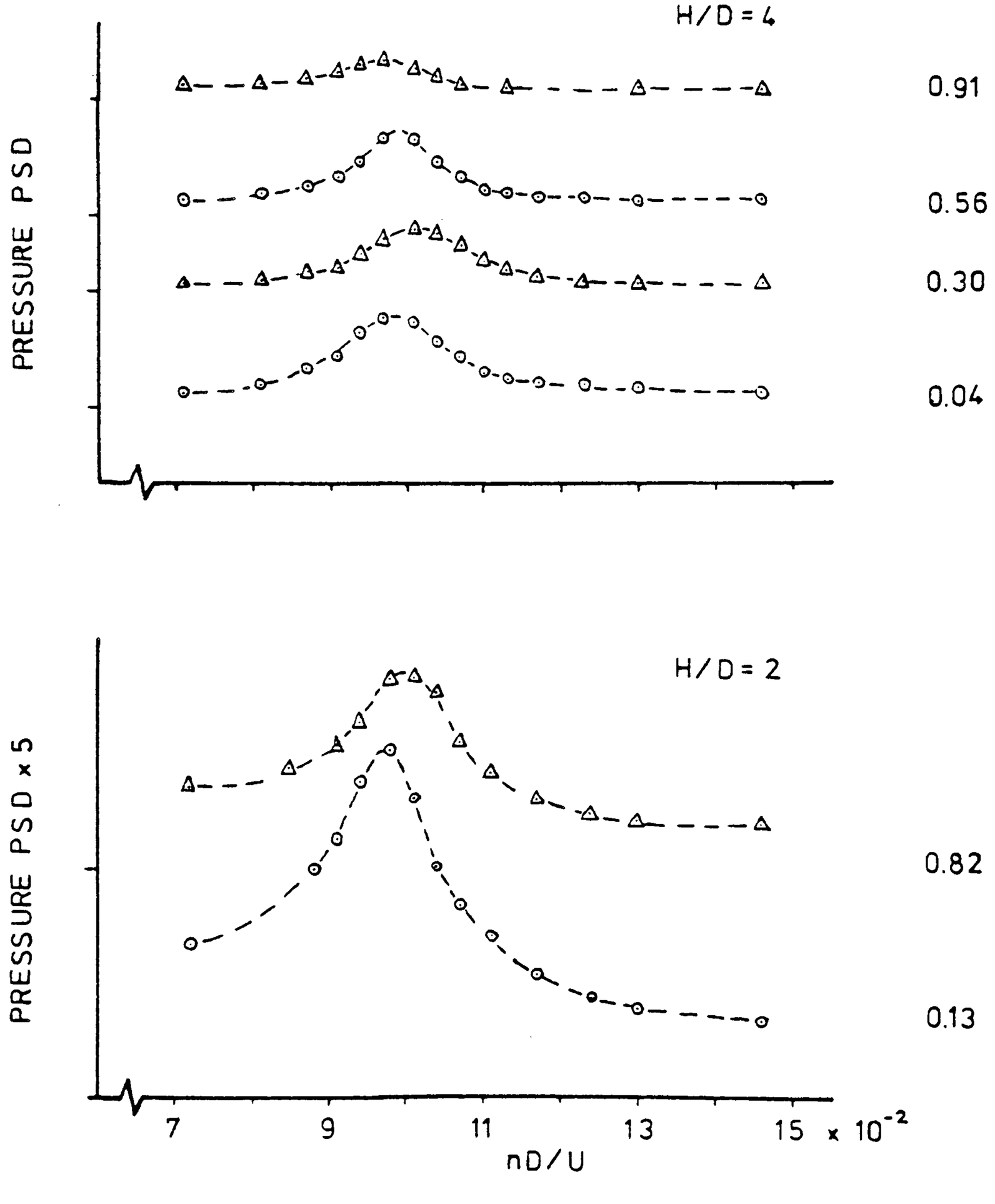

PRESSURE PSD IN UNIFORM FLOW GR1

FIGURE 49

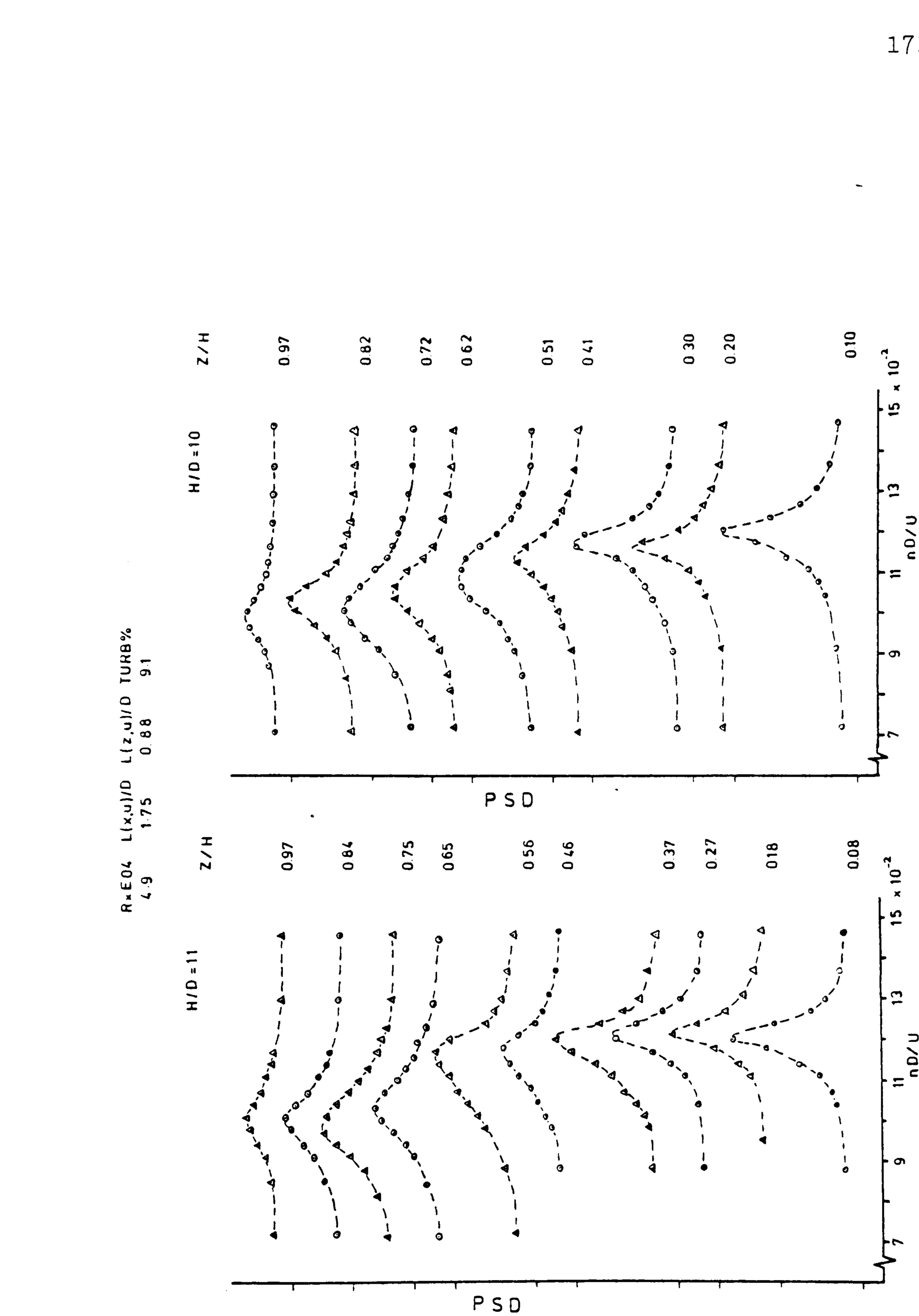

PRESSURE P S D IN UNIFORM FLOW GR2 ON 48mm MODEL AT $\alpha = 0°$

FIGURE 50

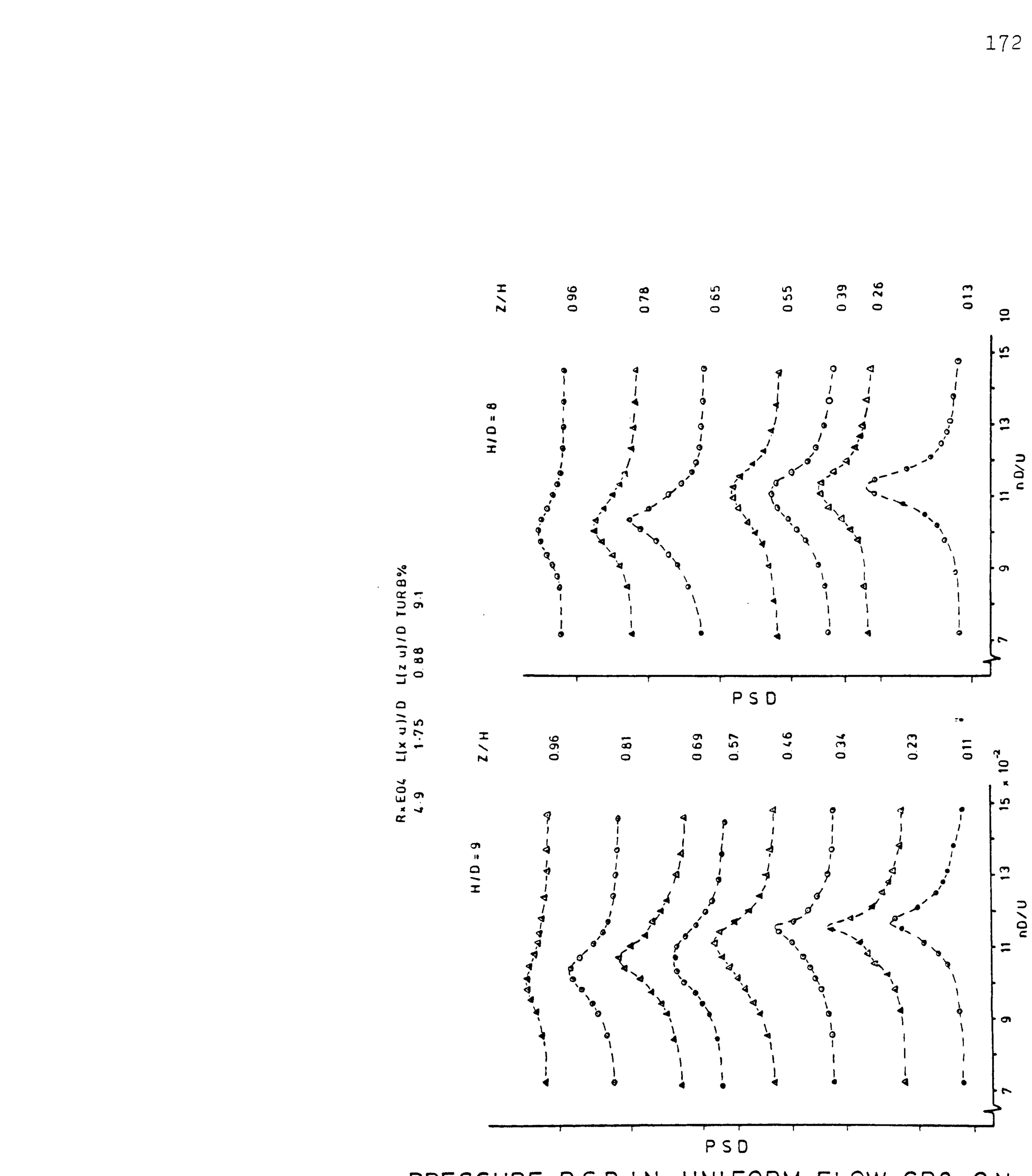

PRESSURE PSD IN UNIFORM FLOW GR2 ON 48mm MODEL AT $\alpha = 0°$

FIGURE 51

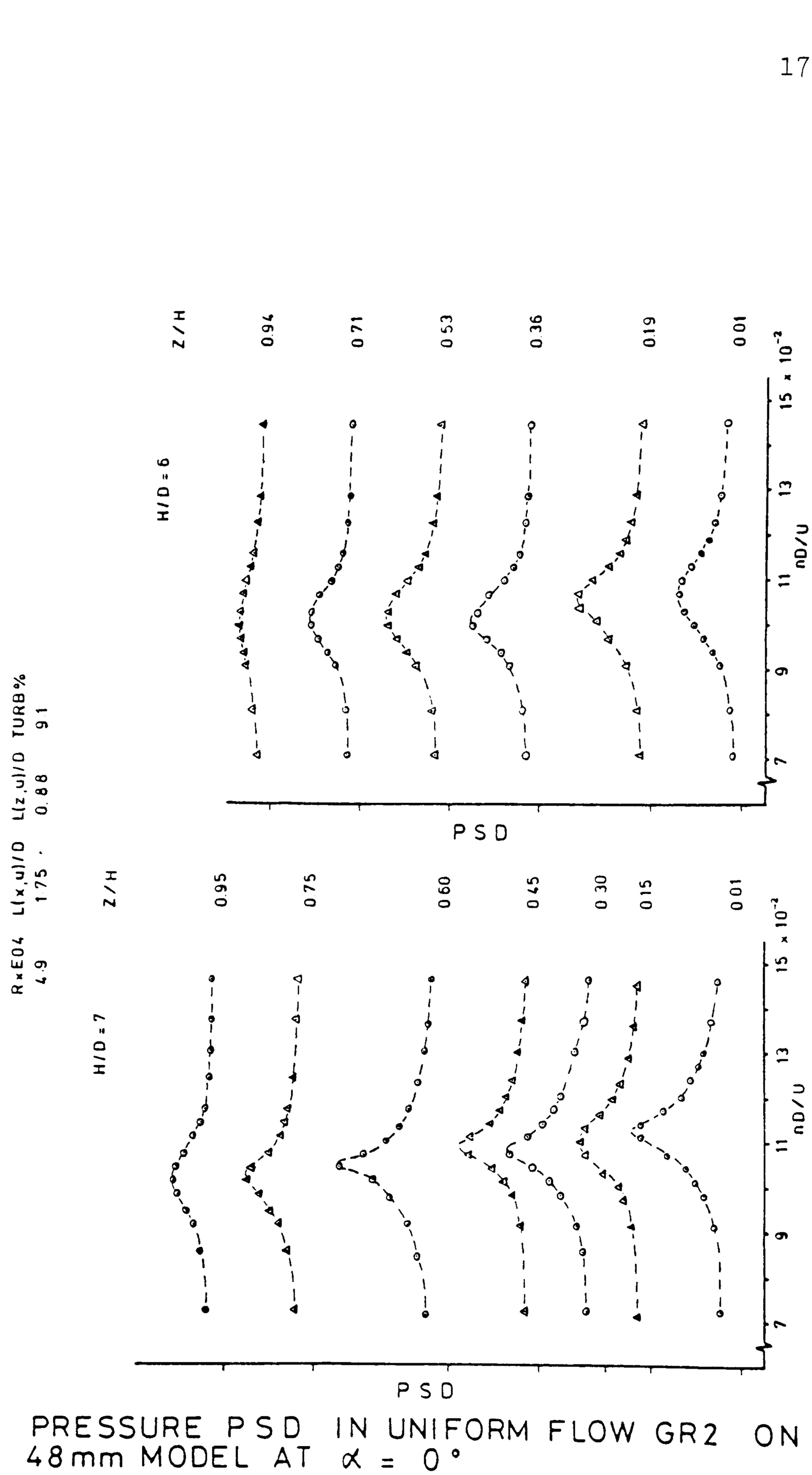

PRESSURE PSD IN UNIFORM FLOW GR2 ON 48mm MODEL AT $\alpha = 0°$

FIGURE 52

R×E04	L(x,u)/D	L(z,u)/D	TURB %
4.9	175	0.88	9.1

D = 48 mm

$\alpha = 0^{\circ}$

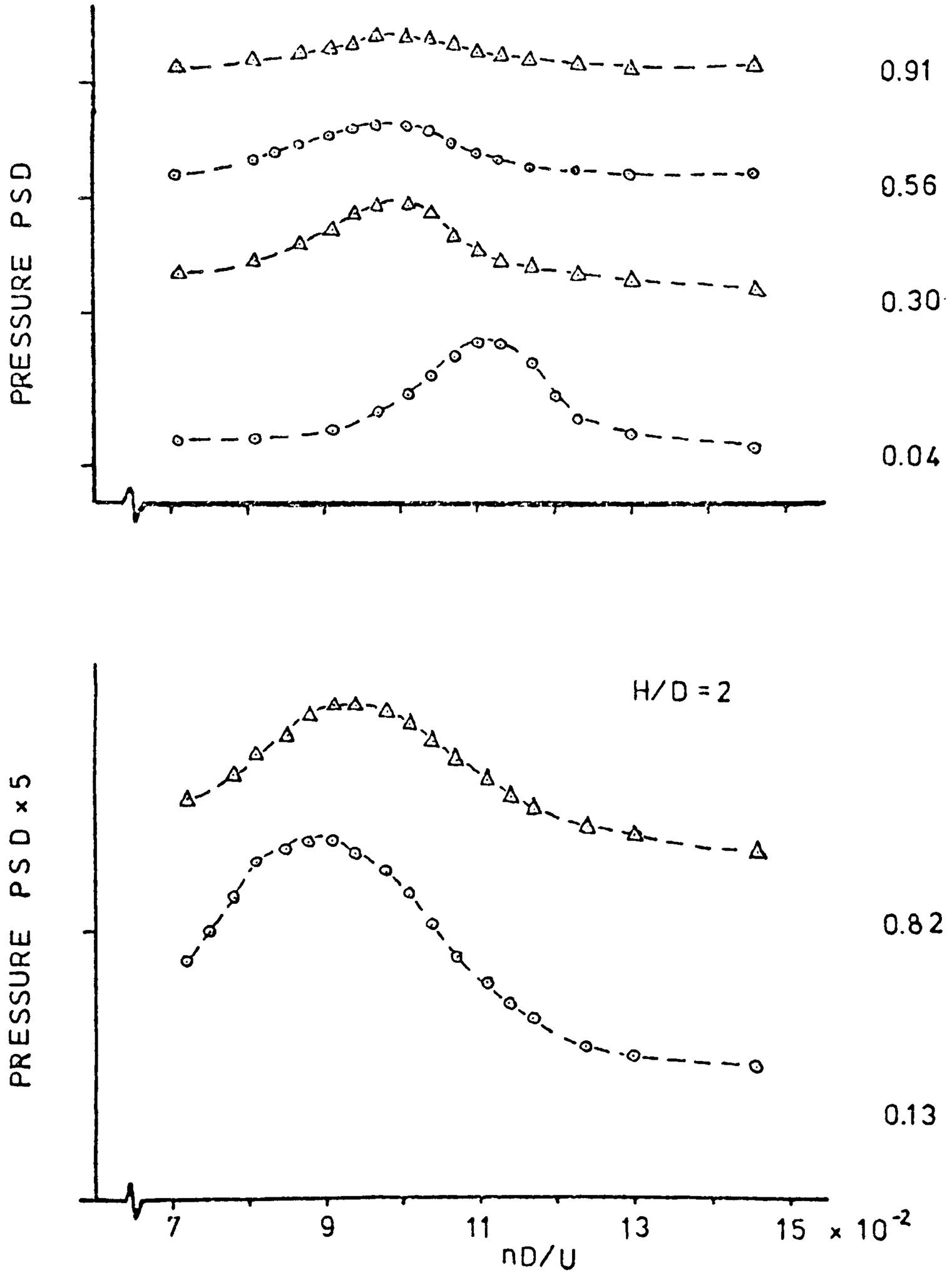

PRESSURE PSD IN UNIFORM FLOW GR2

FIGURE 53

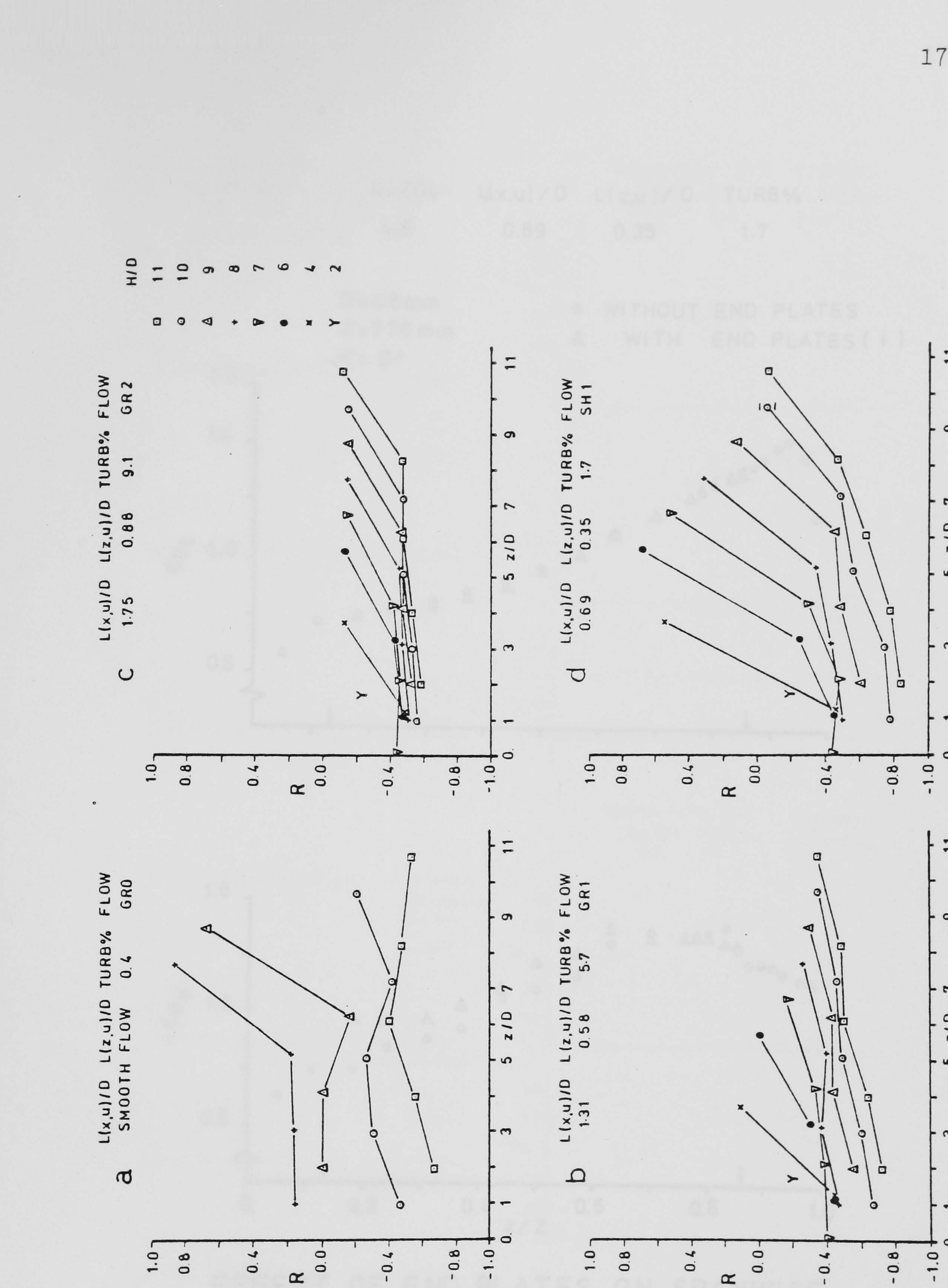

SPANWISE CORRELATION COEFFICIENT IN UNIFORM AND SHEAR FLOWS ON 48mm MODEL AT $\alpha = 0°$

FIGURE 54

Rx E04	L(x,u) / D	L(z,u) / D	TURB%
4.8	0.69	0.35	1.7

D = 48 mm
Z = 770 mm
α = 0°

○ WITHOUT END PLATES
△ WITH END PLATES (↓)

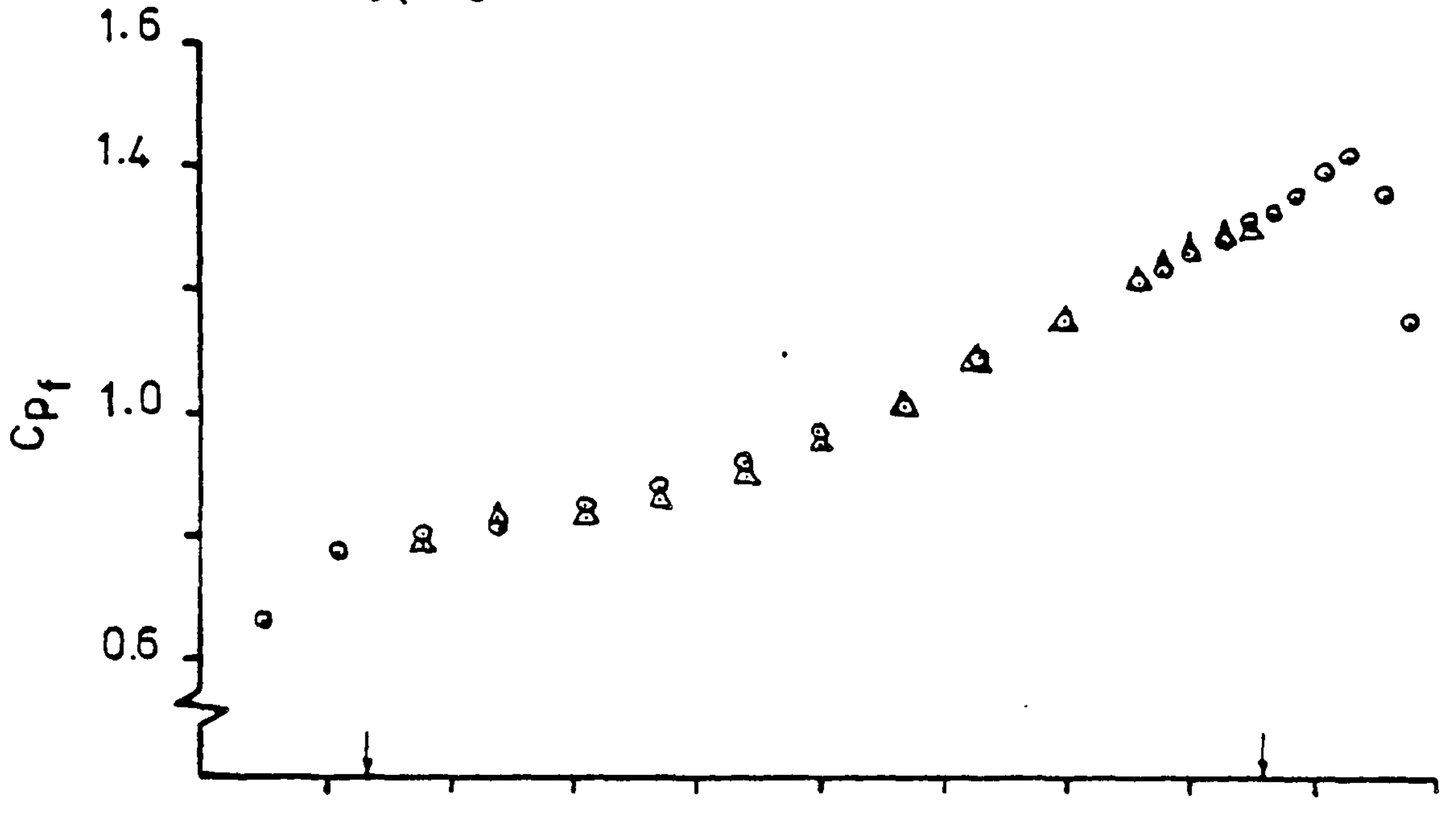

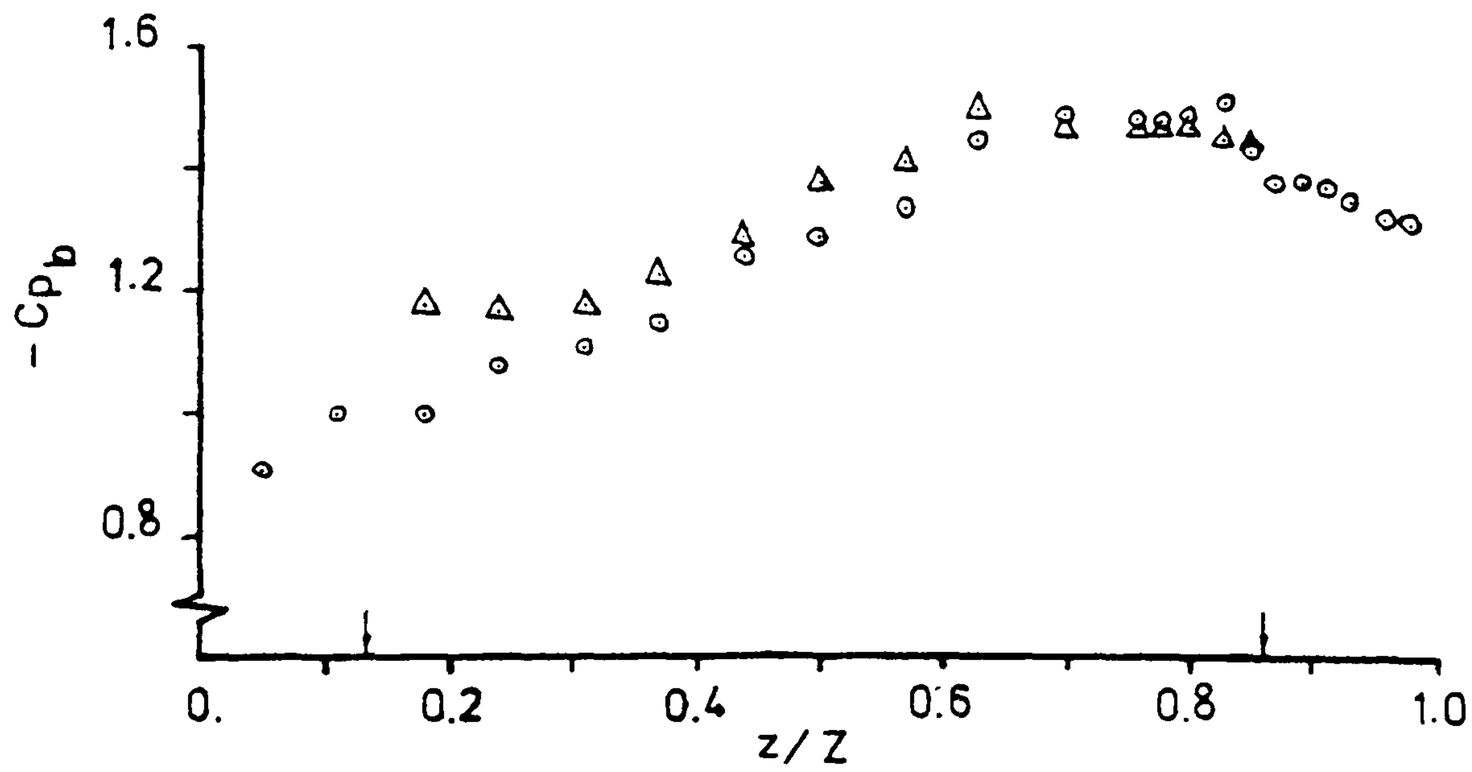

EFFECT OF END PLATES ON SPANWISE MEAN Cp IN SHEAR FLOW SH1

FIGURE 55

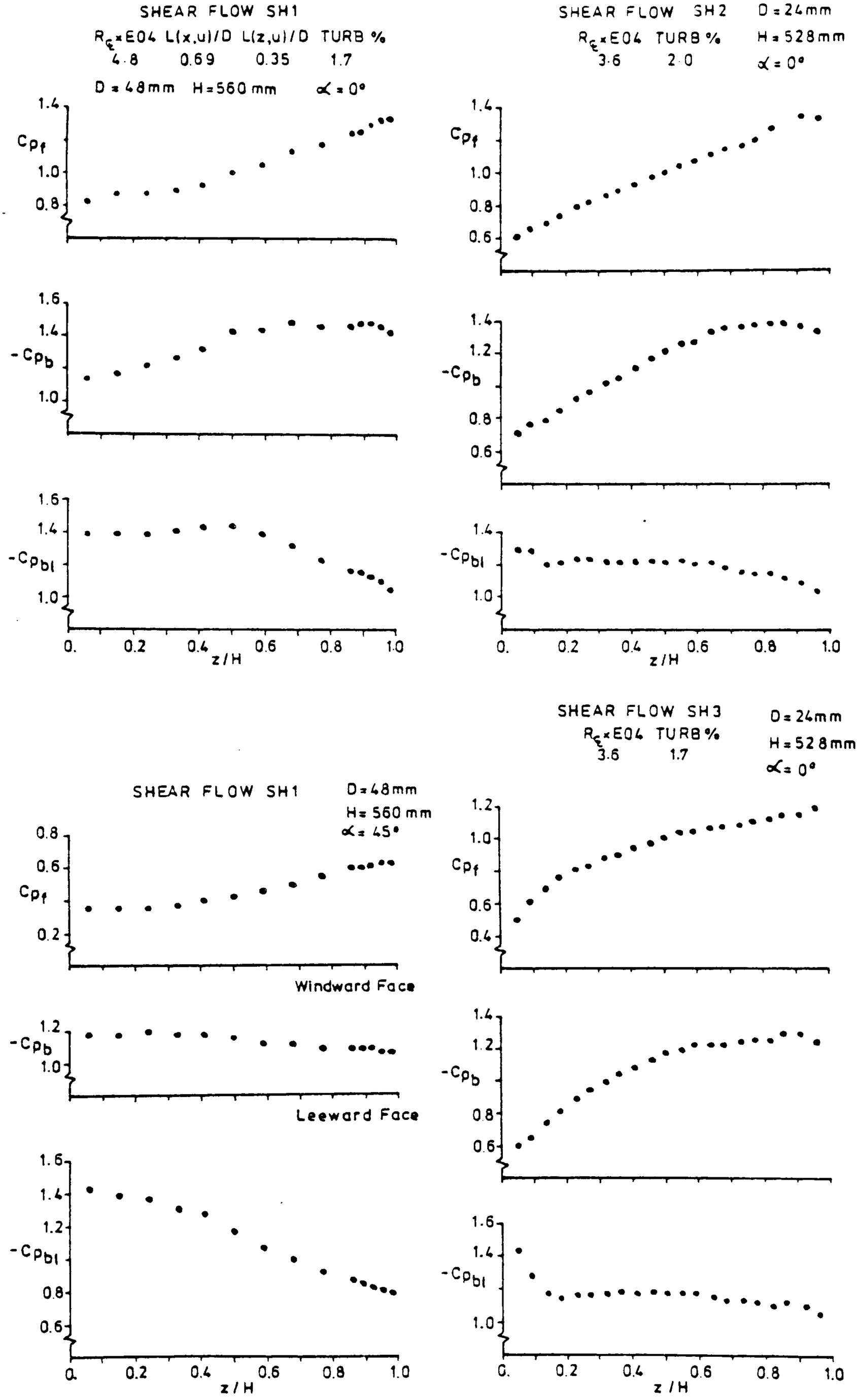

SPANWISE MEAN Cp IN SHEAR FLOWS FOR MODEL SPANNING TUNNEL

FIGURE 56

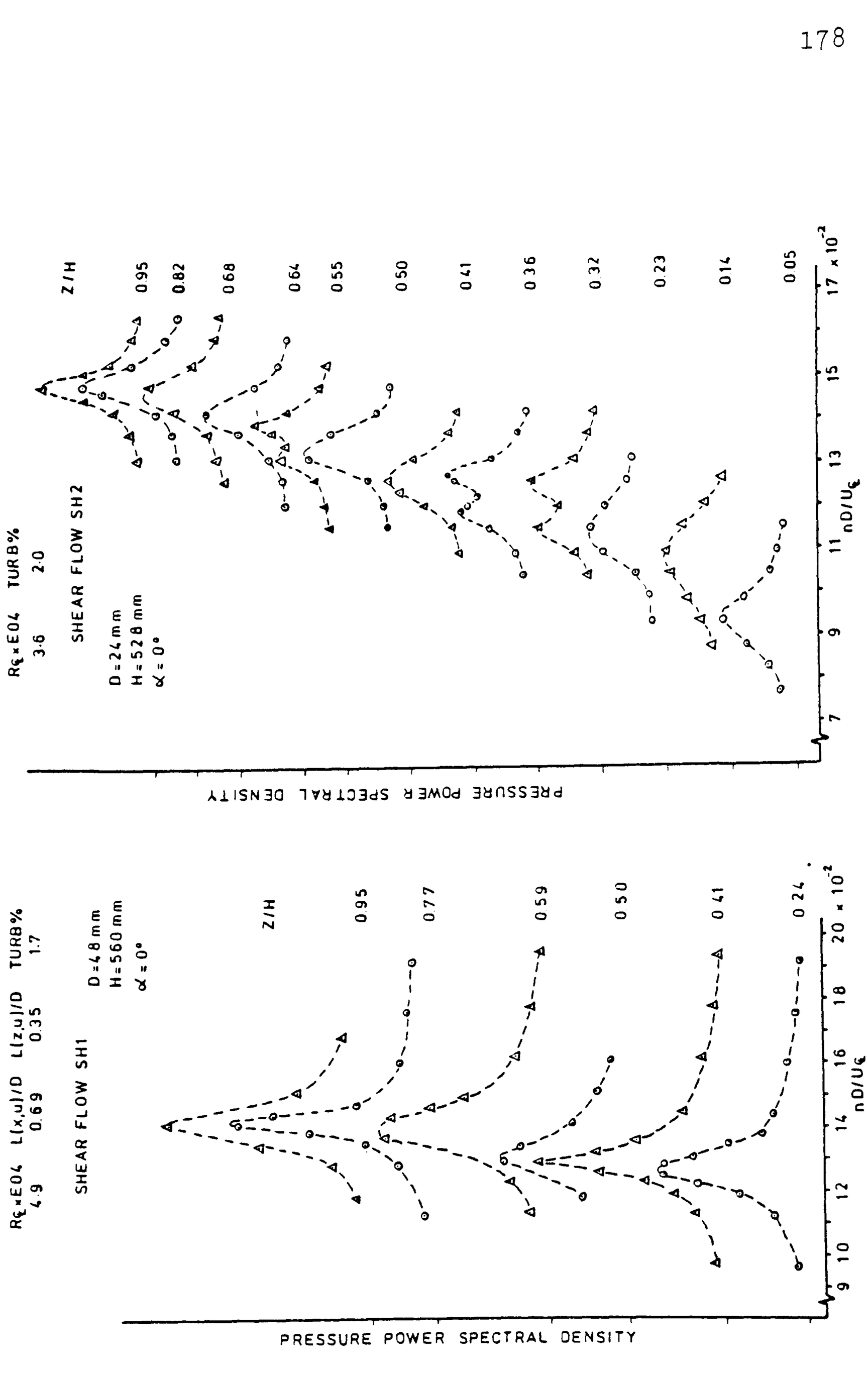

PRESSURE PSD IN SHEAR FLOWS ON MODEL SPANNING TUNNEL

FIGURE 57

	R_{ξ} E04	TURB%	D(mm)	H(mm)	FLOW
⊙	4.9	1·7	48.	560.	SH1
△	3·6	2·0	24.	528.	SH2
+	3·6	1·7	24.	528.	SH3

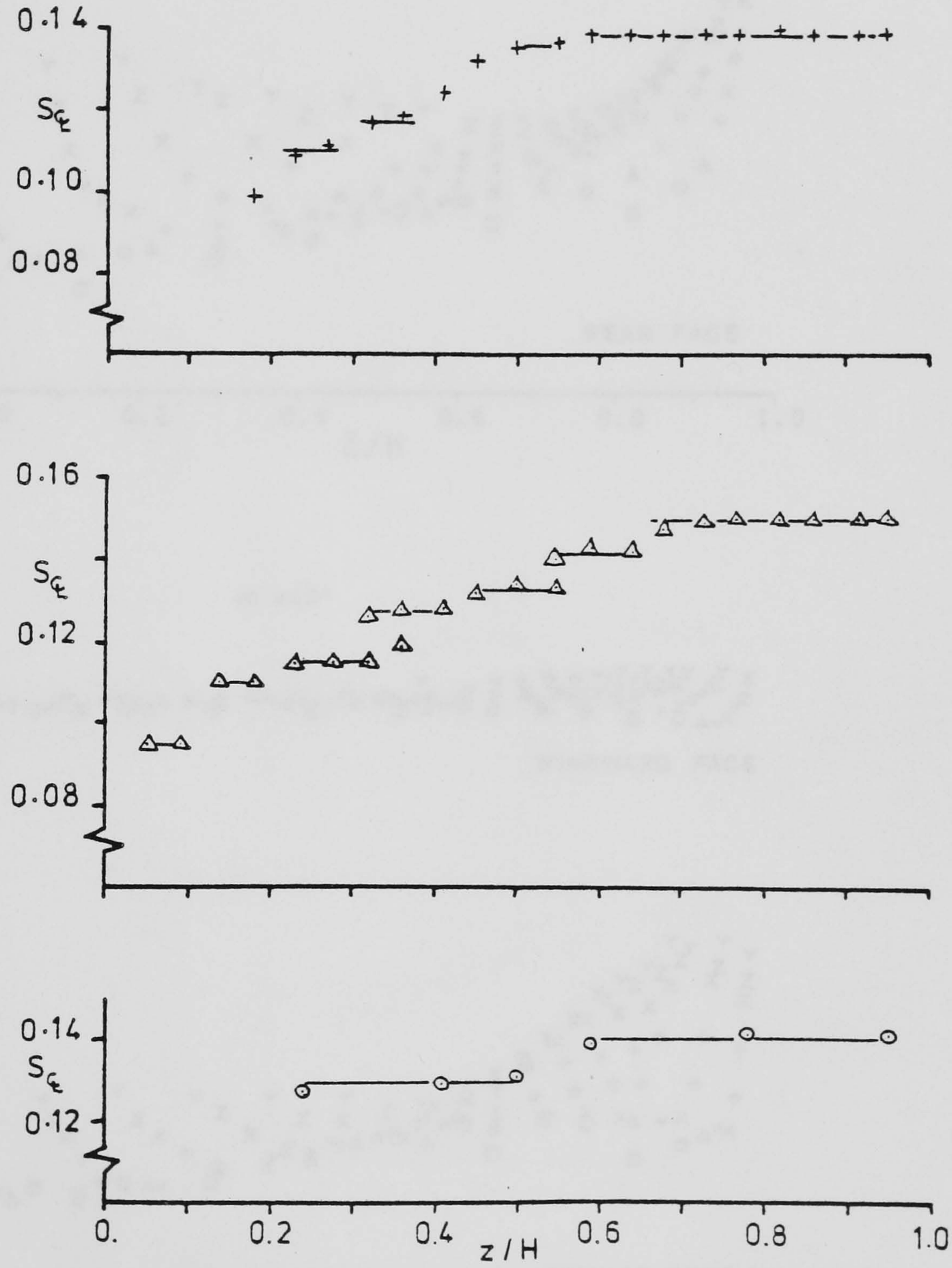

SPANWISE STROUHAL NUMBER IN SHEAR FLOWS

FIGURE 58

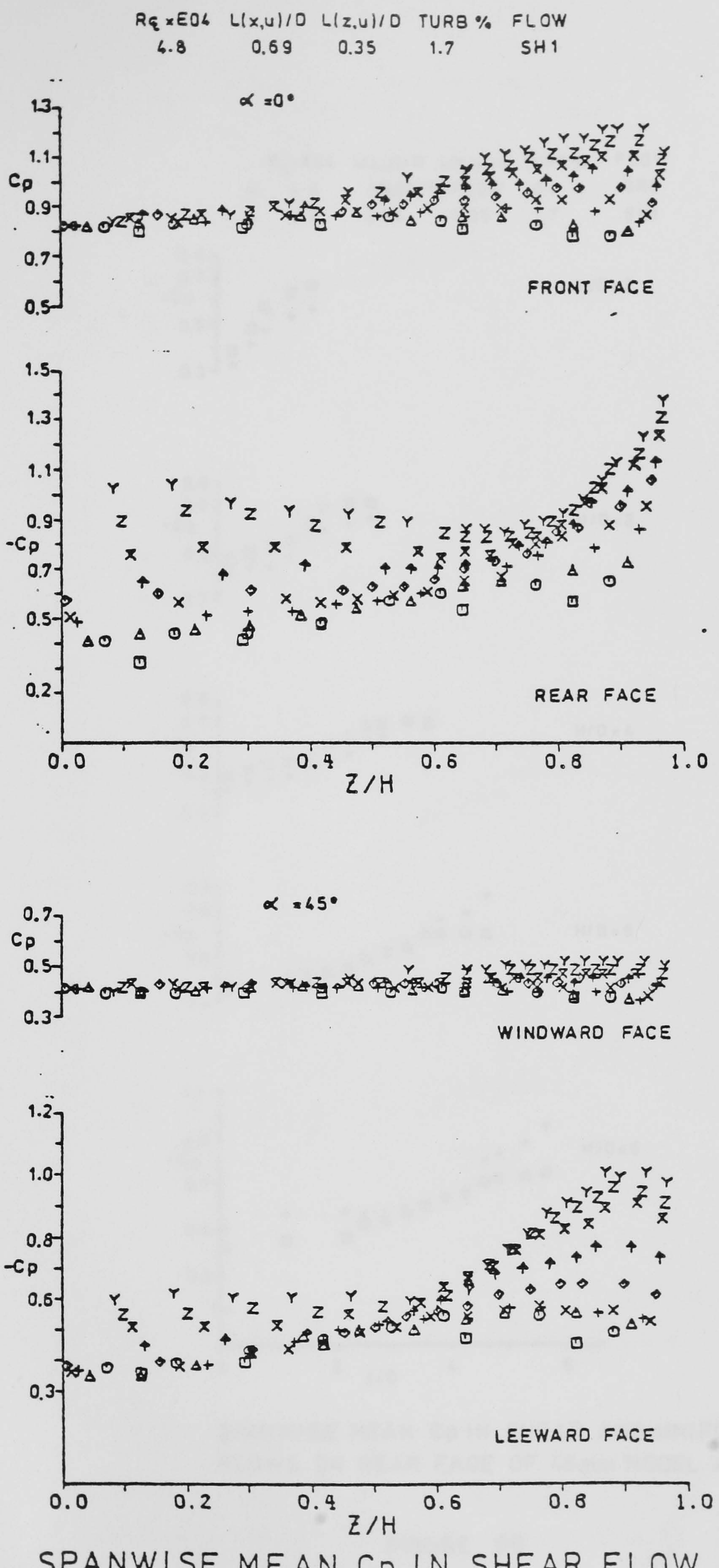

SPANWISE MEAN Cp IN SHEAR FLOW SH1 ON 48mm MODEL FOR $2 \leq H/D \leq 11$

FIGURE 59

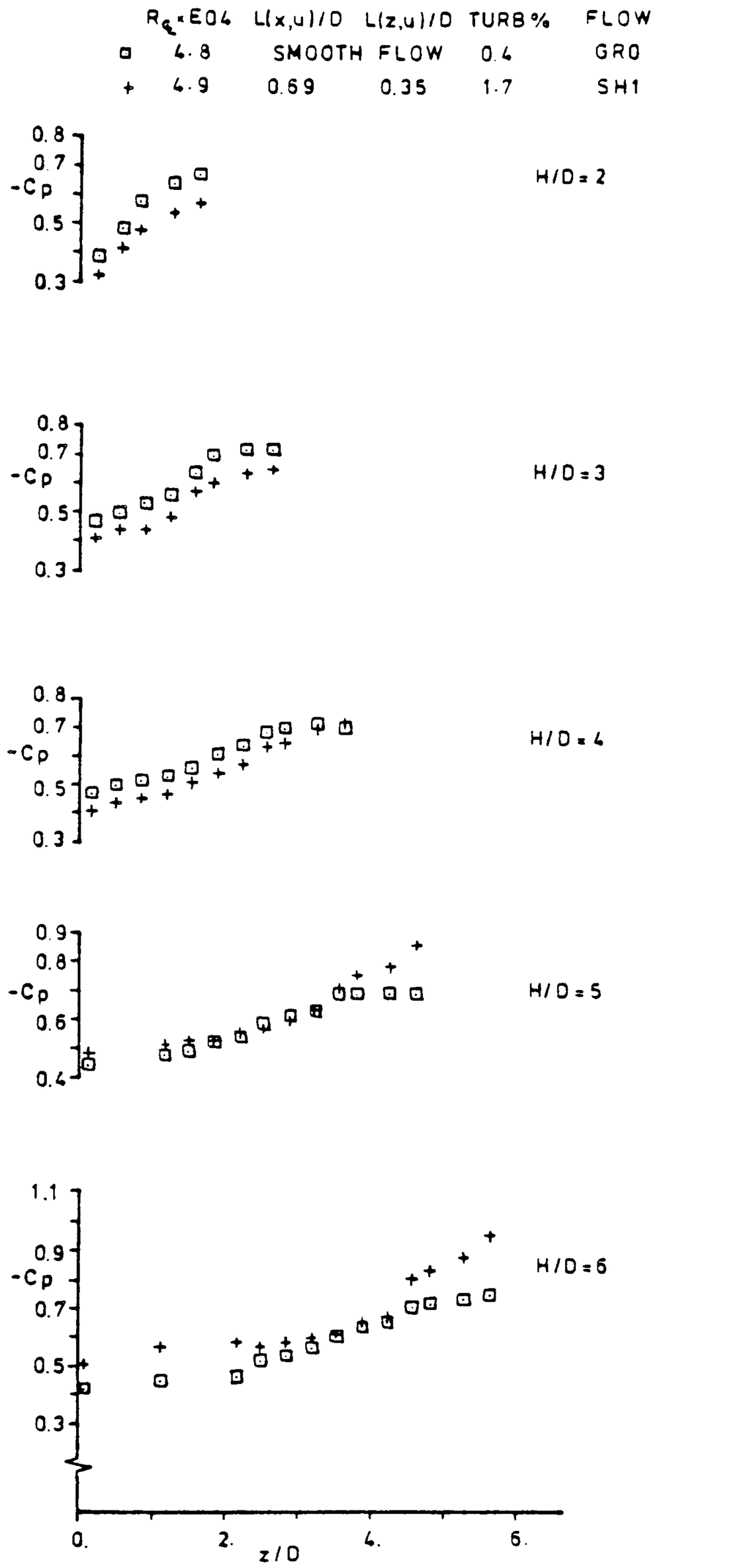
R_e = E04 L(x,u)/D L(z,u)/D TURB % FLOW
□ 4.8 SMOOTH FLOW 0.4 GRO
+ 4.9 0.69 0.35 1.7 SH1
-Cp
H/D = 2
H/D = 3
H/D = 4
H/D = 5
H/D = 6
z/D
SPANWISE MEAN Cp IN SHEAR AND UNIFORM FLOWS ON REAR FACE OF 48mm MODEL AT α = 0°

FIGURE 60

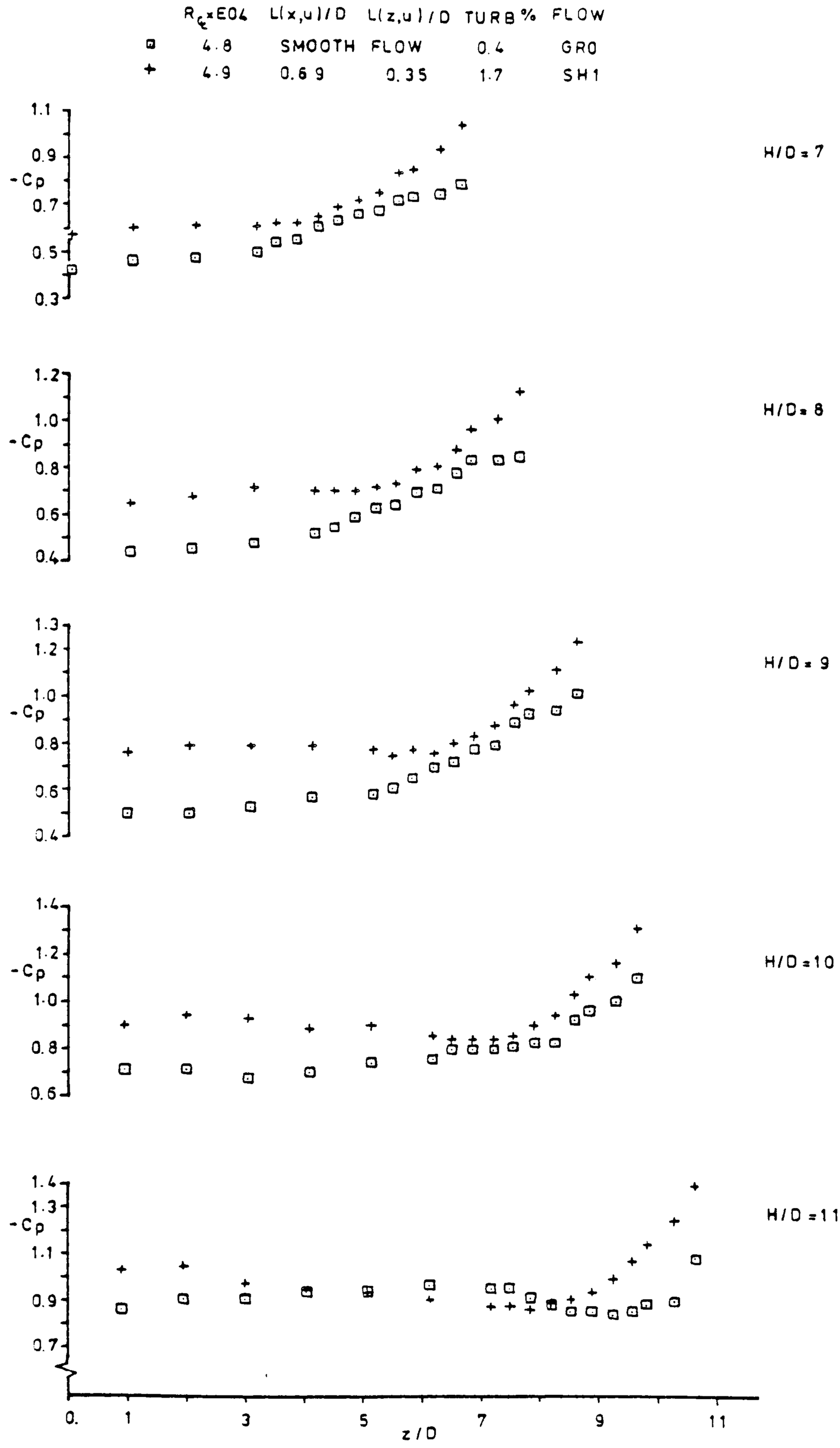

SPANWISE MEAN Cp IN SHEAR AND UNIFORM FLOWS ON REAR FACE OF 48mm MODEL AT $\alpha = 0°$

FIGURE 61

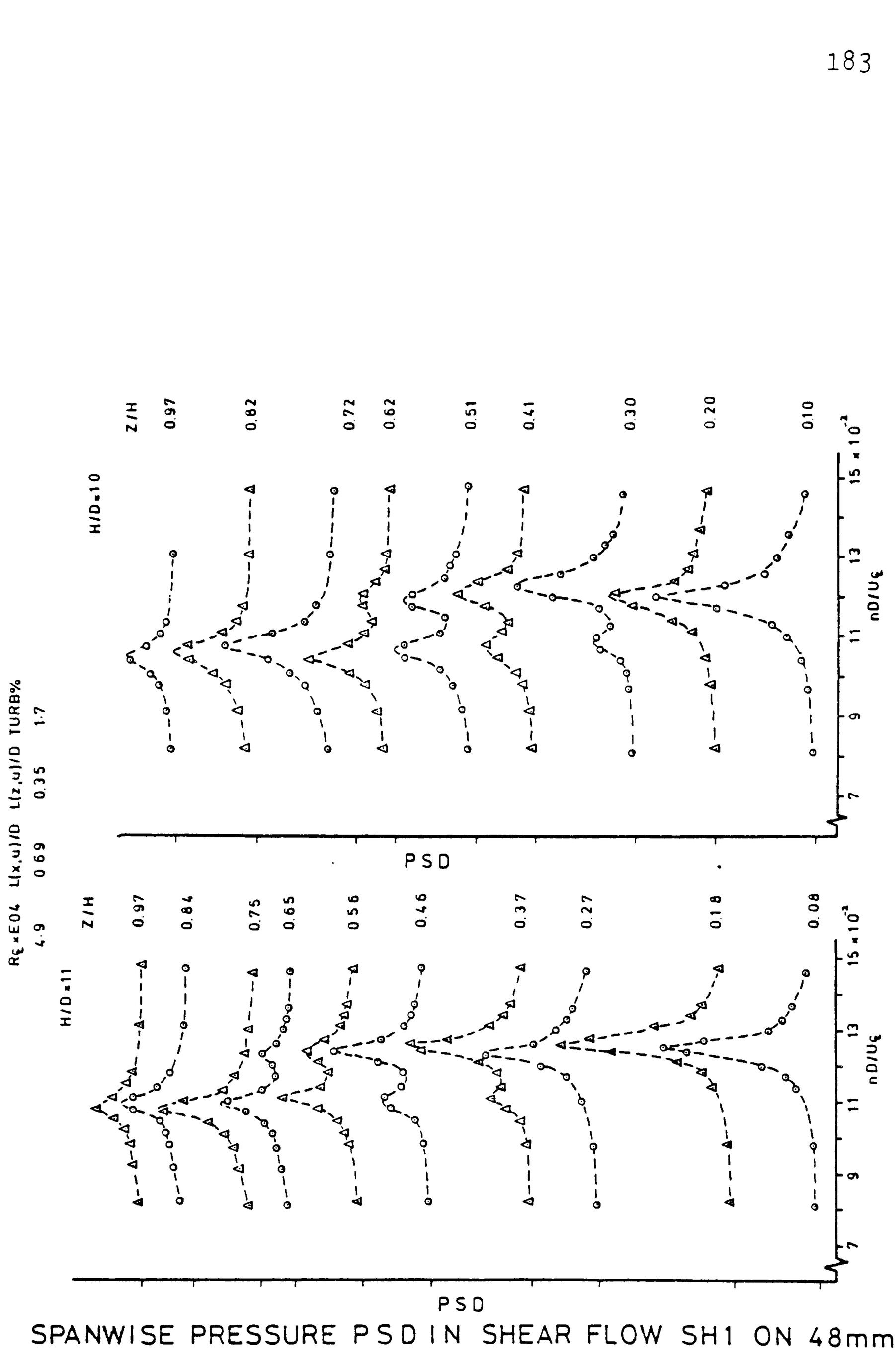

SPANWISE PRESSURE PSD IN SHEAR FLOW SH1 ON 48mm MODEL AT $\alpha = 0°$

FIGURE 62

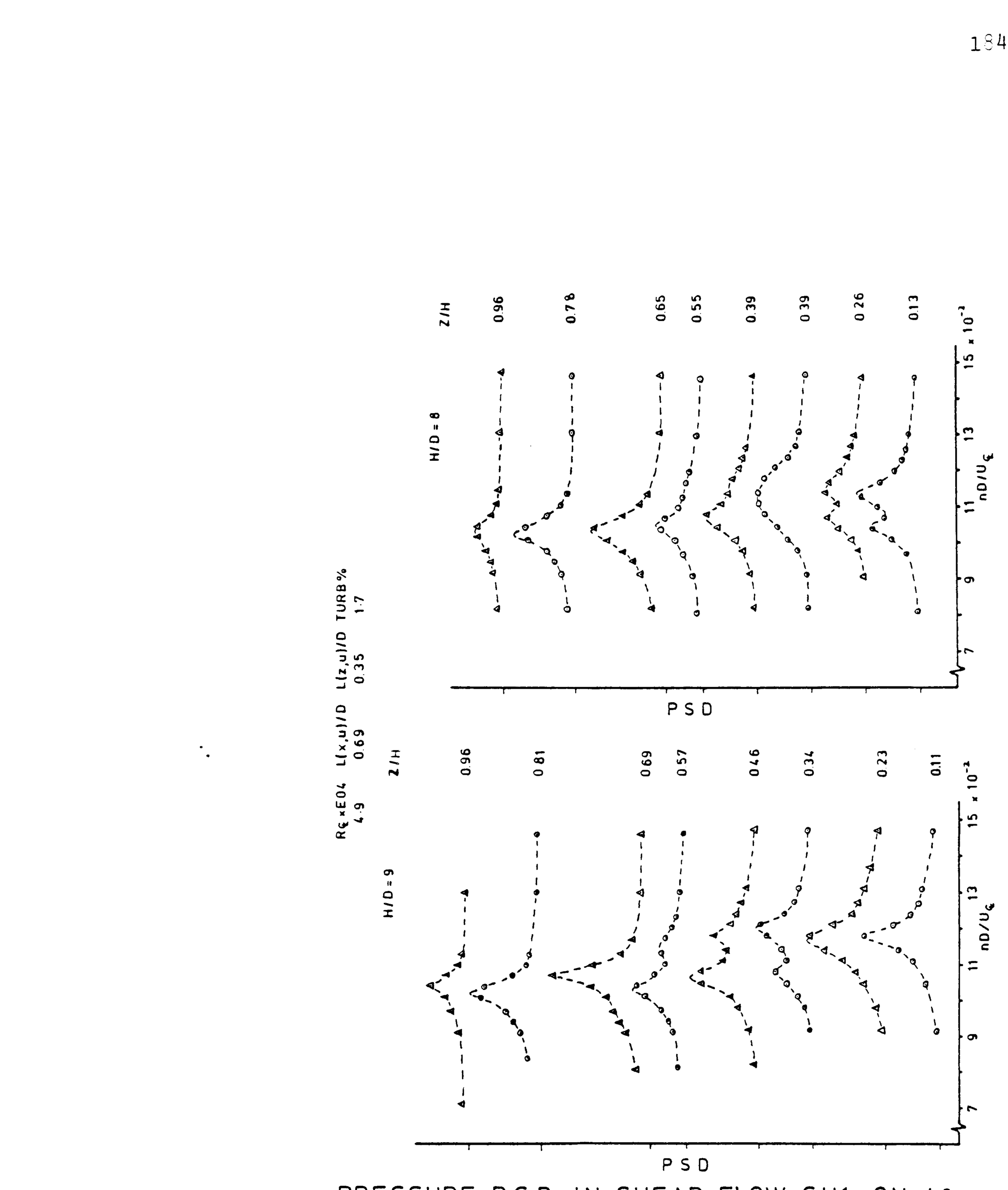

PRESSURE PSD IN SHEAR FLOW SH1 ON 48mm MODEL AT $\alpha = 0°$

FIGURE 63

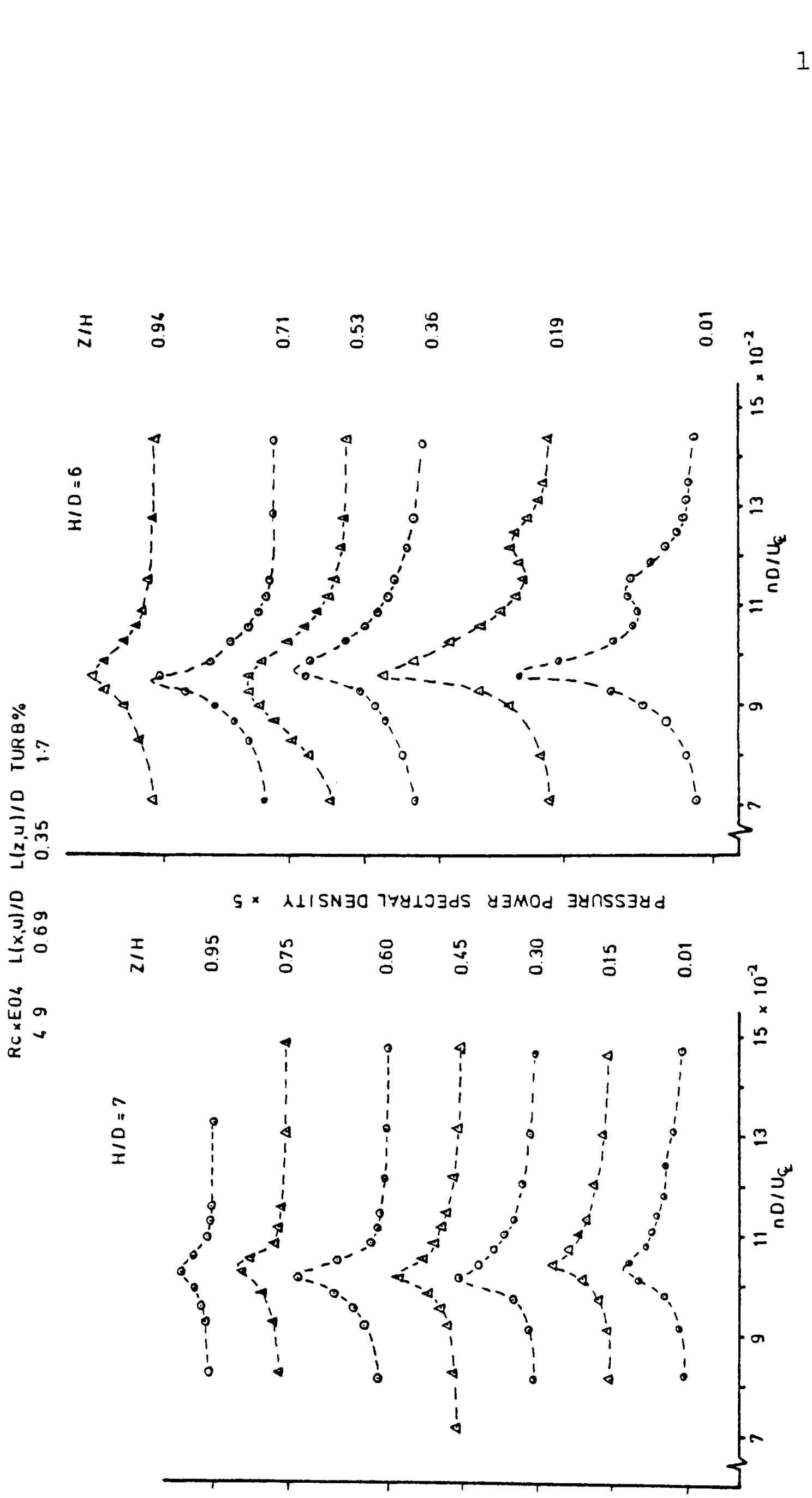

PSD

PRESSURE PSD IN SHEAR FLOW SH1 ON 48mm MODEL AT $\alpha = 0°$

FIGURE 64

$R_{\ell} \times E04$	L(x,u)/D	L(z,u)/D	TURB %
4.9	0.69	0.35	1.7

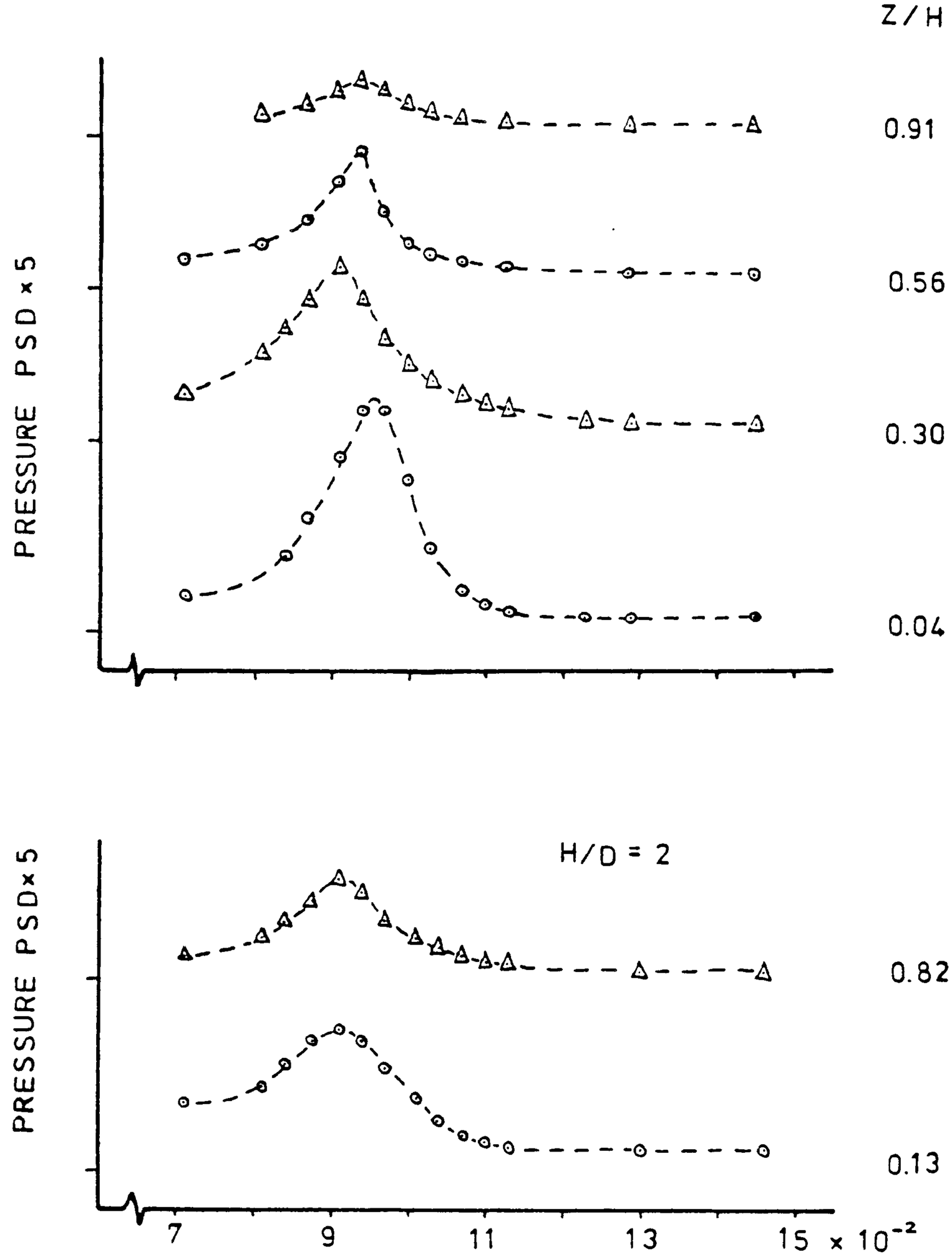

PRESSURE PSD IN SHEAR FLOW SH1 ON 48 mm MODEL AT $\alpha = 0^{\circ}$

FIGURE 65